THE UNIVERSITY OF CHICAGO

# EVALUATION OF GLYCOSYLATED ANTIGEN THERAPIES FOR B CELL-MEDIATED AUTOIMMUNE DISEASE

A DISSERTATION SUBMITTED TO

THE FACULTY OF THE PRITZKER SCHOOL OF MOLECULAR ENGINEERING

IN CANDIDACY FOR THE DEGREE OF

DOCTOR OF PHILOSOPHY

BY

JENNIFER ANTANE

CHICAGO, ILLINOIS

DECEMBER 2022

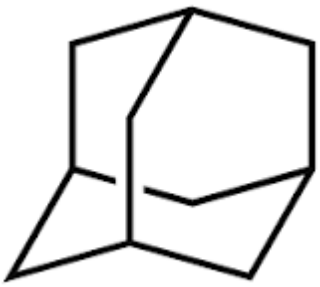

Adamantane

My namesake and a molecule that is both rigid and virtually stress-free.

## TABLE OF CONTENTS

## LIST OF FIGURES

## LIST OF TABLES

## ACKNOWLEDGEMENTS

I am incredibly grateful for and indebted to this very long list of people. Without them, none of this work would have been possible.

First, I want to thank my graduate advisor, Professor Jeffrey Hubbell. He fosters a lab environment unlike any other I have seen. He is an incredibly inspirational leader and his drive for translational research has brought meaning into every day I have spent in the lab for the last six years.

I would like to thank my committee members Melody Swartz and Jun Huang for taking the time to review my thesis.

I would like to thank Scott Wilson for inventing pGal, and the Anokion team for continuing to develop pGal therapies. Their work is the basis for Chapter 2. I would also like to thank the Anokion team, namely Stephan Kontos, Rafael Larocca, Stephanie Morgan, Tom Thornley, and Dina Wassaf, for their contributions during biweekly meetings during most of the pemphigus project. Their questions and guidance were pivotal in shaping the study, and their partnership enabled us to progress much faster than I could have without them.

I would like to thank Rachel Wallace for jumping in with both feet, and being a full member of “Team Pemphigus”. She was always willing to bounce ideas around with me and patiently taught me any technique I needed. Most importantly she became a friend and kept spirits high through some disappointing results and sac day disasters. I would like to thank the other Team Pemphigus member, Mindy Nguyen, for all the hours and care she put into this work. I would also like to thank honorary Team Pemphigus member and animal procedure extraordinaire, Ani Solanki, for lending his expertise during hundreds of delicate procedures.

I would like to thank Elyse Watkins for being my mentor through all the craziness of working

with LSECs. She was my role model as a graduate student and a force to be reckoned with. I am grateful she took the initiative to invite lab members to form friendships and see each other as a group socially outside of the lab. The Hubbell lab is better for having her.

The Hubbell Lab is a uniquely fun and supportive place, and I want to thank all of the members who make that a reality– Suzana Gomes, Tiffany Marchell, Joe Reda, Aaron Alpar, Andrew Tremain, Taylor Gray, Abigail Lauterbach, J-M Williford, Sarah Macewan, Erica Budina, Kirsten Refvik, Shijie Cao, Samir Hossainy, Anna Slezak, Lisa Volpatti, and Marcin Kwissa. Many of these people selflessly gave their time to the work presented in this thesis.

I would like to thank my first research mentor at Northwestern University, Dylan McCreedy, for believing in me and giving me great responsibility. The time he invested in me set me on this path, and gave me the confidence to pursue independent research.

I would like to thank the third cohort of PhD students to start at the PME. They were a great community of people dedicated to learning, and the first group I felt like I belonged to at the University of Chicago. I especially want to thank Rachel Weathered and Viviana Palacio for their enduring friendship.

I want to thank my parents. My father, Schuyler Antane, has always been and will forever be my biggest fan regardless of what I accomplish, and I do not take that for granted. My mother, Madelene Antane, has been my teacher, mentor, cheerleader, role model, therapist, and best friend. She taught me to think like a scientist and has been with me every step of the way since.

Finally, I want to thank my partner, Alejandro Rincon. He was with me from day one of this journey and has supported me through emotional highs and lows and physically taxing late nights in the lab. He never lost faith in me during the moments I doubted myself, and brought love and fun into my life when I needed it the most.

## ABSTRACT

The immune system delicately balances immunity against threats and tolerance to self-proteins. A dysfunction in this balance often leads to illnesses such as cancer, autoimmune diseases, and life-threatening allergies. As rates of autoimmune disease and allergy rise, the need for effective treatments becomes urgent. The current standard of care involves systemic immune suppression that puts the patient at risk for opportunistic infections. Consequently, a major goal of immunotherapy is to generate antigen-specific tolerance to only the antigen or antigens causing disease. Our lab has previously provided evidence that antigen delivered to and processed via endogenous pathways in the liver can result in antigen-specific T cell tolerance both in prophylactic and therapeutic settings. It was also shown that liver sinusoidal endothelial cells (LSECs) are the major hepatic cells that play an active role in the liver's mechanisms for inducing antigen-specific tolerance. In this project, we aim to test the boundaries of our current technologies in autoimmune disease models that rely on B cell responses. We also aim to understand endogenous pathways to design the next generation of therapeutics.

In this thesis, I investigate two approaches to generate antigen-specific tolerance by using endogenous pathways in the liver. The first approach uses a mouse model to test the *in vivo* feasibility of a glycopolymer-conjugated antigen in preventing a B cell-mediated autoimmune disease. The second approach furthers the development of an LSEC-specific promoter to modify LSEC gene expression *in vivo* using a lentiviral delivery method. This tool can probe the cellular pathways involved in LSEC antigen presentation and tolerance induction by knocking down or modulating gene expression related to antigen presentation and tolerance.

# CHAPTER 1

# INTRODUCTION

## 1.1 Loss of Immunological Tolerance

Autoimmune disease and allergy results from a loss of immunological tolerance which activates the body's immune system to attack itself or innocuous antigen. These immunologic disorders are widespread, deadly, and costly. In 2012 a report by the National Institute of Environmental Health Sciences identified more than 80 autoimmune diseases (e.g., Type 1 diabetes, multiple sclerosis, rheumatoid arthritis) that affect more than 23.5 million Americans [1]. Another study has examined data and demonstrated that over the last 30 years in Western countries autoimmune diseases have steadily increased [2]. Life-threatening food allergies, triggered by a loss of tolerance, affect 5% of children and 4% of adults in the United States [3]. In 2009 the National Institute of Allergy and Infectious Diseases estimated that in the United States alone the direct and indirect costs of autoimmune disease exceeded 100 billion dollars [4].

Current therapies for autoimmune diseases have life-threatening side effects caused by systemic immune-suppression. Autoimmune diseases are heterogeneous in pathogenesis, but roughly half of autoimmune diseases are associated with well-defined autoantigens [5]. An attractive approach to prevent or treat these autoimmune diseases and allergies is to induce antigen-specific tolerance through an endogenous pathway. Diverging from traditional global immune suppression, antigen-specific immunotherapies are being tested and aim to re-establish tolerance through the delivery of protein or peptide antigens that cause the disease [6, 7, 8]. The presentation of antigens as "self" invokes peripheral tolerance through anergy, deletion of potential effector T cells, or induction of regulatory T cells. Coupling antigens to nanoparticles for delivery has successfully induced immune tolerance to those antigens for treatment of autoimmune diseases

such as multiple sclerosis and type-1 diabetes [9, 10]. In a 2017 study, antigen encapsulated biodegradable nanoparticles were used to induce antigen-specific tolerance in the relapse-remitting experimental autoimmune encephalomyelitis model [11]. Because they did not need co-delivery with immunosuppressive drugs or the presence of a spleen (splenectomized mouse) for tolerance induction, they concluded that their nanoparticles target endogenous tolerogenic pathways in the liver. Knowledge of the cell types and mechanisms involved would allow for refined and potent therapeutics.

## 1.2 Role of Self-tolerance in Autoimmune Disease

### 1.2.1 Mechanisms of Self-Tolerance: Being Able to Discriminate Self from Nonself

The ability of the immune system to distinguish between one's own antigens, molecules produced by the body, and foreign antigens is important in avoiding autoimmune disease. Distinguishing between self-reactive lymphocytes and nonself-reactive lymphocytes is the immune system's way of creating self-tolerance. This discrimination is accomplished in the thymus as the naïve lymphocytes develop into CD4 or CD8 T cells. When self-reactive lymphocytes encounter self-antigens, autoreactive effector T cells and autoantibodies are generated. As they encounter self-tissues, the host's tissue is damaged causing autoimmune disease. For example, autoreactive T cells cause psoriasis, rheumatoid arthritis, Crohn's disease, multiple sclerosis, and type 1 diabetes. Autoimmune diseases such as systemic lupus erythematosus, Hashimoto's thyroiditis, and Sjögren's syndrome are caused by a combination of autoantibodies and autoreactive T cells. For the most part the immune system is efficient at identifying and eliminating self-reactive lymphocytes. It is when self-reactive lymphocytes escape elimination that autoimmune disease ensues [12].

Induction of self-tolerance, the recognition between self and nonself, begins in the thymus

in a process called central tolerance. After arriving from the bone marrow, immature lymphocytes begin to express their T cell receptors (TCRs), followed by the cell surface protein CD3, which forms a TCR-CD3 complex needed for T cell receptor signaling. The majority of thymocyte TCRs are made up of α and β chains, which eventually become helper or cytotoxic T cells. A small group of thymocyte TCRs are composed of γ and δ chains, which lack expression of CD4 and CD8 co-receptors. They are exported into the periphery to reside in epithelial and mucosal sites. Not much is known about the function of these γδ T cells. In the next stage, αβ thymocytes begin to express both co-receptor proteins CD4 and CD8 on their cell surface and become double-positive thymocytes. These double-positive thymocytes express both the CD4 and CD8 co-receptors and low levels of the T cell receptor. If the TCRs on a double-positive thymocyte can interact with self-peptide:self-MHC complexes on the thymic cortical epithelial cells, then they are selected for survival. Double-positive thymocytes that recognize self-MHC class II molecules become naïve CD4 T cells, which will only recognize MHC class II molecules on antigen presenting cells (APCs) that present antigens from extracellular bacteria and ingested proteins. Those that recognize self-MHC class I molecules mature into naïve CD8 T cells, which will only recognize MHC class I molecules on APCs that present endogenous proteins made from ordinary cellular proteins, viruses, and parasites. This process called positive selection determines the cell surface phenotype of a T cell and also ensures that the T cell will be able to recognize a self MHC molecule and its presented peptide. The final stage of thymocyte development in the thymus is called negative selection. Naïve CD4 or CD8 T cells with self-reactive receptors that bind to the self-peptide:self-MHC complexes too strongly are eliminated by apoptosis. In this way self-tolerance is created by the removal of the naïve T cells that react to self-antigens [12, 13].

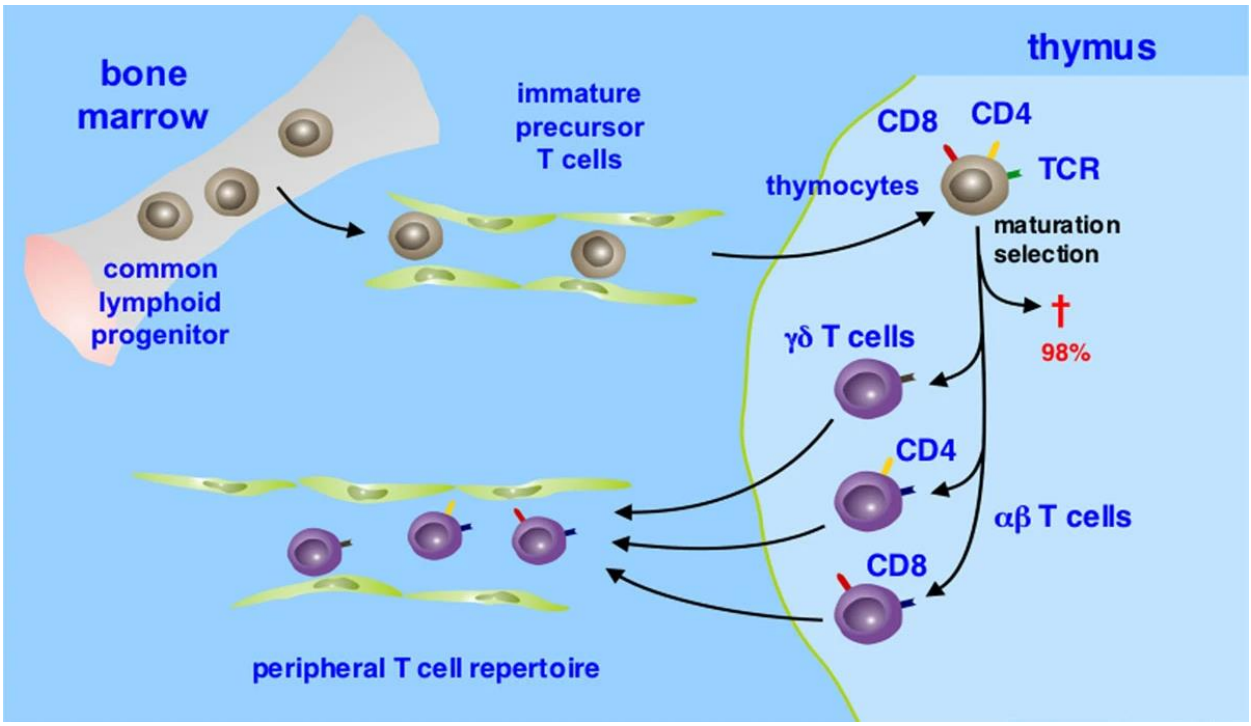


**Figure 1.1 | Schematic representation of T cell development.** T cells originate from the common lymphoid progenitor cells in the bone marrow. They migrate as immature precursor T cells via the bloodstream into the thymus, which they populate as thymocytes. The thymocytes go through a series of maturation steps including distinct changes in the expression of cell surface receptors, such as the CD3 signaling complex (not shown) and the coreceptors CD4 and CD8, and the rearrangement of their antigen receptor (*T cell receptor*, *TCR*) genes. More than 98% of the thymocytes die during maturation by apoptosis (†), as they undergo positive selection for their TCR's compatibility with self-major histocompatibility molecules, and negative selection against those T cells that express TCRs reactive to autoantigenic peptides. In humans, the vast majority of peripheral blood T cells expresses TCRs consisting of α and β chains (αβ *T cells*). A small group of peripheral T cells bears an alternative TCR composed of γ and δ chains (γ/δ *T cells*). αβ and γδ T cells diverge early in T cell development. Whereas αβ T cells are responsible for the classical helper or cytotoxic T cell responses, the function of the γδ T cells within the immune system is largely unknown. αβ T cells that survive thymic selection (Figure 1.1 continued) lose expression of either CD4 or CD8, increase the level of expression of the TCR, and leave the thymus to form the peripheral T cell repertoire. From Skapenko 2005 *Arthritis Res Ther* [13].

By the end of the development and selection process that occurs in the thymus, 98% of the thymocytes have been removed by apoptosis. The successful candidates leave the thymus and travel to the various peripheral lymphoid organs (e.g., spleen, lymph nodes, mucosa-associated lymphoid tissues) where they encounter antigen presented on MHC-I or MHC-II of APCs and

grow into mature naïve CD8 or CD4 T cells, respectively. The process of recognizing self and nonself in the peripheral lymphoid organs is called peripheral tolerance. A mature naïve T cell with self-reactive TCRs can undergo deletion, anergy, or survival when it encounters self-antigen in the periphery. Three mechanisms in the periphery are used to induce tolerance. First, when a self-reactive T cell is repeatedly activated by ever-present self-antigens, they are eliminated by apoptosis. Second, under non-infectious conditions, when pro-inflammatory cytokines and co-stimulatory molecules are absent, a high concentration of self-antigen that creates a sustained signal is recognized as self. In this case, a self-reactive mature naïve T cell becomes either tolerant or anergic to that self-antigen. Third is the development of "induced" regulatory T cells (iTregs) that can suppresses autoreactive effector T cell responses [12].

### 1.2.2 Utilizing the Liver to Induce Tolerance

The liver is a central organ that receives and filters circulating blood from the hepatic artery and gut-derived blood from the portal vein. As a result, the liver is exposed to a variety of antigens resulting from microbes, pathogens, degradation products, damaged cells, and toxins. Although these products can produce an inflammatory response, the cells in the liver work to actively suppress this response. As the blood flows through the liver sinusoids, it slows down so interactions with the resident liver scavenger cells, such as Kupffer cells (KCs) and the liver sinusoidal endothelial cells (LSECs), can occur. The KCs are liver macrophages that remove large particles by phagocytosis. The LSECs are endothelial cells that create a permeable barrier between the blood and the hepatocytes, whose primary function in addition to inducing tolerance is metabolism, detoxification, and protein synthesis in the liver [14].

LSECs' active receptor-mediated endocytosis mechanism distinguishes it from all other liver cells. It gives the LSECs the ability to clear blood of soluble antigens and waste material with

great speed and high capacity. The endocytic receptors on the LSEC surface, which include mannose receptor, stabilin-1, stabilin-2, and FcgRIIb2, enable the removal of small particles (< 200 nm) and macromolecules. To target these endocytic receptors on the LSECs, specific ligands are incorporated onto lipid nanoparticles and used as a strategy to deliver therapeutics to the liver LSECs [15, 16]. It is important to note that Kim et al. [16] have demonstrated, although with less efficiency, the uptake by LSECs of lipid nanoparticles, which lack the specific ligands targeting the LSEC endocytic receptors. They also have shown that molecules with a particle size of approximately 45-80 nm can pass through the fenestrae of the LSECs and are readily taken up by hepatocytes, which are also known to induce tolerance.

KCs and LSECs are not only highly efficient scavengers but also antigen-presenting cells. The particles that are taken up during their scavenging activities are presented as antigens to passing lymphocytes to induce tolerance. After interacting with an antigen-presenting LSEC, a CD8 T cell is tolerized or becomes a memory T cell. A CD4 effector cell is transformed into Foxp3 regulatory T cell after interaction with an antigen-presenting LSEC and exposure to TGF-β. Foxp3 regulatory T cells can suppress autoreactive T cells. Although KCs can also induce tolerance in autoreactive lymphocytes, they also have a high plasticity. This means that under a state of inflammation KCs can readily switch between being tolerogenic to activating T cells and causing inflammation. In contrast LSECs have a low plasticity and remain tolerogenic even during inflammatory conditions [14].

In summary the liver is an attractive target for antigen-specific tolerance induction due to its APCs such as LSECs, KCs, and hepatocytes. These cells use their antigen-presenting ability to lymphocytes and induce tolerance by deletion or anergy of self-reactive T cells and by induction of regulatory T cells. LSECs and KCs are also ideally located in the liver sinusoid where they can

survey circulating blood as well as blood from the gut. This allows them to rapidly clear antigens that can be presented for antigen-specific tolerance induction. The low plasticity of LSECs is an additional advantage for utilizing the liver to induce tolerance.

### 1.3 Current Therapeutics for Immune Tolerance

#### 1.3.1 Antigen-specific Immunotherapies that Target the Liver

Current therapies for autoimmune disease span from experimental mouse models to ones in clinical trials. Summarized below are antigen-specific immunotherapies that utilize the liver's antigen-presenting cells to induce tolerance by suppressing autoreactive T cells and by activating regulatory T cells.

Gene transfer to hepatocytes

In the field of gene therapy, a viral vector system based on adeno-associated virus or lentivirus is used to deliver a functional copy of a missing or deficient gene. In this way the missing protein in a genetic disease is produced. This strategy has the limitation that the missing protein (i.e., the transgene product) can trigger an immune response when it is perceived as foreign. Seeking to induce tolerance to the transgene product, the concept of delivering the transgene to an anatomically privileged site (e.g., liver, central nervous system, eyes, and hematopoietic cells) was developed. The liver known for its tolerogenic abilities through the suppression of self-reactive T cells and the induction of regulatory T cells makes it an attractive site for transgene delivery. Once delivered, tolerance induction to the missing protein occurs in the liver by the production of regulatory T cells [17].

In a similar way viral vector-based antigen-specific immunotherapies use a hepatocyte-directed gene transfer strategy for tolerance induction in the treatment of autoimmune disease. Adeno-associated viral (AAV) or lentiviral vectors containing a hepatocyte-specific promoter

delivers genes that can only be expressed in hepatocytes. Akbarpour et al. [18] used a lentiviral vector with a hepatocyte-specific promoter (i.e., enhanced transthyretin) to target hepatocytes in the nonobese diabetic (NOD) mice for the expression of insulin B chain 9-23 ($InsB_{9–23}$) transgene. They showed that antigen-specific Tregs to $InsB_{9–23}$, an immunodominant epitope of insulin, are induced in the liver and accumulate in the pancreatic lymph nodes and pancreatic islets. These $InsB_{9–23}$–specific Tregs lead to a state of immune tolerance protecting NOD mice from type 1 diabetes.

In another study an AAV8 vector was constructed with a liver-specific promoter and full-length myelin oligodendrocyte glycoprotein (MOG), which is known to produce a potent T cell response in multiple sclerosis patients. When used in experimental autoimmune encephalomyelitis (EAE) mouse model for multiple sclerosis, they found that AAV8.MOG induced long-term expression of MOG. This resulted in antigen-specific immune tolerance and prevented long-term development of EAE in mice for 200 days [19]. While the viral vector-based gene transfer strategy for antigen-specific tolerance induction shows promise in animal models, the immunogenicity of the vector and transferred gene product remains a limitation [14].

Antigen-loaded erythrocytes

The body removes aging erythrocytes using a mechanism called eryptosis, a form of programmed cell death. These dying erythrocytes express phosphatidylserine on their cell surface, and are recognized by macrophages in the spleen and liver where they undergo phagocytosis. Thus, an autoantigen bound to dying erythrocytes can be presented by MHC on APCs to autoreactive T cells to induce tolerance [20]. With 80% of the macrophages present as Kupffer cells, this approach is an ideal therapeutic for targeting the liver [14].

Kontos et al. was able to attach a peptide islet β-cell autoantigen (p31) to an erythrocyte-

binding antibody fragment (TER119). TER119-p31 can specifically target and in situ bind to circulating erythrocytes in the NOD BDC2.5 mouse model. Treatment with TER119-p31 resulted in the deletion of diabetogenic CD4+ T cells and prevented the development of diabetes [21]. Clinical candidates that target autoimmune diseases by using antigen-loaded erythrocytes include ETIMS (Phase 1b, NCT01414634) [22] for multiple sclerosis.

The use of antigen-loaded erythrocytes as an antigen-specific immunotherapy is limited by the high degree of plasticity of KCs and macrophages. Thus, during inflammatory conditions there is a risk of aggravating the autoimmune disease [14].

Antigen-specific nanoparticles targeting the liver

Synthetic nanoparticles (NPs) have several advantages. First their large surface-to-volume ratio gives them an increased capacity to carry autoantigen peptides for delivery to specific targets. Second, NPs are versatile because they can be functionalized with various ligands that can recognize specific cell surface receptors. This guarantees that the NP and its peptide cargo will be only taken up by specific cell types. Third, NPs are readily taken up by APCs, which have MHC protein on their cell surface. This results in the presentation of the NP's peptide cargo to T cells, and in the induction of tolerance to the specific peptide through the suppression of self-reactive T cells and activation of regulatory T cells. Fourth, after systemic application NPs are known to accumulate in the liver where the tolerogenic function of APCs, such as KCs and LSECs, can be utilized [14, 23].

Casey et al. [24] investigated the properties and mechanism of tolerance induction by highly negatively-charged antigen-containing poly(lactide-co-glycolide) nanoparticles (PLG-Ag) coated with a stabilizing anionic surfactant poly(ethylene-alt-maleic acid). When given intravenously this platform was effective at inducing tolerance in mouse models for multiple

sclerosis and type 1 diabetes. PLG-Ags with a particle size between 300-800 nm had a 10-fold greater cell distribution in the liver as compared to the lung and spleen. Casey et al. also demonstrated that the scavenger cells of the liver could utilize the PLG-Ag platform to promote tolerance to the antigen proteolipid protein (PLP), which was used to induce disease in EAE (experimental autoimmune encephalomyelitis) mouse model for multiple sclerosis. For example, KCs were shown to mitigate EAE symptoms in an adoptive transfer experiment using Cy5.5-labeled PLG-PLP-containing KCs. In addition, when KC-depleted (i.e., using clodronate liposomes) splenectomized mice were treated with PLG-PLP, EAE symptoms were reduced indicating that LSECs also play a central role in tolerance induction through the PLG-Ag platform. They also found that *in vivo* treatment of OT-II mice with PLG-OVA showed an upregulation of CD86 and CD40, and an increased expression of coinhibitory molecule PD-L1 in both KCs and LSECs.

Freitag et al. used a PLG-Ag platform encapsulating gliadin protein in mouse models for celiac disease. They observed a reduction of gliadin-specific T cell proliferation, a decrease in inflammatory cytokine secretion, and an increase in Foxp3 expression in regulatory T cells [25]. Similarly, Prasad et al. used a PLG-Ag platform that contained either a single diabetogenic epitope (e.g., p31 or NRPA7) or a linked tripeptide of p31, NRPA7, and $InsB_{9-23}$. They discovered that onset of hyperglycemia was prevented or reversed in an adoptive transfer model of type 1 diabetes (i.e., transfer of activated BDC2.5 CD4+ T cells and/or NY8.3 CD8+ T cells into NOD.SCID mice) [26]. Although not specifically designed to target KCs, NPs still accumulate in the liver due to the liver's high scavenging and clearance ability. However, the plasticity of KCs remains a safety concern for this approach where immune activation instead of tolerance will occur [14].

Topas Therapeutics conjugated antigen-specific peptides onto the surface of small

polymer-coated superparamagnetic iron oxide particles. Because of its small particle size, this technology platform, called Topas Particle Conjugates (TPCs), has been shown to specifically target LSECs via passive targeting or localization of nanoparticles within LSECs. TPCs have also been validated in several mouse models of autoimmune disease [27]. Carambia et al. demonstrated that through passive LSEC-targeting antigen-loaded TPCs can induce immune tolerance. In the case of CD8 T cell-driven autoimmune disease, primary biliary cholangitis, SIINFEKL-conjugated TPCs resulted in LSEC cross-presentation of SIINFEKL and induction of CD8 T cell tolerance, which reduced severity of the disease [28]. In another study they demonstrated that TPCs conjugated with MPB or MOG antigen prevented the onset of disease in EAE mouse model for multiple sclerosis through the induction of CD4+ Foxp3+ regulatory T cells [29].

In yet another LSEC-targeting platform, Liu et al. took advantage of LSECs' natural preference for small particles and its scavenger receptors. They developed a poly(lactide-co-glycolide) nanoparticle encapsulating OVA ($NP^{OVA}$) whose surface was conjugated to a ligand, such as ApoB protein, that targets the stabilin receptor specific to LSECs. When the surface of $NP^{OVA}$ was covalently bound to the ApoB protein ($NP^{OVA}$/ApoBP), particles the size of 230-290 nm were recognized by the scavenger receptor stabilin. They not only observed $NP^{OVA}$/ApoBP distribution to the liver and increase uptake by LSECs, but also an increase in TGF-β production and the recruitment of Foxp3+ regulatory T cells. Thus they were able to demonstrate that $NP^{OVA}$/ApoBP reduced allergic inflammation in a mouse model of OVA-induced allergic inflammation in the lung [30]. The targeting of LSECs has several advantages. LSECs are effective at inducing immune tolerance due to their high efficiency in taking up NPs, their generation of regulatory T cells, and their ability to cross-present antigens to induce CD8 T cell tolerance. In addition, their low plasticity offers a good safety profile [14].

Two of the antigen-specific nanoparticle technologies have clinical candidates. The PLG-Ag platform developed by Cour Pharmaceuticals [31] has clinical candidates TAK-101 (Phase 2, NCT04530123) for celiac disease, CNP-104 (Phase 2a, NCT05104853) for primary biliary cholangitis, and CNP-201 (Phase 1b/2a, NCT05250856) for peanut allergy. Topas Therapeutics TPCs platform has TPM203 in Phase 1 (EUCTR2019-001727-12-DE) for pemphigus vulgaris [32, 33].

Antigen-glycopolymer conjugates

N-acetylgalactosamine (GalNAc) is a ligand that is readily recognized by the asialoglycoprotein receptor (ASGPR) on the cell surface of liver hepatocytes, and are taken up by receptor-mediated endocytosis. Taking advantage of this property, GalNAc has been developed into an effective hepatocyte-targeting delivery platform. Conjugation of siRNA or antisense oligonucleotides (ASO) to a trivalent cluster of GalNAc results in the targeted delivery of these substances to hepatocytes. This promising hepatocyte-targeting technology has resulted in 29 different GalNAc conjugates of siRNA or ASO that are in the various stages of clinical development (Phase 1-3) [34, 35].

Using a similar strategy Wilson et al. [36] uses glycopolymers (e.g., of GalNAc) to deliver disease-causing antigen to hepatic APCs, such as hepatic DCs, KCs, LSECs, and hepatocytes. By taking advantage of the liver's tolerogenic environment they wanted to induce antigen-specific immune tolerance. Hepatic APCs induce tolerance upon presentation of antigen to T cells through TGF-β signaling. In the absence of co-stimulation, the production of TGF- β mediates the conversion of CD4+ T cells into regulatory T cells. TGF- β also inhibits T cell proliferation and production of proinflammatory cytokines. In addition, suppression of effector T cells is accomplished by the expression of programmed death-ligand 1 (PD-L1) on KCs and LSECs. To

accomplish antigen-specific immune tolerance, they chose ligands that would target the C-type lectin receptor found on hepatic APCs. Both GalNAc and N-acetylglucosamine (GluNAc) are residues on apoptotic debris that bind to C-type lectin receptors of hepatic APCs during hepatic clearance. Taking advantage of this, Wilson et al. conjugated the antigen OVA to glycopolymers 1) GalNAc, known to bind to asialoglycoprotein receptor (ASGPR) found on hepatocytes [34, 35], and 2) GluNAc, known to bind to the mannose and LSECtin [15] receptors present on multiple hepatic APCs.

When fluorescently labelled OVA was used, they found that *in vivo* administration resulted in preferential accumulation of both OVA-p(GalNAc) and OVA-p(GluNAc) in the mouse liver over the heart, kidneys, lungs, lymph nodes, and spleen. They also showed that OVA-p(GalNAc) and OVA-p(GluNAc) caused antigen uptake and MHC I presentation of SIINFEKEL (i.e., immunodominant MHC I epitope of OVA) by hepatic APCs, most notably LSECs and hepatocytes. Splenectomized mice were adoptively transferred with OTI and OTII T cells, and followed by treatment with OVA-p(GalNAc) or OVA-p(GluNAc). When compared to saline treated mice, they observed in draining lymph nodes a decrease in $IFN\gamma^+$ OTI and OTII T cells and an increase in Foxp3 regulatory OTII cells, indicating that both antigen-glycopolymer conjugates suppressed OVA-specific T cell responses [36].

The antigen-conjugated glycopolymers of GalNAc and GluNAc were tested in several mouse models of autoimmune disease. In an experiment with BDC2.5 T cell adoptive transfer model of type 1 diabetes, activated BDC2.5 T cells were transferred into NOD/SCID mice. The mice that were treated with p31-p(GluNAc) was free of disease for 35 days, whereas saline treated mice developed hyperglycemia within 10 days [36]. In another study Damo et al. [37] showed that hepatocytes have the ability to cross-present extracellular antigen on MHC-I to induce CD8 T cell

tolerance. When comparing the cross-presentation of unmodified OVA and OVA-p(GalNAc), they found that OVA-p(GalNAc) had a 1.2-fold increase of cross-presentation of SIINFEKL in hepatocytes. Thus, they used the antigen-glycopolymer, OVA-p(GalNAc), in a mouse model of skin transplantation. Mice were pretreated with OVA-p(GalNAc)-incubated hepatocytes prior to tail skin graft from $OVA^{+/+}$ C57BL/6 mice. At the end of 60 days mice who retained $OVA^{+/+}$ skin grafts showed after *ex vivo* restimulation of spleen cells, lower frequencies of SIINFEKL-specific CD8 T cells and higher frequencies of Foxp3 regulatory T cells. By using GalNAc as a hepatocyte targeting strategy, they demonstrated that hepatocytes can induce tolerance of antigen-specific CD8 T cells.

Anokion uses an "antigen-based, novel synthetic glycosylation platform" to specifically deliver antigen to the liver and utilize its tolerogenic environment. At present they have several clinical candidates to treat autoimmune disease that include KAN-101 (Phase 1, NCT04248855) for celiac disease, ANK-700 (Phase 1, NCT04602390) for multiple sclerosis, and KAN-201 (pre-clinical) for type 1 diabetes [38].

### 1.3.2 Liver Sinusoidal Endothelial Cells (LSECs) and Antigen Specific Tolerance

A strong candidate for a major contributing cell type in liver-mediated antigen specific tolerance are liver sinusoidal endothelial cells. LSECs are the most efficient scavengers in the body with many types of receptors for endocytosis. Interestingly, they can present and cross-present antigens they take in similar to professional antigen presenting cells [39]. LSECs are important in their interactions with lymphocytes because they can 1) silence T cell activation by inhibiting T cell activation, proliferation, and effector function, 2) promote a tolerogenic response by inducing tolerance in CD8 T cells through programmed death-ligand 1 signaling, and 3) transform CD4 T cells into Tregs. However, the problem with the current literature involving LSECs is the lack of

uniformity in how the cells are isolated and the lack of characterization of the cells after *in vitro* culture to confirm their identity and preserved phenotype. This has led to conflicting reports of LSEC behavior, function, and expressed markers that could be due to contaminating cell types during isolation, or by favoring the isolation of different subsets of LSECs. In 2017, distinct subsets of LSECs were observed in the human liver through immunofluorescence [40]. Further support for LSEC subsets is the two embryological origins identified by fate tracing experiments [41]. Single cell RNA sequencing (scRNA-seq) on wild type LSECs shows the full picture of the heterogenous population of LSECs and helps to identify unique subsets. scRNA-seq has proven very useful in immunology in being able to sensitively and accurately reveal previously unidentified immune cell subsets and associated cellular pathways [42].

**1.4 RNAseq: A Powerful Tool**

Analysis of the proportion of G and C nucleotides in a region of interest (GC content), duplicated reads, and other aspects of the raw reads is used to detect artifacts, contaminations, or sequencing errors. The quality of the reads should be consistent across samples. FastQC is a popular tool to perform quality control analyses [43]. Low quality reads are discarded. Reads are then mapped onto a genome or transcriptome. Mapping onto a transcriptome prevents the discovery of new transcripts. Reads are either mapped to a single position in the reference or they are multi-mapped reads (multireads) due to repetitive sequences or shared domains. Good read alignment has a high percentage of mapped reads and uniformity of read coverage on exons. Beyond examining the individual samples, there should be reproducibility between the replicates. The biological replicates within the conditions (healthy, autoimmune disease, germ-free) should cluster together in a principal component analysis (PCA).

The RNA-seq data is used for differential gene expression analysis. In order to compare

gene expression values among samples, normalization methods are used to account for varied sequencing depth between samples and heterogeneous transcript distributions that skew the count distribution towards highly expressed genes. There are many options for packages for sample normalization including NOISeq R, TMM, and DESeq [44]. There are also many packages for the visualization of RNA-seq data at the level of reads or heatmaps across samples. The final and crucial step is to use the identified differentially expressed genes (DEGs) to characterize molecular functions or pathways. RNA-seq functional analysis tools use functional annotation data from resources available for model species, and implement enrichment analysis similar to approaches developed for gene microarray technology. They essentially compare the DEGs against the genome searching for overrepresented function, or they rank the transcriptome according to differential expression in what is called gene set enrichment analysis (GSEA). Our goal is to identify changes in the molecular functions and pathways active in LSECs in healthy mice, mice with autoimmune disease such as diabetes, and germ-free mice on an antigen-free diet that does not have the antigenic load of gut-derived antigens on the liver. For example, changes in the active pathways from a mouse with diabetes could provide possible pathogenesis or targets for therapeutics, whereas differences in the gene expression of LSECs in germ-free mice could point to how tolerance is promoted under antigenic load by showing what pathways are missing when the gut-derived antigens are removed.

## 1.5 Overview of Research

### 1.5.1 Approaches to Induce Tolerance

Two studies were done to investigate approaches to induce tolerance. First, a mouse model for pemphigus vulgaris was explored to see if a carbohydrate polymer could induce tolerance. Second, the goal of the LSEC study was to use genetic approaches to isolate the role of LSECs in

antigen-specific tolerance and pinpoint specific mechanisms of tolerance induction. This would provide greater understanding of endogenous peripheral tolerance pathways and crucial information for the intelligent design of therapeutics. The successful development of an LSEC-specific promoter would make future studies of LSEC behavior possible in immunology and hepatology fields.

### 1.5.2 Autoimmune Disease and Allergy

The understanding of mechanisms for inducing antigen-specific tolerance would have far-reaching implications in the design of therapies to tolerize autoantigens, allergens, or drugs that elicit antibodies. Dysfunction in the generation of tolerance can manifest as an autoimmune disease. Without immune tolerance, allergens can cause allergies. The generation of anti-drug antibodies is the result of biological therapeutics eliciting an immune response.

Current strategies to treat or lessen the symptoms of autoimmune diseases and allergies utilize methods that non-specifically suppress the immune system, which exposes the patient to a risk of opportunistic infection and induces numerous side effects [45]. The strategy of globally suppressing the immune system does not target the original immune dysfunction that causes disease. Pathways to develop antigen-specific tolerance are desirable as an entry point for potential treatment for autoimmune diseases and allergies. Antigen-specific tolerance would not evoke systemic side effects and would treat the source of the disease. One approach would utilize a glycopolymer linked to an antigen to induce antigen-specific tolerance in autoimmune diseases [36]. Another approach would employ the liver's ability for peripheral tolerance induction. A robust therapeutic could be developed by studying and understanding the role of LSECs in antigen-specific peripheral tolerance induction (e.g., antigen-specific Tregs) [46].

### 1.5.3 Drug Immunogenicity and Antigen-specific Therapy

Life-saving drugs for chronic autoimmune illnesses such as rheumatoid arthritis or multiple sclerosis are administered in repeated does for extensive periods of time. These drugs are often large proteins, which are foreign to the patient, and therefore have the potential to elicit an immune response. When the immune response results in formation of anti-drug antibodies (ADAs), the drug loses its effectiveness with an increase in side effect occurrences [47]. This phenomenon of immunogenicity is a common problem faced by protein therapeutics. A therapy that involves an antigen-specific tolerance to these biological drugs could be developed by using the endogenous tolerance pathways in the liver. The ADA-inducing drug could then be tolerized. This therapy would allow for the continued use of effective drugs in the 30% of patients with autoimmune diseases such as rheumatoid arthritis or multiple sclerosis that develop ADAs [48]. The implementation of an antigen-specific tolerance therapy will not only impact the long-term success of currently available therapies, but also generate the development of new therapies that are currently held back by ADA production. With antigen-specific tolerance induction, successful biological therapeutics could expand in areas such as cancer therapy, where numerous trials are abandoned as patients develop ADAs [49].

# CHAPTER 2

# USING A CARBOHYDRATE POLYMER TO INDUCE TOLERANCE IN A PEMPHIGUS VULGARIS MURINE MODEL

## 2.1 Abstract

Current treatments for autoimmunity generate broad immunosuppression that puts patients at risk for opportunistic infections and malignancy. Recent efforts have focused on regulating antigen-specific T cell responses, but to treat autoimmune diseases we will have to regulate antigen-specific B cell responses as well. In this project we evaluate the feasibility of using a glycopolymer-conjugated antigen for the treatment of a B cell-mediated autoimmune disease. Specifically, we examined the use of pGal-Dsg3 both prophylactically and therapeutically in naïve or immunized adoptive transfer pemphigus vulgaris mouse models. When delivered intravenously, pGal targets the delivery of a conjugated antigen to carbohydrate scavenging receptors on antigen presenting cells in the liver. Upon uptake, the antigen is released by a self-immolative linker. This results in antigen presentation in the immunosuppressive environment of the liver. This strategy has been shown to therapeutically suppress previously activated T cells, even in the presence of antibodies to the conjugated antigen. We show that this is dependent on the conjugated antigen, and specifically, Dsg3 activates T cells even when conjugated to pGal. We also show that pGal-Dsg3 is not able to suppress the production of anti-Dsg3 IgG. Ultimately, we are able to show that pGal-peptide antigen therapy was less immunogenic than peptide antigen therapy in a pemphigus vulgaris mouse model.

## 2.2 Introduction

### 2.2.1 Pemphigus Vulgaris: An Autoimmune Disease of the Skin

Autoimmune bullous skin diseases consist of two main subtypes, pemphigus and pemphigoid, both causing blistering of the skin and mucous membranes. Pemphigus affects the desmosomes, which are structural proteins for the cell-cell adhesion of the keratinocytes in the epidermis. Pemphigoid occurs in the subepidermal layer affecting the hemidesmosomes that connect keratinocytes to the basement membrane. The blistering results because of a loss of cellular adhesion between keratinocytes, which is caused by IgG autoantibody binding to the desmosomal structural proteins desmoglein (Dsg) 1 and Dsg3. Studies have shown that autoantibodies from pemphigus patients recognize the extracellular domains EC1 and EC2 of Dsg, which targets the NH2-terminal of Dsg. Two major mechanisms have been identified in the loss of cellular adhesion between keratinocytes (Figure 2.1). First the binding of IgG autoantibody to the amino-terminal domain of Dsg results in a steric interference preventing Dsg binding and leading to keratinocyte dissociation. Second IgG autoantibody binding to Dsg results in cellular signaling that affects several pathways including p38 MAPK, protein kinase C (PKC), c-Jun N-terminal kinases (JNK), RhoA, and caspases 3, 6, 8 and 9. Activation of signaling pathways causes internalization of Dsg from the cell surface resulting in Dsg depletion and keratinocyte cell adhesion. Additionally binding of IgG autoantibodies to the keratinocyte α-acetylcholine receptor (AChR) results in cellular signaling that disassembles the desmosome (i.e., keratin filaments from desmoplakin) causing the loss of keratinocyte adhesion [50, 51].

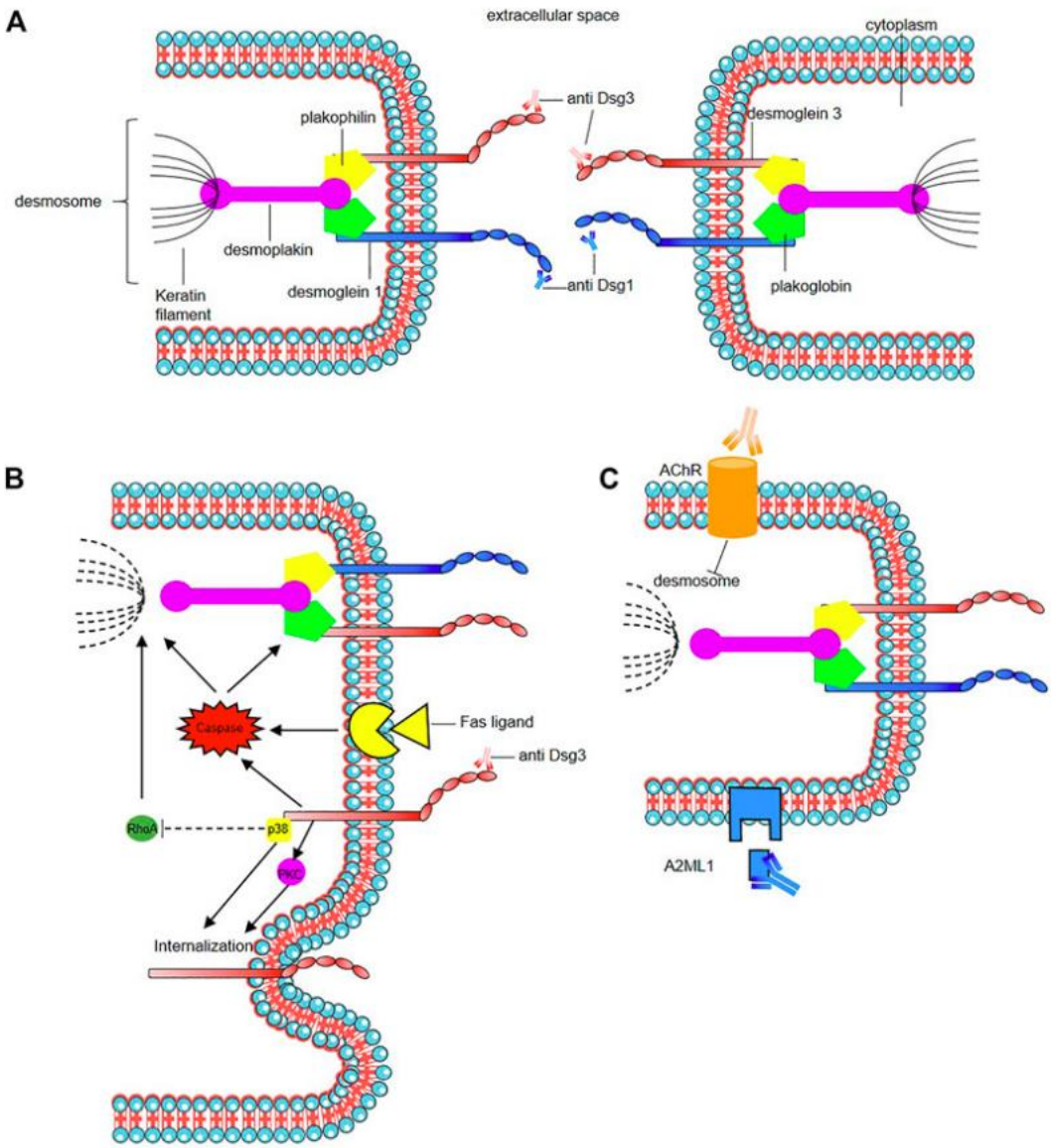


**Figure 2.1 | Mode of action of the pathogenic autoantibodies in pemphigus.** (**A**) Interaction of pathogenic autoantibodies the NH2-terminal of desmosomal protein leading to steric hindrance of trans-Dsg binding. (**B**) Binding of autoantibodies to desmoglein induce an alteration of cellular signaling affecting components of multiple pathways including p38 MAPK (p38), protein kinase C (PKC) including an internalization of Dsg3. The autoantibodies binding reduce the RhoA activity in the p38MPAK-dependent manner which impact the reorganization of the actin cytoskeleton and drive further loss of desmosomal integrity. Caspace signaling may be activated by signal induced by the binding of autoantibodies to desmoglein by the Fas ligand/receptor pathway including pre-apoptotic caspase signaling. (**C**) Anti-keratinocyte α-acetycholine receptor (AChR) IgG autoantibodies induce signal causing disassembly of desmosomes, leading to acantholysis and blistering. In PNP, autoantibody binding also seems to inhibit A2ML1 (α-2 microglobulin-like 1) impacting the activation of a protease inhibitor. From Lim 2022 *Front. Mol. Biosci.* [51].

Pemphigus consists of several different forms, which are pemphigus vulgaris (PV), pemphigus foliaceus (PF), paraneoplastic pemphigus (PNP), pemphigus herpetiformis (PH), and IgA pemphigus. Among the different forms of pemphigus, PV accounts for 70% of all pemphigus cases. The mucosal-dominant type of PV is caused by the primary autoantigen Dsg3, which is responsible for producing blisters and lesions in mucous membrane. The mucocutaneous type of PV, caused by both Dsg3 and Dsg1, results in blisters and lesions in mucous membrane and the skin [50, 51]. Research has shown that the majority of PV patients have a strong genetic connection between PV and HLA alleles DRB1*04:02 and DQB1*05:03, which are found in Jewish and mixed European populations, respectively. The DRB1*04, DRB1*14 and DQB1*05:03 HLA alleles are found predominantly in Han Chinese and Japanese populations. [51, 52].

### 2.2.2 Existing Therapeutic Approaches for Pemphigus Vulgaris

The initial goal in treatment of PV is to control disease progression and maintain remission. Initially, systemic corticosteroids with or without an immunosuppressive adjuvant is used. During the tapering off of corticosteroid dose, 50% of patients undergo relapse and the remainder are in remission after an average of 3 years. However long term use of corticosteroids can result in side effects of osteoporosis, infection, and abnormal glucose tolerance [50].

Patients with moderate to severe PV are initially treated with rituximab, a murine-human chimeric anti-CD20 monoclonal antibody (mAb) that targets $CD20^+$ B cells. Rituximab rapidly depletes autoreactive B cells from peripheral blood. It also depletes $CD20^+$ B cells, such as pre-B cells in the bone marrow, as well as the mature B cells, memory B cells, and short-lived plasma cells in the secondary lymphoid organs. Rituximab also inhibits IgM to IgG class switching, which reduces circulating anti-Dsg3 IgG autoantibodies [51]. Rituximab also shows a decrease in anti-Dsg antibody titers without a decrease in antibody titers to tetanus toxoid or Pneumococcal

polysaccharides. This supports the conclusion that short-lived plasma cells, and not long-lived plasma cells of humoral immunity, are responsible for Dsg3 autoantibodies [52]

Limitations of rituximab therapy include 1) patient susceptibility to infections, specifically of the respiratory tract and skin, and 2) patient resistance (10-20%) to rituximab caused by persistent memory and germinal autoreactive B cells [51]. Despite these limitations 89% of PV patients treated with rituximab are in remission and off-corticosteroids after 2 years [50]. Relapse after rituximab therapy most likely occurs because of incomplete B cell depletion in bone marrow and secondary lymphoid organs. A longitudinal epitope-mapping study supports an incomplete B cell depletion premise as the same anti-Dsg clones are found during active disease and in a subsequent relapse. Strategies, as either a single or adjunct therapy, are needed to completely eliminate Dsg3-reactive B cells allowing PV patients to remain in remission [52].

Novel therapies for PV in clinical trials include 1) targeting the autoreactive B cell or autoantibodies, 2) using regulatory T cells, and 3) inducing antigen-specific tolerance. Therapies that target the autoreactive B cell are 1) humanized anti-CD20 mAb and 2) Dsg3 chimeric autoantibody receptor T cell (Dsg3-CAART). Veltuzumab, a humanized anti-CD20 mAb, is less immunogenic than rituxamib, a murine-human chimeric anti-CD20 mAb. It has higher binding affinities and improved B cell depletion. Veltuzumab was granted orphan drug status in 2015 for PV [50, 51]. In Dsg3-CAART therapy the PV patient's T cells are engineered to express the autoantibody Dsg3 receptor. These engineered T cells can recognize anti-Dsg3 B cells and eliminate them. A major advantage of Dsg3-CAART therapy is the specific targeting of anti-Dsg3 B cells which results in reduced immunosuppression since normal B cells are not eliminated [51, 53]. Cabaletta Bio's clinical candidate "DSG3-CAART" (NTC04422912, Phase 1) for mucosal-dominant PV utilizes the pathogenic epitopes of Dsg3 (i.e., extracellular domains 1-4 of Dsg3). In

2020 they received FDA “Orphan Drug Designation” for the treatment of PV and “Fast Track Designation” for improving healing of mucosal blisters [54].

Therapies that target autoantibodies are 1) mAbs targeting the neonatal Fc receptor and 2) intravenous immunoglobulins (IVIG). The normal function of the neonatal Fc receptor (FcRn) is to bind IgG and prevent the endocytosed IgG from lysosomal degradation within the endothelial cells. In this way IgG is recycled and released back into the blood. High affinity mAbs block the binding of anti-Dsg1 and anti-Dsg3 IgG antibodies (subclass 1 and 4; IgG4 is major pathogenic Ab in PV) to FcRn. This produces an increase in the lysosomal degradation of unbound IgG autoantibodies, resulting in reduced anti-Dsg1 and anti-Dsg3 IgG plasma levels. Anti-FcRn therapeutics include 1) ALXN1830 (NCT03075904, phase 1/2), a humanized affinity-matured IgG4-kappa monoclonal antibody, and 2) Efgartigimod, a human IgG1 antibody Fc-fragment, which is undergoing two phase 3 clinical trials (NCT04598451 and NCT04598477) to assess long-term efficacy and safety [50, 51].

IVIG consists of human plasma containing > 95% IgG antibodies. It works by saturating the IgG receptor FcRn with the infused IgG antibodies leaving the Dsg3 autoantibodies unbound and exposed to lysosomal degradation [55]. IVIG therapy alone is used when rapid decreases in serum levels of IgG1 and IgG4 antibodies against both Dsg1 and Dsg3 is needed. IVIG in conjunction with rituximab or corticosteroids is used to treat severe recalcitrant PV. IVIG with rituximab has been shown to reduce autoantibody titers resulting in long-term remission and a lower risk of infection. The combination therapy of rituximab and IVIG for PV is in a phase 2 clinical trial (NTC04400994) [51, 53].

Adoptive cell therapy using polyclonal regulatory T cells (Tregs) is being used in clinical trials for various autoimmune diseases which include type 1 diabetes, systemic lupus

erythematosus, inflammatory bowel disease (i.e., Crohn disease, ulcerative colitis), pemphigus, and autoimmune hepatitis. Tregs with $CD4^+$ $CD25^+$ $CD127^-$ expression are isolated from peripheral blood, expanded *ex vivo* with potent stimulation through the T cell receptor, followed by infusion of Tregs into the patient [56]. Tregs play an important role in autoimmune disease, using several mechanisms to suppress autoreactive T cells. These mechanisms include 1) the production of anti-inflammatory cytokines (i.e., TGF-β, IL-10, IL-35), 2) killing of target cells by granzyme mediated cytolysis, 3) disruption of metabolic pathways (i.e., binding of IL-2 on CD25 receptors of Tregs depletes IL-2 needed for autoreactive T cell development; expression of CD39

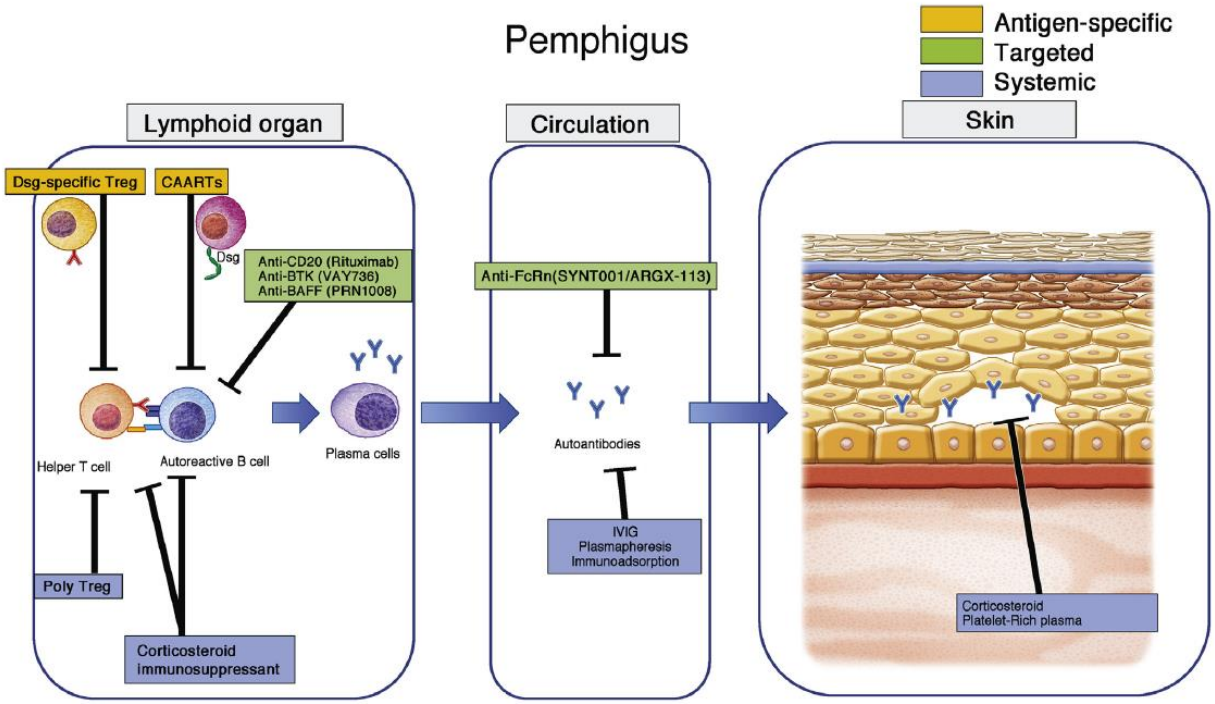


**Figure 2.2 | Current and future therapeutic strategies for pemphigus according to mechanism of action.** The strategies were categorized into 3 groups: systemic (blue box), targeted (green box), and antigen-specific (yellow box). Conventional treatments such as systemic steroids and immunosuppressive agents affect a broad range of cells and tissues, whereas antigen-specific treatments targeted against pathogenic autoimmune cells or IgG are potentially safer. CAARTs (yellow box) and Dsg-specific Treg cells are antigen-specific therapies that show promise for treatment of autoimmune diseases and are unlikely to induce general immunosuppression. BAFF, B-Cell–activating factor; BTK, Bruton tyrosine kinase. From Egami 2020 *J Allergy Clin Immunol* [50].

and CD73 generates adenosine which suppresses T cell function), and 4) inhibition of dendritic cell maturation and function (e.g., via CTLA-4 binding to CD80/CD86) [57, 58]. The use of polyclonal Tregs as an adoptive transfer therapy for PV is supported by mouse studies in which anti-Dsg3 antibody levels increase when Tregs are depleted, and decrease upon adoptive transfer of Tregs. In addition, the blood of PV patients have exhibited lower levels of Tregs as compared to healthy individuals [51]. A polyclonal Treg-cell therapy clinical trial (NCT03239470) for PV is presently in phase 1 to explore safety and effect of Treg therapy on patients with PV [50].

Antigen-specific tolerance induction takes advantage of natural endogenous pathways in the tolerizing environment of the liver and utilizes autoantigen presentation by hepatic APCs (discussed in section 1.3.1). A novel PV therapy using antigen-specific tolerance induction is the small polymer-coated superparamagnetic iron oxide nanoparticle that specifically targets LSECs. Topas Therpeutics PV candidate, TPM203, is presently in phase 1 clinical trial (EUCTR2019-001727-12-DE) [32, 33].

### 2.2.3 Antigen-conjugated Glycopolymers of GalNAc as a Potential Therapeutic for B Cell-mediated Autoimmune Disease

PV is a B cell-mediated disease to which we would like to apply an antigen-specific tolerance induction strategy. This strategy relies on the presentation of autoantigens by APCs to induce tolerance by the deletion or anergy of autoreactive T cells or by induction of Tregs. To make a case for antigen-conjugated glycopolymers (i.e., antigen-p(GalNAc) discussed in section 1.3.1) as a therapy for PV we need to understand not only the relationship between autoantibodies, autoreactive B cells, and T cells, but also their role in PV disease. Through the analysis of peripheral blood from PV patients, research has found the presence of Tregs, IgG autoantibodies

against Dsg1 and Dsg3, and various helper T cells, such as Th1, Th2, Th17, and T follicular helper cells.

Evidence for IgG autoantibodies and CD4 T cell subsets in PV patients

Tregs are generated during T cell development in thymus or peripheral lymphoid organs when naïve CD4 T cells differentiate into Tregs after receiving a T cell receptor signal of intermediate strength in the presence of TGF-β. Tregs play an important role in tolerance induction by secreting anti-inflammatory cytokines (i.e., IL-10, IL-35, TFG-β) to suppress autoreactive CD4 T cell activation and convert CD4 T cells into Tregs [59]. Studies have shown that Treg populations are 10 times smaller in patients with active PV disease compared to healthy individuals [60]. Veldman et al. has also identified a Dsg3-specific type 1 regulatory T (Tr1) cell that primarily secretes IL-10 and smaller amounts of TGF-β in 80% of healthy carriers with PV-associated HLA alleles (see section 2.2.1). Contrastingly Dsg3-specific Tr1 cells were found in only 17% of patients with active PV disease. The authors suggest that Dsg3-specific Tr1 cells are involved in tolerance against Dsg3 autoantibodies [61].

It is known that IgG autoantibodies against Dsg1 and Dsg3 cause the loss of cellular adhesion between keratinocytes (i.e., epidermal cells of skin) by binding to the desmosomal structural proteins. Similarly, AChR IgG autoantibodies bind to the AChR of keratinocytes inducing the disassembly of demosomes that results in loss of cellular adhesion [51]. Each PV disease variant has a different profile of autoantibodies against Dsg1 and Dsg3. In the mucosal-dominant type of PV, detection by ELISA found autoantibodies against only Dsg3, whereas autoantibodies against both Dsg1 and Dsg3 were detected in the mucocutaneous type of PV [53]. Additionally, AChR IgG antibodies were found in 85% of PV patients [51]. Interestingly ELISA positivity for Dsg1 and Dsg3 were found in 46% of PV patients in remission from prednisolone (>

3 months), although at consistently lower levels than in patients with active disease [62].

Several subtypes of CD4 helper T cells were found in PV patients. The subtypes and their primary functions are as follows: 1) Th1 cells secrete IFNγ to activate infected macrophages to destroy ingested pathogens; 2) Th2 cells secrete IL-4 to promote B cell class-switching to IgE antibody responsible for allergies, and IL-5 to promote eosinophil recruitment that contributes to allergic reactions; 3) Th17 cells produce cytokines IL-17 for neutrophil recruitment; 4) T follicular helper (Tfh) cells are found in the B cell follicle where they help B cells with antibody production and class switching [12].

Autoreactive helper T cells has been extensively studied in PV patients. Research has shown that PV patients have both Dsg3-reactive Th1 and Th2 cells. In comparison with healthy individuals, Dsg3-reactive Th2 cells were significantly higher in serum of PV patients, concurrently with elevated levels of Th2 cytokines IL-4 and IL-10 [51, 53]. In addition, Dsg3-reactive Th2 cells can only be found in PV patients, whereas Dsg3-reactive Th1 cells were found in healthy individuals that carry the PV HLA class II alleles. This finding agrees with the observation that PV patients have high levels of IL-4 which can sustain autoreactive B cell production of autoantibodies [53]. In yet another study comparing patients in remission versus active disease, patients in remission showed slightly higher numbers of Th2 and Th1 cells, whereas Th17 cells predominated in patients with active disease [63].

The role of T follicular helper cells was examined in a recent study of 63 PV and 11 PF patients. Holstein et al. [63] identified the dominant disease-inducing CD4 T cell subset as IL-17A-producing Tfh17 cells. In a comparison of whole RNA-seq data of skin biopsy specimens from healthy individuals and pemphigus patients, they showed the dominance of IL-17 signaling pathway. Analysis of peripheral blood of pemphigus patients with active disease showed

significantly ($P < 0.01$) higher percentages of circulating Tfh17, whereas Tfh1 and Tfh2 levels were the same for patients with active disease or for those in remission. Further evidence for the significance of Tfh17 cells in pemphigus was shown by the coculture of isolated Th (e.g., Th1, Th2, Th17) and Tfh (e.g., Tfh1, Tfh2, Tfh17) cells of pemphigus patients with CD27+ memory B cells. Compared to patients in remission, Tfh cells of patients with active disease were more effective in stimulating autoreactive B cell production than their corresponding Th (e.g., Th1, Th2, Th17) cells. Amongst all the Tfh cell subsets, Tfh17 cells from patients with active disease induced the greatest Dsg3/Dsg1-specific autoantibody production, whereas patients in remission barely produced autoantibodies. In addition, high levels of Dsg3-autoreactive Tfh17 cells were found in pemphigus patients with acute disease, and are significantly decreased for patients in remission. Based on their data, an important role for the T follicular helper cell in PV is indicated. Holstein et al. [63] "speculate that Th17 cells and Tfh17/Tfh17.1 cells play different roles in pemphigus pathogenesis. Whereas Th17 cells are presumably involved in the peripheral effector phase, Tfh17/Tfh17.1 cells sustain B-cell autoantibody production in GCs" (Germinal Centers).

Mechanism of B cell-mediated autoimmune disease

The relationship between autoantibodies, autoreactive B cells, and T cells can be visualized by examining the path of B cell development. The elimination of autoreactive B cells and prevention of autoimmune diseases relies on multiple self-tolerance checkpoints starting with the immature B cell in the bone marrow to the development of naïve B cells in the periphery into long-lived plasma cells and memory B cells, as described in Bonasia et al. [64]. Helper T cells and T follicular helper cells are important players in both B cell development and prevention of autoreactive B cell evasion of self-tolerance checkpoints.

B cell development begins in the bone marrow where the first checkpoint for autoreactive

B cell elimination exists. Depending on the strength of interaction between self-antigen and the B cell receptor (BCR) of an immature B cell, a decision for survival or elimination is made. A strong interaction indicates an autoreactive B cell and induces anergy (i.e., downregulation of BCR expression), clonal deletion (i.e., apoptosis), or receptor editing of the light chain of a BCR to change its antigen specificity. Of the remaining immature B cells approximately 40% remain autoreactive following this first checkpoint in the bone marrow [64].

The surviving immature B cells travel to the spleen as transitional B cells where the second checkpoint for autoreactive B cell elimination occurs, and the autoreactive B cell population is further reduced to 20%. Once again, a strong interaction between antigen and BCR results in anergy or clonal deletion. A moderate interaction promotes further development of transitional B cells into naïve B cells, which go on to circulate in the blood and lymphatic system. Accumulation within the follicular sites of the spleen and lymph nodes exposes naïve B cells to the third checkpoint where autoreactive B cell elimination occurs. In this location naïve B cells encounter antigens that are presented as peptides on MHC II. Recognition by CD4 helper T (Th) cells results in binding of Th cells to MHC II. The naïve B cells are then activated. In the absence of binding to Th cells, autoreactive naïve B cells are eliminated through anergy or clonal deletion [64].

Upon activation naïve B cells in the extrafollicular sites of the spleen and lymph nodes either differentiate into short-lived plasma cells or enter the germinal center, where they undergo somatic hypermutation and isotype switching. The fourth checkpoint for autoreactive B cell elimination occurs in the germinal center. Activated naïve B cells that have the highest affinity for the same antigen as follicular dendritic cells and CD4 T follicular helper (Tfh) cells survive to form memory B cells and long-lived plasma cells. Autoreactive naïve B cells are eliminated by the absence of Tfh cell interaction. This absence is due to the removal of autoantigen-specific Tfh cells

by central and peripheral tolerance mechanisms during T cell development [64].

Future for a Dsg3-specific Treg therapy for PV

The discovery of decreased levels of Tregs in PV patients supports a therapeutic for Dsg3-specific Tregs. Furthermore, the involvement of Tfh17 cells as a dominant disease-causing T follicular helper cell in PV disease indicates a need for Tregs that can control the activation and proliferation of not only Th17, but other Th and Tfh cells that are responsible for the production of Dsg3-reactive antibodies.

Presently polyclonal Tregs are being used in multiple clinical trials for different autoimmune diseases including PV. Polyclonal Treg therapy, however, is not an antigen-specific therapeutic and has the risk of non-specific immunosuppression. It is also costly (> $450,000) with an involved labor-intensive manufacturing process and requires a large number of infused cells to be effective [56, 65].

There are multiple advantages to an antigen-specific therapy that can generate Tregs in situ. For example, using a Dsg3-specific glycopolymer conjugate of GalNAc takes advantage of the endogenous tolerogenic pathways in the liver that can generate Dsg3-specific Tregs in situ. The work of Wilson et al. [36] has demonstrated in mouse models that Treg formation can be induced *in vivo* by OVA-p(GalNAc) (i.e., in OVA challenge model) and p31–p(GluNAc) (i.e., in BDC2.5 diabetes induction model). A Dsg3-specific glycopolymer conjugate as a therapeutic approach for PV would avoid costly Treg isolation and expansion manufacturing, minimize the risk of non-specific immunosuppression, and avoid handling of live cells.

### 2.2.4 Mouse Models for Pemphigus Vulgaris

Mouse models are effective tools for studying diseases. The creation of a Dsg3 knockout mouse was accomplished by Koch et al. [66] by deleting from the Dsg3 gene the first coding

sequence starting at the first exon. mRNA from this modified gene would encode a polypeptide missing the first extracellular domain of Dsg3, thereby functionally inactivating the Dsg3 gene. Analysis of Dsg3 mRNA expression showed that $Dsg3^{-/-}$ mice were missing Dsg3 mRNA, but detected in $Dsg3^{+/+}$ and $Dsg3^{+/-}$ animals. $Dsg3^{+/-}$ mice were healthy, whereas homozygous $Dsg3^{-/-}$ mice showed reduced bodyweight within 8-10 days after birth, oral mucosal lesions, a cycle of hair loss and regrowth eventually resulting in bald spots at 3-4 weeks, snout lesion and conjunctivitis.

Aoki-Ota et al. [67] investigated two mouse model protocols (e.g., naïve vs immunized) using the $Dsg3^{-/-}$ mice to study PV, and compared their effectiveness in producing disease. $Dsg3^{-/-}$ mice had the mixed genetic background of 129/SV ($H\text{-}2^b$) and C57BL/6J ($H\text{-}2^b$). Splenocytes from either naïve or immunized $Dsg3^{-/-}$ mice were adoptively transferred into C57BL/6J $Rag2^{-/-}$ mice through the tail vein. Naïve $Dsg3^{-/-}$ mice were used without immunization and the number of transferred splenocytes needed to produce disease was 5x that of splenocytes from immunized mice (i.e., $5 \times 10^7$ for naïve, $1 \times 10^7$ for immunized). Splenocytes from immunized $Dsg3^{-/-}$ mice were obtained from 6- to 8-week-old $Dsg3^{-/-}$ mice that were subcutaneously primed once with mouse recombinant Dsg3 (rDsg3, 10 μg) in complete Freund's adjuvant, twice (day 7, 14) with mouse rDsg3 in incomplete Freund's adjuvant, then boosted with mouse rDsg3 only (day 21, 28; intraperitoneal) [67, 68]. For the naïve and immunized groups, transferred splenocytes containing both CD4+ T cells and B220+ B cells were required for anti-Dsg3 IgG production.

Significant anti-Dsg3 IgG levels were detected on day 14 after transfer for mice that received immunized $Dsg3^{-/-}$ splenocytes compared to mice receiving naïve $Dsg3^{-/-}$ splenocytes (still negligible). By day 28 IgG levels of both mice groups had reached a peak with the immunized group having an anti-Dsg3 IgG titer that was 6x higher ($P < 0.001$). Significant weight loss was

first observed at day 14 for the group receiving immunized Dsg3$^{-/-}$ splenocytes, whereas the recipients of naïve Dsg3$^{-/-}$ splenocytes began at day 21. Both groups reached a plateau at day 28. Active disease phenotype (e.g., patchy hair loss, lesions on snout and eyes) was seen on day 14 for the immunized group and on day 28 for the naïve group [67].

A large study conducted by Holm et al. [69] at Nova Nordisk provided details about the naïve Dsg3$^{-/-}$ mouse model protocol described by Aoki-Ota et al. The paper by Holm et al. compared intravenous (i.v.) vs intraperitoneal (i.p.) transfer of Dsg3$^{-/-}$ splenocytes (5 x $10^7$) from naïve Dsg3$^{-/-}$ mice into 8- to 10-week-old Rag2$^{-/-}$ mice. Their data revealed the induction of disease in Rag2$^{-/-}$ mice was as follows: 1) 55% (16/29) of mice in the i.v. group had hair loss or lesions compared to 32% (7/22) in the i.p. group; 2) 17% (5/29) of mice in the i.v. group had weight loss or acantholysis compared to 9% (2/22) in the i.p. group; 3) 79% (23/29) of mice in the i.v. group had circulating anti-Dsg3 IgG (as determined by ELISA) compared to 72% (16/22) in the i.p. group; 4) 59% (17/29) of mice in the i.v. group showed *in vivo* IgG deposition on keratinocyte cell surfaces of esophagus and oral mucosa on day 56 compared to 50% (11/22) in the i.p. group. They also note that their maximum PV score was 4 for Dsg3$^{-/-}$ mice, and 5 for Rag2$^{-/-}$ mice in contrast to PV score of 4-10 (day 28) by Aoki-Ota et al. The authors conclude that despite the low incidence of phenotype development (e.g., 14% had weight loss, 45% developed hair loss) and heterogeneity (e.g., 76% had circulating Dsg3 IgG levels with a variable PV score ranging from 1-5) in disease development, the naïve Dsg3$^{-/-}$ mouse model is a useful mouse model for PV disease.

Kim et al. [70] used a PV mouse model to show that Dsg3-specific ICOS+ Tfh cells are important for the production of anti-Dsg3 antibodies in PV disease. They grafted 1 $cm^2$ tail skins from Dsg3-expressing WT C57BL/6 mice onto the backs of Dsg3$^{-/-}$ mice. After 3 weeks PV

phenotypes were present. The spleens and grafted skin-draining auxiliary and inguinal lymph nodes were harvested. CD19+ B cells and CD4+ T cells were isolated and purified (>90%). A mixture of the purified B and T cells (1 x $10^6$ cells of each) were adoptively transferred into Rag1$^{-/-}$ mice. Consistent with PV phenotype observed by Aoki-Ota et al., the PV mouse model protocol developed by Kim et al. (i.e., adoptively transferring purified B and T cells from Dsg3$^{-/-}$ mice immunized with a skin graft from a Dsg3-expressing mouse) resulted in weight loss, mucosal lesions on the eyelids and mouth, acantholysis, *in vivo* IgG deposition in epidermis, and circulating anti-Dsg3 IgG.

The method of using Dsg3$^{-/-}$ mice immunized with a skin graft from a Dsg3-expressing mouse is based on a PNP model of pemphigus reported by Hata et al. [71]. After adoptive transfer into Rag2$^{-/-}$ mice of splenocytes from Dsg3$^{-/-}$ mice that had received two skin grafts, this method created mice with high numbers of CD4+ and CD8+ T cells and showed robust development of PV disease phenotype of acantholysis and interface dermatitis in skin and oral mucosa. In contrast to the mice of Aoki-Ota's PV model (i.e., adoptive transfer of splenocytes from naïve or recombinant Dsg3-immunized Dsg3$^{-/-}$ mice), the mice of PNP model additionally developed anti-envoplakin IgG, a characteristic autoantibody in PNP, and had significantly higher mortality rates than did mice of Aoki-Ota's PV model (i.e., on day 49, 46% for PNP mice compared to 81% for PV mice survived).

## 2.3 Results

### 2.3.1 Pemphigus vulgaris mouse model validation

We first sought to reproduce the naïve transfer model in our facility due to the variability reported in the model, and to further characterize the cellular phenotype of the disease. The experimental timeframe of the pilot study is shown below in Figure 2.3a. The original design was to transfer 50 million splenocytes from Dsg3$^{-/-}$ mice or a healthy control, Dsg3$^{+/-}$ mice, into Rag2$^{-/-}$ mice, but due to limitations in breeding we did not have enough splenocytes (Figure 2.3b). Our collaborators at Anokion were also attempting to establish this model in their labs and had not seen disease induction after transferring 20 million splenocytes per mouse. For this reason, rather than pooling cells and transferring a lower number of cells per mouse, we decided to transfer the total splenocytes from each Dsg3$^{-/-}$ or Dsg3$^{+/-}$ mouse into each Rag2$^{-/-}$ mouse. This resulted in a range of 21-43 million splenocytes transferred.

Clinical scores and weights were measured daily, and we saw hair loss in all five mice that received Dsg3$^{-/-}$ splenocytes and no hair loss in the five mice that received Dsg3$^{+/-}$ splenocytes (Figure 2.3c). Interestingly, the two mice that received more than 40 million Dsg3$^{-/-}$ splenocytes were also the mice that developed the highest clinical scores. Mice were bled weekly, and we measured anti-Dsg3 IgG antibody abundance by titer (data not shown) and the area under the curve (AUC) of the OD across the dilutions (Figure 2.3d). Differences were more pronounced using the AUC quantification method, and as expected, mice receiving Dsg3$^{-/-}$ splenocytes developed anti-Dsg3 antibodies.

We also took this opportunity to search for differences between lymph nodes in the T cell and B cell compartments. At this time we had a technical limitation in not being able to look at antigen-specific cells with flow cytometry and we did not see any significant differences looking

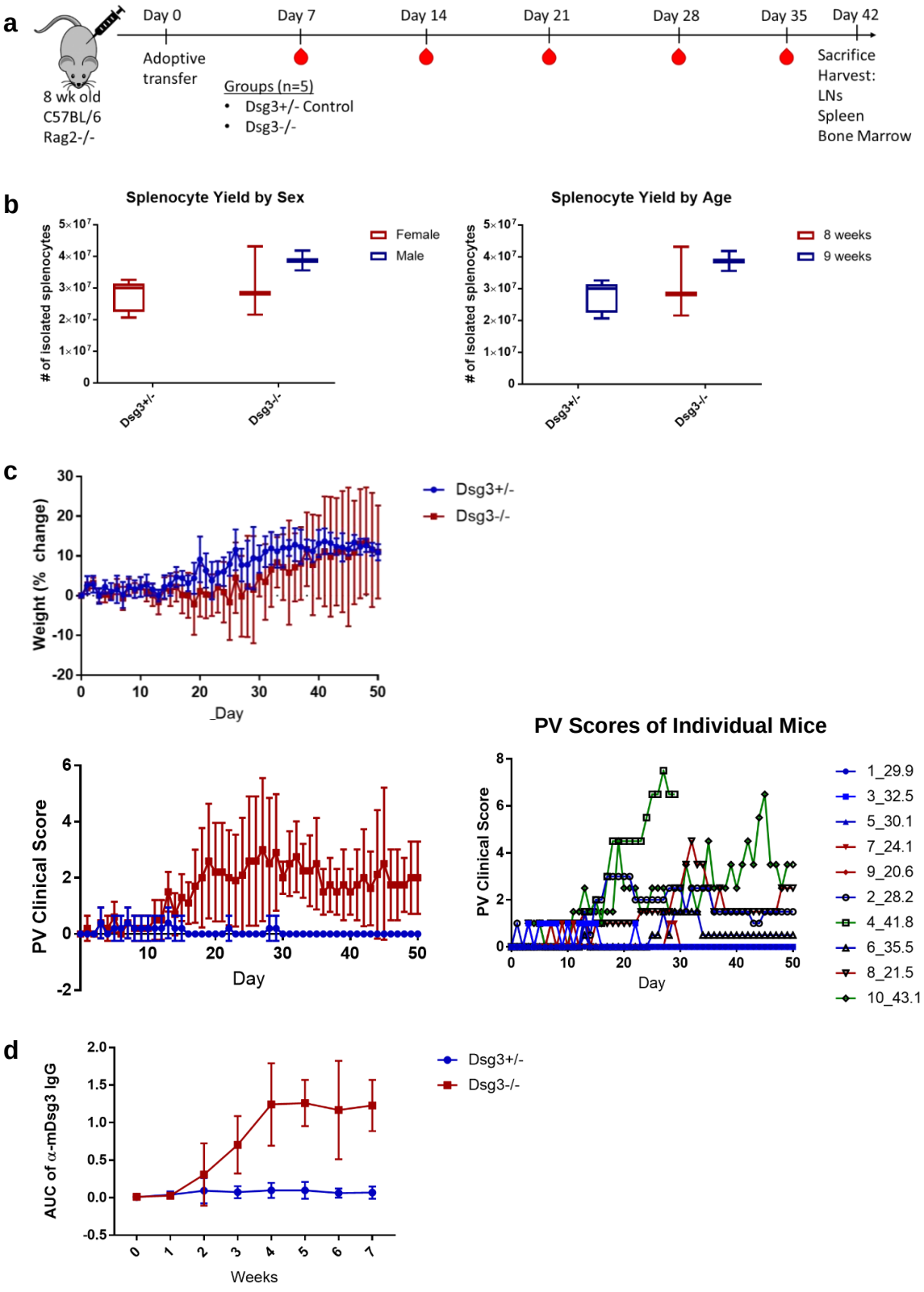


**Figure 2.3 | Adoptive transfer of naïve Dsg3$^{-/-}$ or Dsg3$^{+/-}$ splenocytes into Rag2$^{-/-}$ mice.**

**Figure 2.3, continued.** (A) Experimental design. (B) Splenocyte distribution by sex and age of $Rag2^{-/-}$ mice. (C) PV clinical score and weight change shown as a percent difference from the weight on Day 0. Individual PV clinical scores with legend indicating mouse number and number of cells transferred. Solid symbols show mice that received $Dsg3^{+/-}$ splenocytes and unfilled symbols show mice that received $Dsg3^{-/-}$ splenocytes. (D) anti-Dsg3 IgG is greater in $Rag2^{-/-}$ mice that received $Dsg3^{-/-}$ splenocytes.

at nonspecific responses (Supplemental Figure 2.1). We had a hypothesis that certain lymph nodes would contain more germinal centers in the disease group, and that these lymph nodes might correspond to which areas of the mice had hair loss or lesions. To test this, we harvested five types of lymph node and processed them separately. Figure 2.4a shows a correlation plot between disease score, ICOS+ Tfh cells and class switched memory B cells in the lymph nodes and spleen, and the anti-Dsg3 IgG AUC for week 0-4. The $Dsg3^{+/-}$ (het) transfer group on the left shows positive correlations between the spleen and lymph nodes for Tfh and class switched B cells. This is lost in the ICOS+ T cells in the homozygous transfer disease group, but there is a strong positive correlation between disease score and the percent of class switched B cells in the inguinal LN, with a less significant correlation in the iliac LN. To investigate antigen-specific B cell responses, we coated ELISPOT plates with Dsg3 and used a CTL kit to measure IgG secreting cells (Figure 2.4b). We did not see consistent differences between groups but did see at least one mouse in the $Dsg3^{-/-}$ transfer group with an increased concentration of IgG secreting cells in either the spleen or the bone marrow. The fact that the same mouse did not have high concentrations of IgG secreting cells in both the spleen and bone marrow led us to hypothesize that there could be a shift of IgG producing cells from the spleen to the bone marrow as the disease progresses. The mouse with the highest concentration of IgG producing cells in the bone marrow had the highest disease score at the experiment endpoint. Overall, we were encouraged to use the naïve transfer model as we were successful in recapitulating disease and antibody production.

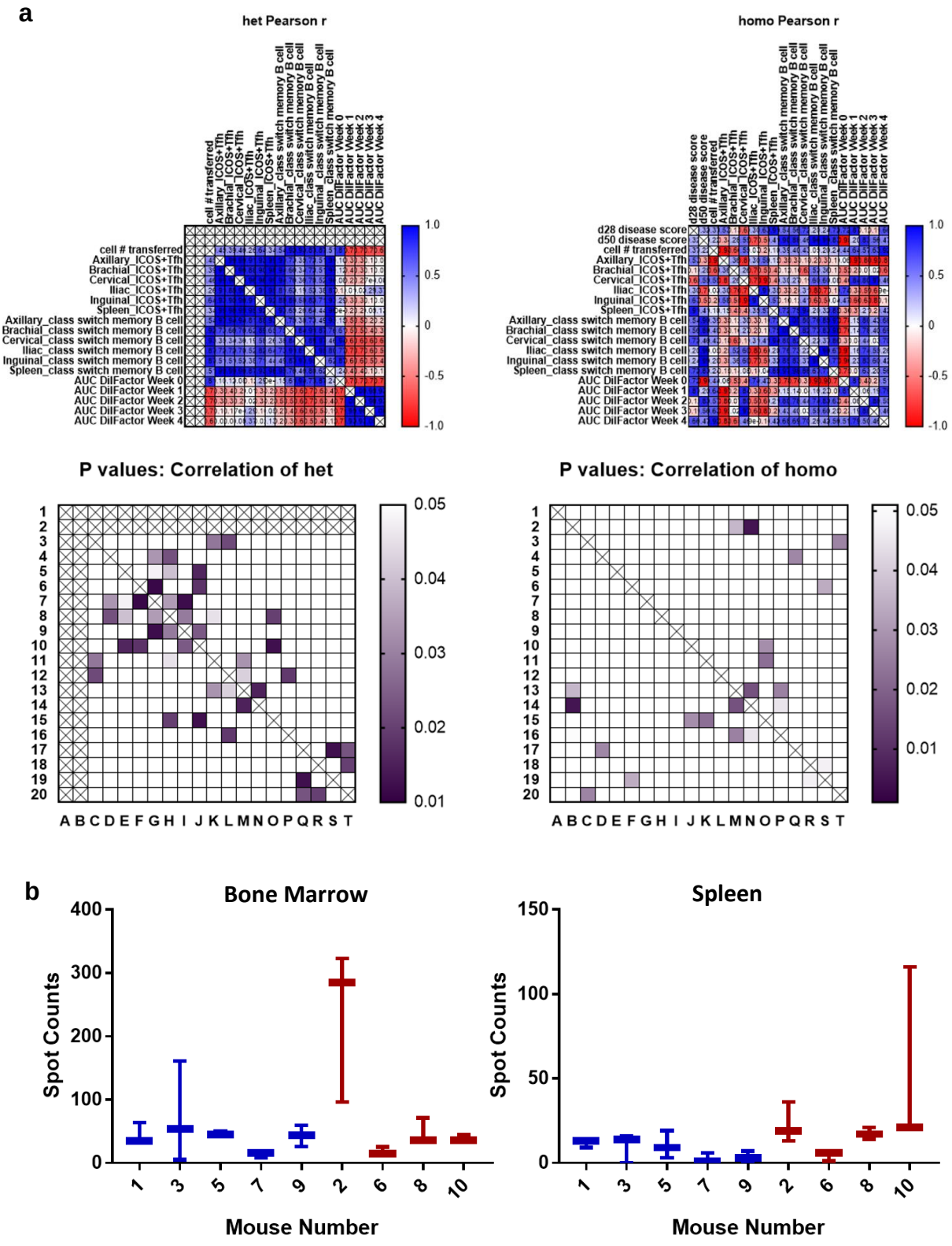


**Figure 2.4 | T and B cell responses in naïve transfer model.**

**Figure 2.4, continued.** (A) Pearson's correlations shown as heatmaps between disease score, ICOS+ Tfh cells and class switched memory B cells in the lymph nodes and spleen, and the anti-Dsg3 IgG AUC for week 0-4. Blue shows positive correlation and red shows negative correlation. P-values of correlations shown in purple. (B) ELISPOT measuring anti-Dsg3 IgG secreting cells in spleen and bone marrow with mice that received $Dsg3^{-/-}$ splenocytes in red and mice that received $Dsg3^{+/-}$ splenocytes in blue. All statistical comparisons were performed by one-way ANOVA using Tukey correction.

### 2.3.2 B cell depletion in pemphigus vulgaris immunized model

In assessing the potential PV disease models available, we were concerned about the variability of the naïve transfer model and wanted to also develop an immunized transfer model that would be more robust while adding B cell depletion to create an opportunity for treatment. Our hypothesis was that without first weakening the ongoing B cell response, reprogramming the T cell response with pGal therapy would not be likely to stop the ongoing B cell response and there would be no meaningful reduction in disease scores. Therefore, we tested multiple B cell depletion strategies to identify a strategy that slowed or weakened disease progression without completely abrogating the disease.

Shortening the immunization protocols previously published, $Dsg3^{-/-}$ mice were immunized subcutaneously with Dsg3 emulsified in CFA followed with two boosters in IFA given one week apart. Two weeks after the last booster, splenocytes are collected and transferred via tail vein injection to $Rag2^{-/-}$ mice (Figure 2.5a). $Rag2^{-/-}$ mice do not produce mature B or T cells, so when the splenocytes are transferred, they are able to fill the niches and survive. The Dsg3 experienced cells are now able to cause an autoimmune attack against Dsg3 in the skin which results in hair loss and lesions.

We tested three different B cell depletion strategies. The first was using anti-CD20 to deplete B cells one day post-transfer. The proposed mechanisms of action of anti-CD20 include directly inducing apoptosis by binding the CD20 receptor, complement activation by the Fc portion

of the antibody and subsequent cell lysis, or antibody-dependent cellular cytotoxicity (ADCC) in which effector cells are activated by binding to the Fc portion of the anti-CD20 antibodies coating B cells and short-lived plasma cells. We hypothesized that this would be highly effective as a higher percentage of B cells would still be circulating and not have navigated to niches in the bone marrow or skin associated lymphoid tissue, and there would not be time for mature B cells to become long-lived plasma cells which do not express CD20. The second strategy was to administer anti-CD20 four days post-transfer. We hypothesized that this would be less effective as B cells would have time to become long-lived plasma cells. The final strategy was to give anti-CD20 four days post-transfer followed by bortezomib. Bortezomib is a potent chemotherapy that inhibits proteasomes and has been demonstrated to eliminate malignant plasma cells in multiple myeloma patients. The proteasome inhibition causes an accumulation of proteins within the endoplasmic reticulum and activates apoptotic signals. Short- and long-lived plasma cells have a high rate of protein expression due to their IgG production, and so they are particularly sensitive to proteasome inhibition. We included this group with the hypothesis that in the case that the long-lived plasma cells were sufficient for disease progression, then depleting these cells would be necessary to lower disease scores and not accomplished by anti-CD20.

First mice were sacrificed 9 days post splenocyte transfer to confirm B cell depletion and investigate any effects on the T cell compartment. Figure 2.5b shows total cell counts in the spleen, lymph node, and bone marrow. B cells were depleted in the spleen and lymph node as shown by flow cytometry (Figure 2.5c), and in the bone marrow as shown by ELISPOTs detecting nonspecific IgG secreting cells (Figure 2.5d). Bortezomib also decreased the number of T cell in the lymph nodes, which was a concern for use with a pGal therapy that would act through an effect on the T cell compartment. It is important to remember that in the $Rag2^{-/-}$ mice, transferred cells

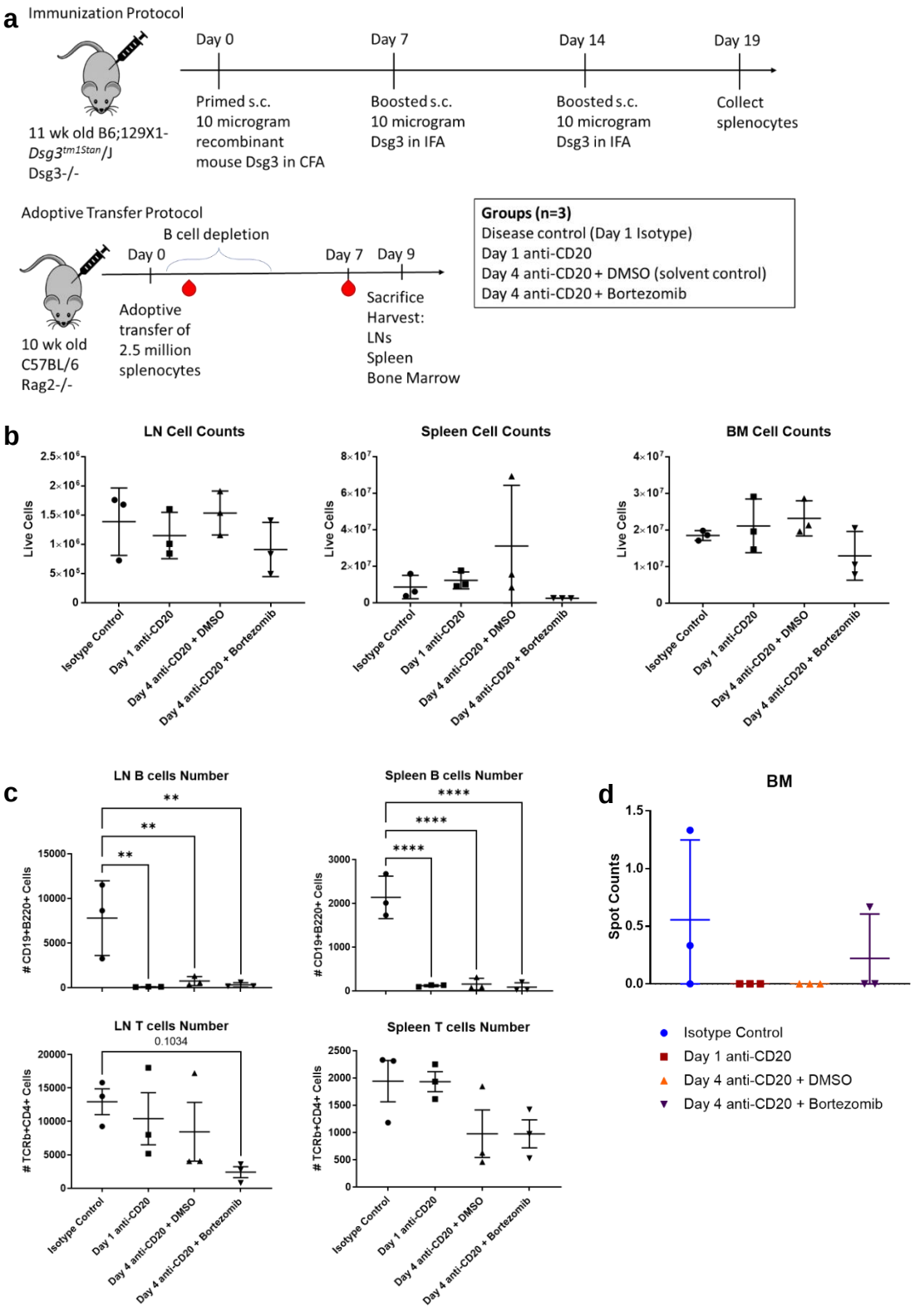


**Figure 2.5 | B cell depletion study to confirm B cell depletion in PV immunized model.**

**Figure 2.5, continued.** (A) Experimental design. (B) Total cell counts of B and T cells in lymph node, spleen, and bone marrow. No significant effects on total cell counts. (C) Flow cytometry data showing depletion of B cells, but not T cells after various B cell depletion regimens. (D) ELISPOT analysis of bone marrow showing nonspecific IgG secreting cells. All statistical comparisons were performed by one-way ANOVA using Tukey correction.

are the only source of mature B and T cells, so enough cells must remain to multiply and either cause disease progression or be affected by the therapies being tested.

Once B cell depletion had been confirmed, the experiment was repeated, and mice were sacrificed 47 days post splenocyte transfer (Figure 2.6a). Mice were bled weekly, and scored and weighed daily. Figure 2.6b shows disease progression. Supplemental Figure 2.2 shows weight changes. Anti-CD20 administered one day post adoptive transfer completely abrogated disease, whereas anti-CD20 given on day 4 with and without bortezomib only delayed disease progression and decreased disease severity. The results are similar in anti-Dsg3 IgG present in the serum shown in Figure 2.6c. The disease control group that was given an isotype control for the anti-CD20 antibody shows the highest levels of anti-Dsg3 IgG, followed by anti-CD20 given on day 4, anti-CD20 given on day 4 with bortezomib, and then anti-CD20 given on day 1 and the wildtype (WT) control which is a healthy control that received WT splenocytes instead of $Dsg3^{-/-}$ splenocytes. Splenocyte and lymphocyte non-antigen-specific responses were analyzed by flow cytometry and ELISPOT (Supplemental Figure 2.3 and Supplemental Figure 2.4), and show B cell, plasma cell, and plasmablast populations recovered from the lymph nodes, spleen, and bone marrow. Given these results, we decided to move forward with anti-CD20 given on day 4 as the B cell depletion strategy that dampened but did not eliminate disease progression and that did not deplete T cells.

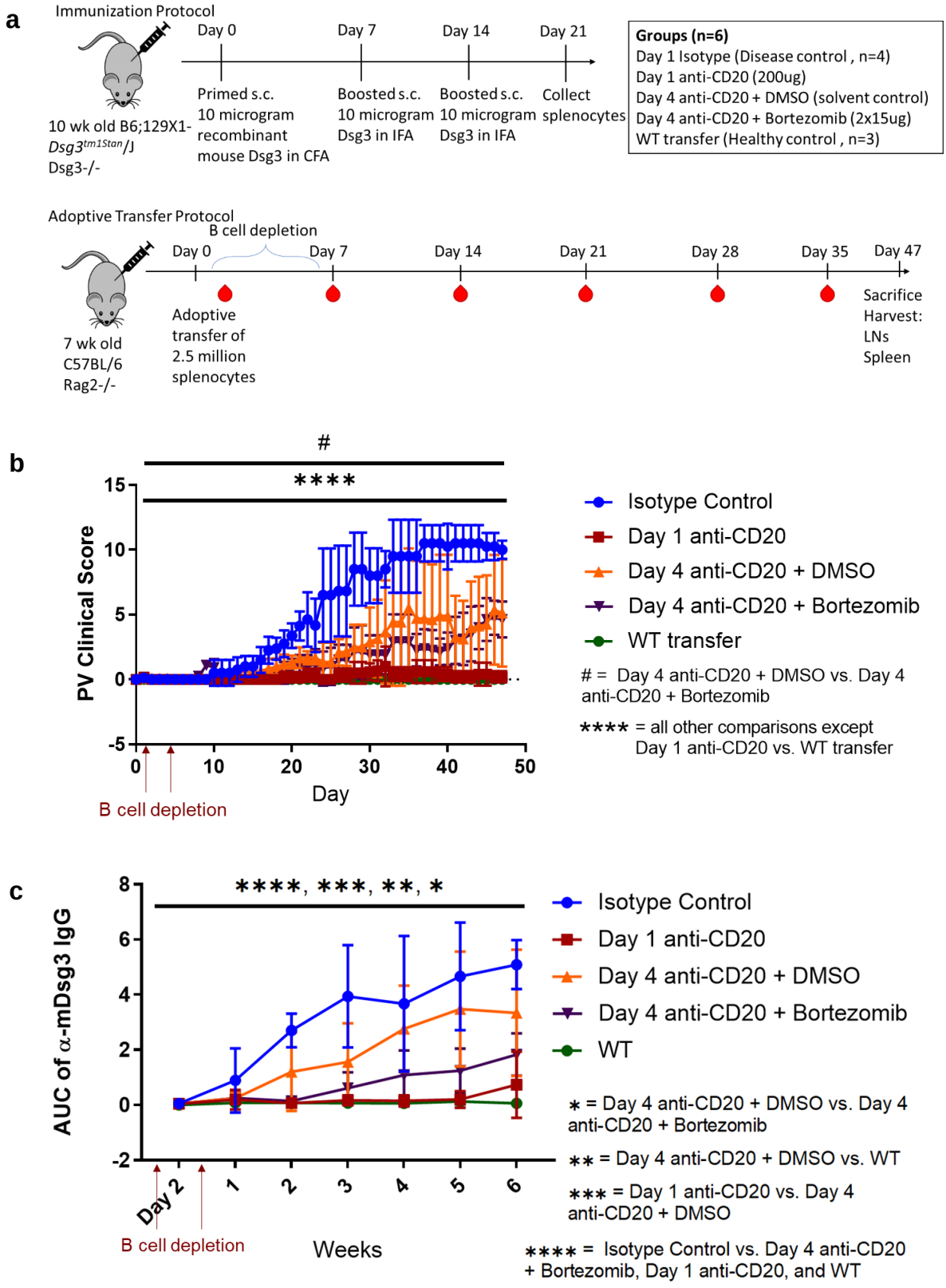


**Figure 2.6 | B cell depletion study in pemphigus vulgaris immunized model.**

**Figure 2.6, continued.** (A) Experimental design. (B) PV clinical score showing disease progression in isotype control and anti-CD20 treated mice showing lower scores. (C) anti-Dsg3 IgG levels elevated in isotype control and decreased levels in anti-CD20 treated mice. Horizontal bars atop the graph indicate significant differences via AUC.

### 2.3.3 pGal-Dsg3 therapy in pemphigus vulgaris naïve model

The naïve transfer model was an ideal candidate to attempt to induce tolerance to Dsg3 because at the time of transfer the splenocytes have no prior immunity. The first pGal-Dsg3 dose is 12 hours after transfer, so pGal-Dsg3 may be the first context in which splenocytes experience Dsg3, but there is the added complication that Dsg3 is also present in the skin and splenocytes may be educated by antigen presenting cells that collected Dsg3 in the skin and traveled to a lymph node. The skin is an environment that is typically more immunogenic than the liver which is targeted by pGal.

pGal-protein antigen conjugations delivered intravenously have previously been shown to partially prevent anti-drug antibodies when given prophylactically, although the effect was not statistically significant [72]. Here we build upon the complication of simultaneous and competing antigen presentation by having that competing antigen presentation originate in an immunogenic organ. We sought to use a B cell-mediated disease model to test if lower antibody production would lead to a functional difference measured by disease scores. Similar to our first naïve transfer experiment, 45 million naïve splenocytes were transferred from $Dsg3^{-/-}$ mice and mice were bled weekly, and weight and scores were recorded daily (Figure 2.7a). pGal-Dsg3 or a saline control was injected via the tail vein twice, at 2 hours and at 4 days post adoptive transfer. Even though 3 of the 7 saline treated mice did not develop clinical scores, we were encouraged to see a significant difference between the clinical score areas under the curves of the two groups over the course of the experiment (Figure 2.7b). A single pGal-Dsg3 treated mouse developed a lesion on one leg

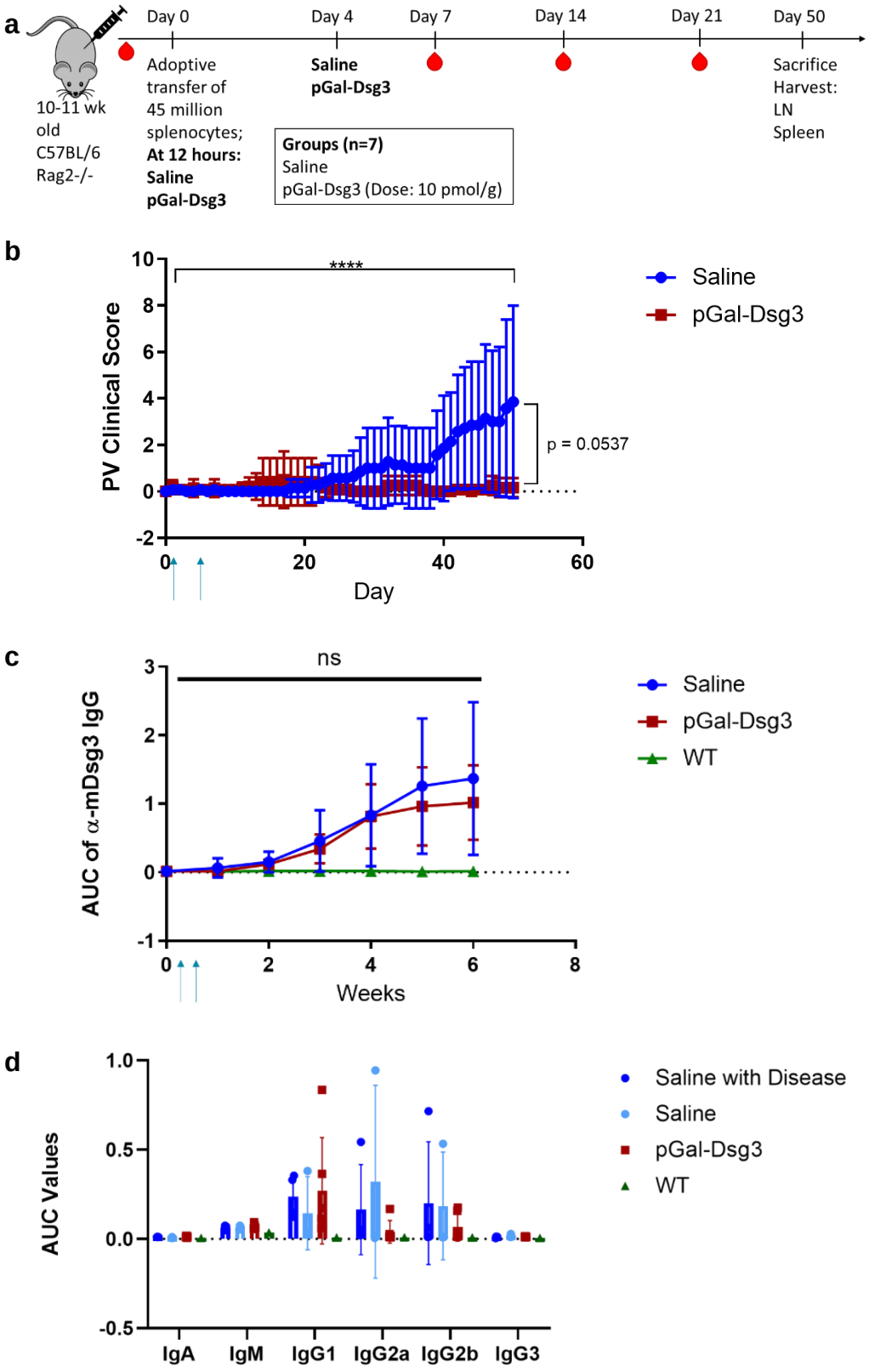


**Figure 2.7 | pGal-Dsg3 suppression of clinical scores in pemphigus vulgaris naïve transfer model.**

**Figure 2.7, continued.** (A) Experimental design. (B) Disease progression as measured by clinical scoring of hair loss and lesions. Blue arrows indicate treatments. (C) anti-Dsg3 IgG levels are not significantly different between treatment groups. A wildtype control shows the background level of the AUC of OD measurements. (D) anti-Dsg3 IgA, IgM, IgG1, IgG2a, IgG2b, and IgG3 levels are not significantly different between treatment groups. Horizontal bars atop the graph indicate significant differences via AUC. All statistical comparisons were performed by one-way ANOVA using Tukey correction.

which then healed as seen by the slight increase in clinical score around day 15. Concerningly, we did not see a difference between groups in anti-Dsg3 IgG antibody abundance (Figure 2.7c). Even after analyzing mice with a disease score as a separate saline with disease group, we still saw no differences in IgG, as well as IgG subclasses, IgA, or IgM at week 6 (Figure 2.7d). We also saw no differences in IgG or IgG1 avidity (data not shown).

Lymph nodes and spleens were harvested and processed for 3 day ex-vivo antigen restimulations. Supernatants were collected and various cytokine concentrations were measured by Legendplex (Supplemental Figure 2.5). Unfortunately, we did not see any cytokine production increases upon restimulation with Dsg3. Anokion saw the same phenomenon in their own Dsg3 protein restimulations of an immunization experiment, which suggests that the issue is not having too few antigen-specific cells. Although we did not have a satisfactory explanation for the persistence of anti-Dsg3 antibodies in the pGal-Dsg3 treated group, we were encouraged by the pGal-Dsg3 treated mouse that had healed and by the statistically significant differences in clinical scores. We hypothesized that if we increased the number of animals in the experiment, that we would then be able to see differences between anti-Dsg3 antibody production.

In this larger repeated experiment, we also included a free protein control to show any tolerogenic effects of pGal-Dsg3 were stronger than Dsg3 alone. (Figure 2.8a). As shown by the clinical scores in Figure 2.8b, we failed to induce disease as rapidly and to the same magnitude in the saline treated group as we had done previously. Even more alarming was the rapid disease

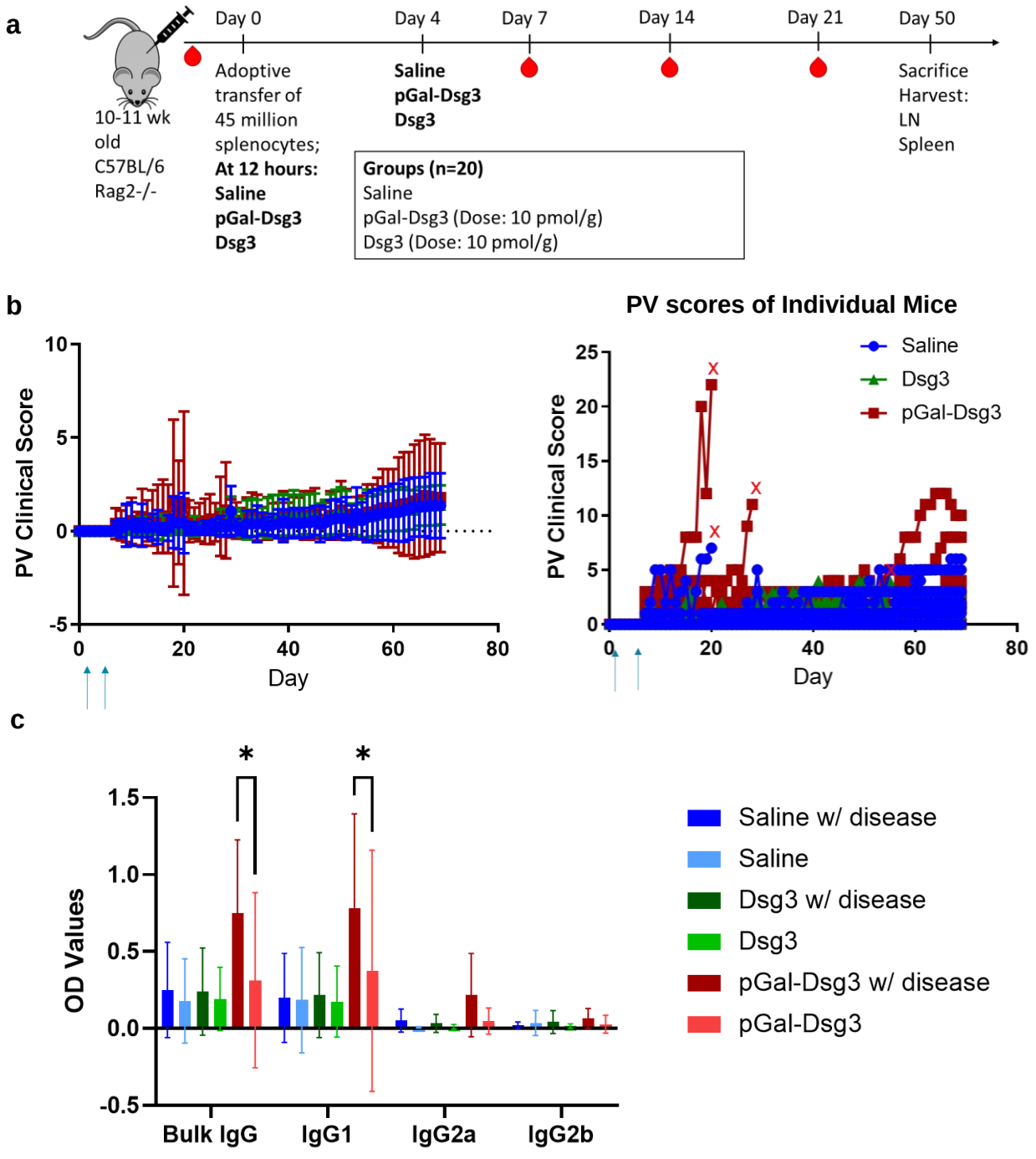


**Figure 2.8 | pGal-Dsg3 suppression of clinical scores in pemphigus vulgaris naïve transfer model, larger group study (n = 20).** (A) Experimental design. (B) Disease progression as measured by clinical scoring of hair loss and lesions. Blue arrows indicate treatments. (C) OD values of anti-Dsg3 IgG, IgG1, IgG2a, IgG2b levels at 7 weeks post adoptive transfer. All statistical comparisons were performed by one-way ANOVA using Tukey correction.

progression and meeting of euthanasia criteria by two of the pGal-Dsg3 treated mice. And finally in examining anti-Dsg3 antibody production (Figure 2.8c) we were able to see differences, but interestingly they were most pronounced between the pGal-Dsg3 treated mice with disease and without disease.

Supplemental Figure 2.6 shows the increased epidermal thickness and percent of cells that are CD3+ infiltrating T cells in skin samples taken from areas of hair loss compared to areas with hair or the border between the two. There were no differences when comparing epidermal thickness or percent of cells that are CD3+ cells across treatment groups (data not shown). We also measured cytokine secretion by splenocytes and lymphocytes after restimulation for 3 days with either PVP1, PVP2, PVP3, or a PV peptide pool (Supplemental Figure 2.7). There were no significant differences outside of the positive control, pooled cells stimulated with PMA + ionomycin. One of the largest differences was a trend towards increased IFNγ in diseased mice splenocytes. We investigated B cell and T cell phenotypes in spleen by flow cytometry and found no significant differences between treatment groups, likely due to poor disease induction (data not shown). However, when comparing healthy and diseased mice regardless of treatment, we did see a significant increase in the percent of B cells, the percent of IgM memory B cells, and the percent of class switched memory B cells that are positively stained with Dsg3 tetramer. All together these results would suggest that pGal-Dsg3 may actually be exacerbating autoantibody production and subsequent clinical features.

### 2.3.4 pGal-Dsg3 therapy in pemphigus vulgaris immunized model

Given the prior success of pGal-antigen, and specifically pGal-OVA, in suppressing previously activated T cell responses in the presence of polyclonal anti-OVA IgG, we hypothesized that pGal-Dsg3 would be able to suppress anti-Dsg3 T cell responses and remove T

cell help from anti-Dsg3 B cells. We tested pGal-Dsg3 in the PV immunized model at the same time that we did naïve model experiment. We followed the same experimental design as in our B cell depletion experiment. As previously discussed, we went forward with the day 4 anti-CD20 B cell depletion strategy (Figure 2.9a). We tested two pGal-Dsg3 doses including a low dose at 2 picomole per gram mouse body weight and a high dose at 10 picomole per gram given at 12h, 3 days and 6 days post adoptive transfer. We included these groups with and without the B cell depletion to test our hypothesis that the B cell depletion was necessary. As shown in Figure 2.9b the disease induction in the saline treated group as well as the day 4 anti-CD20 group was delayed and not as severe as expected from the previous experiment. Both the low dose and high dose pGal-Dsg3 treated groups had no difference from the saline treated group. Interestingly there was a significant increase in the AUC of the clinical score in the high dose pGal-Dsg3 treated group as compared to the low dose pGal-Dsg3 group. There was no significant difference between any of the anti-CD20 treated groups (Figure 2.9c). All three anti-CD20 treated groups had a statistically significant lower clinical score than the groups that did not receive anti-CD20. We were discouraged by the lower disease induction overall in this experiment and rather than further developing this model to increase the clinical score of the anti-CD20 treated group to be able to see a potential decrease in clinical score with pGal-Dsg3 treatment, we decided to investigate the possibility that pGal-Dsg3 was exacerbating anti-Dsg3 production and disease progression. In order to do this, we needed to deliver pGal-Dsg3 in a completely prophylactic manner.

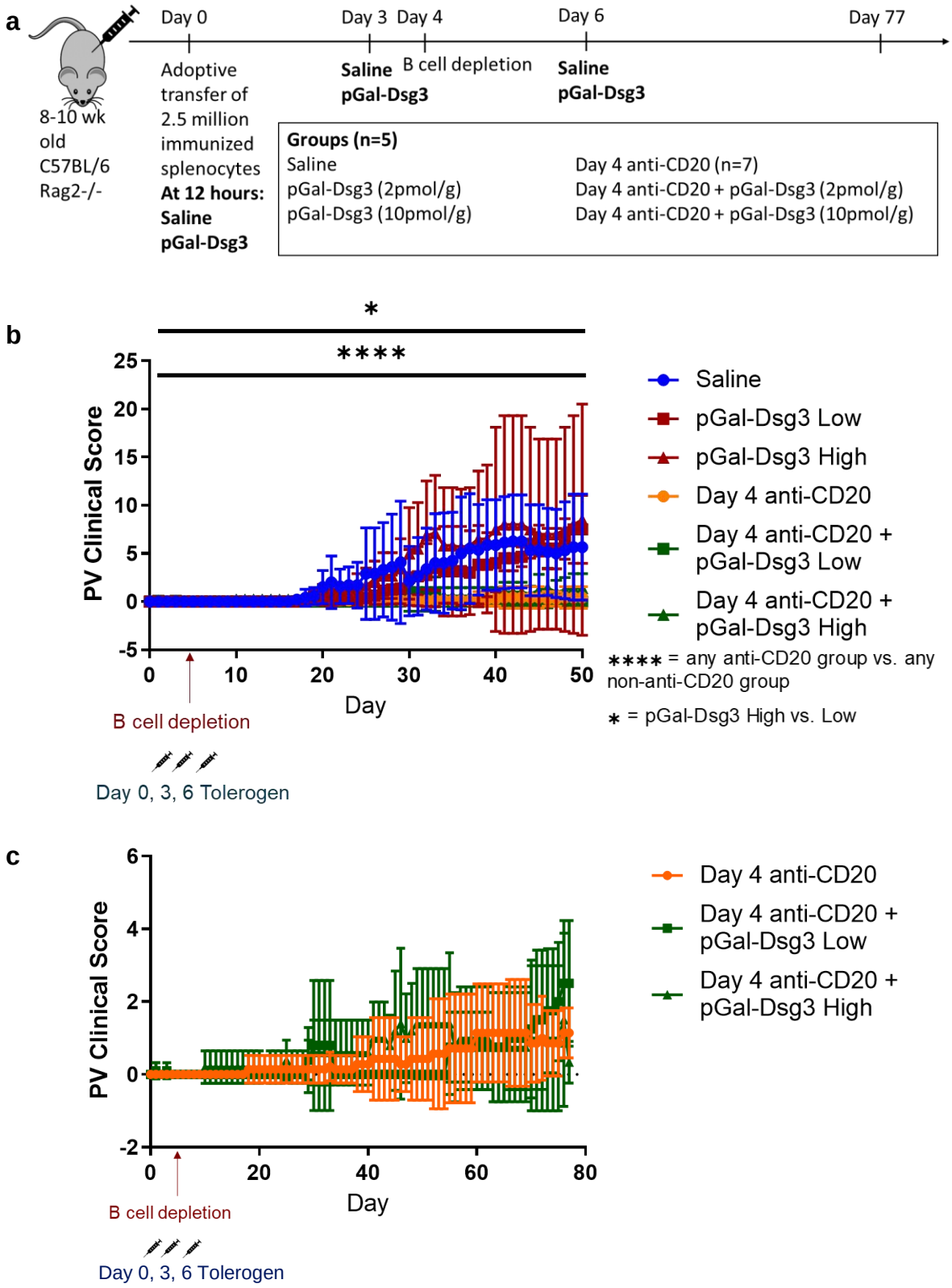


**Figure 2.9 | pGal-Dsg3 suppression of clinical scores in pemphigus vulgaris immunized transfer model.**

**Figure 2.9, continued.** (A) Experimental design. (B) Disease progression as measured by clinical scoring of hair loss and lesions with B cell depletion on day 4 shown by the red arrow. Blue arrows indicate tolerogen treatment. (C) Disease progression as measured by clinical scoring of hair loss and lesions shown only for groups with B cell depletion on day 4 in order to see more clearly. No statistically significant differences. Horizontal bars atop the graph indicate significant differences via AUC.

### 2.3.5 Prophylactic pGal-antigen therapies in pemphigus vulgaris peptide-immunized model

By creating a pemphigus vulgaris model where pGal antigen therapies are delivered prophylactically we are able to test if those pGal antigen therapy are immunogenic in a completely naïve environment and without competing antigen presentation. Our collaborators at Anokion ran the first experiment where Dsg3$^{-/-}$ mice were treated with 3 doses of saline, pGal-Dsg3, or Dsg3 alone given 3 days apart. One week after the last dose the mice were immunized with Dsg3 with no adjuvant. Mice were boosted 2 weeks later again with no adjuvant. Two weeks later splenocytes were transferred into Rag2$^{-/-}$ mice and their body weight and clinical scores were continuously monitored. Anti-Dsg3 IgG1 antibody titers were measured before tolerogen doses, 3 days before the first Dsg3 immunization, one week after the first immunization, two weeks after the first immunization, and on the day of the adoptive transfer. They found that Dsg3 alone and pGal-Dsg3 induced strong antibody titers over 1:1,000,000 (serum:dilutant). The saline treated group did not develop any anti-Dsg3 IgG1 titers until two weeks after the first immunization. At the time of transfer all 3 groups had comparable antibody titers. After the adoptive transfer Rag2$^{-/-}$ mice in the pGal-Dsg3 and Dsg3 treated groups had similar disease progression and mice in the saline treated group had slower disease progression. This confirmed that pGal-Dsg3 was immunogenic in a naïve mouse. Anokion performed a series of liver receptor assays and showed that Dsg3 was broadly binding. If Dsg3 was not adequately shielded from these interactions by conjugation with pGal then there would be competition for cellular uptake of pGal-Dsg3 in the liver.

Knowing that these properties of Dsg3 may not have been a factor in previous pGal applications we decided to test different pemphigus vulgaris antigens. By conjugating pGal to a different PV-associated antigen, we aimed to show that immunogenicity came from Dsg3 and that pGal conjugated to another antigen would be tolerogenic in the same $Dsg3^{-/-}$ mice. As shown in Figure 2.10a we designed a new pemphigus vulgaris model with prophylactic treatment. The tolerogen groups we included were a saline control, pGal-Dsg3, $Dsg3_{516\text{-}530}$ peptide (peptide 1), pGal-peptide 1 (pGal-P1), and a mixture of pGal-peptide1 and pGal-peptide pool. Due to constraints in $Dsg3^{-/-}$ mice we did not include the Dsg3 group in order to have groups of 5 mice. We selected a Dsg3 peptide for multiple reasons. First, we had to use some form of Dsg3 as the model is based on using $Dsg3^{-/-}$ mice. One of our concerns was the size of Dsg3, as it is the largest protein our lab has conjugated to pGal and nearly twice the size of OVA. It is possible that the pGal coverage of Dsg3 by steric hindrance was less than optimal, allowing Dsg3 to bind to various liver receptors. We chose a peptide rather than one or multiple domains of Dsg3 to decrease the likelihood of unintentional cellular uptake. The reason we included pGal-peptide pool is because multiple immunodominant mouse Dsg3 epitopes have been reported and we hypothesized with a pool of peptides we could induce lasting tolerance to the full protein that the treated splenocytes would encounter in the $Rag2^{-/-}$ mouse. The pool consisted of 140 15-mer peptides with 1-3 lysines, at which site the conjugation to pGal is possible.

Considering the high immunogenicity of Dsg3, we also switched from a Dsg3 immunization without adjuvant to a peptide immunization with CFA and IFA. This had the added benefit of boosting our ability to read out antigen-specific responses with a peptide stimulated T cell ELISPOT. Figure 2.10b shows anti-Dsg3 IgG1 titers are only present in the pGal-Dsg3 treated group before immunization. Interestingly, we were able to see an increase in anti-Dsg3 antibody

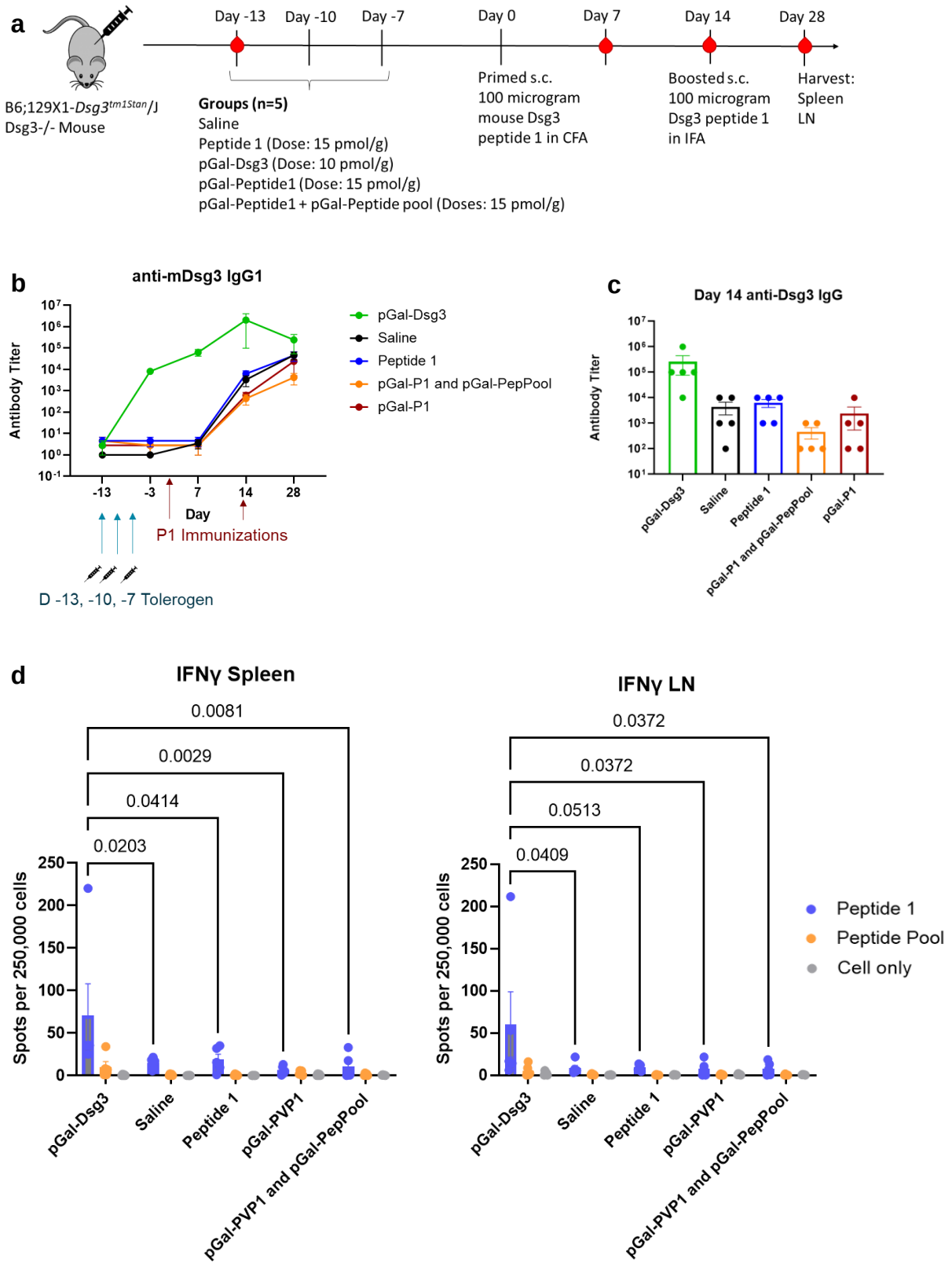


**Figure 2.10 | Prophylactic pGal-antigen treatment of Dsg3$^{-/-}$ mice in pemphigus vulgaris peptide-immunized transfer model.**

**Figure 2.10, continued.** (A) Experimental design. (B) Antibody titer of anti-mDsg3 IgG1 in Dsg3$^{-/-}$ mice. Blue arrows indicate tolerogen treatment. Red arrows indicate peptide 1 immunizations with CFA then IFA booster. (C) Day 14 antibody titers show pGal-Dsg3 at highest level but with no significant difference. (D) IFNγ T cell ELISPOTs of spleen and lymph node show highest concentrations of IFNγ secreting cells in pGal-Dsg3 group. All statistical comparisons were performed by one-way ANOVA using Tukey correction.

titers in all groups after the peptide immunization. Figure 2.10c shows a similar induction of anti-Dsg3 IgG titers. In the case of anti-Peptide 1 IgG1, none of the groups developed anti-Peptide 1 IgG1 antibodies after tolerogen treatment (Supplemental Figure 2.8). All groups developed anti-Peptide 1 IgG1 antibodies after the first peptide 1 immunization with CFA.

On day 28 spleens and lymph nodes were harvested and 5 million splenocytes were transferred to each Rag2$^{-/-}$ mouse. Remaining splenocytes and lymphocytes were used for T cell ELISPOT restimulated with peptide 1 or peptide pool to detect IFNγ or IL-4 secreting cells (Figure 2.10d, Supplemental Figure 2.9). All IFNγ signals were above cell only background control. Comparing between treatment groups only the pGal-Dsg3 treated group had a statistically significant higher concentration of IFNγ secreting cells than all other treatment groups. This suggests that pGal-Dsg3 generated strong antigen-specific B cell and T cell responses.

Figure 2.11a shows the experimental design post adoptive transfer to Rag2$^{-/-}$ mice. The groups were 15 mice each as each Dsg3$^{-/-}$ mouse splenocytes were transferred into three Rag2$^{-/-}$ mice. Supplemental Figure 2.10 shows that there were no significant differences in weight changes over the course of the experiment between treatment groups. As expected, the pGal-Dsg3 treated group induced the highest clinical scores, which were significantly higher than saline, pGal-peptide 1, and the mixture of pGal-peptide 1 and pGal-peptide pool, but there was no difference between peptide 1 at endpoint. Using AUC analysis peptide 1 scores were significantly higher than either pGal-peptide conjugated group, but there was no difference between peptide 1 and saline.

This suggests that the pGal-peptide conjugated groups were less immunogenic than peptide alone. However, we cannot draw a conclusion between the saline (disease control) and pGal-peptide conjugated groups (Figure 2.11b). Anti-Dsg3 IgG1 titers in sera compared using AUC (Figure 2.11c) and at the experimental endpoint (Figure 2.11d) show only a significant difference between pGal-Dsg3 and the other groups. Hard palettes of $Rag2^{-/-}$ mice and wild type control were fluorescently stained for mouse IgG1 (Figure 2.12). This revealed IgG1 deposition on keratinocytes in mice from the pGal-Dsg3 group and peptide 1 treated group. Supplemental Figure 2.11 shows a higher percentage of Dsg3 tetramer+ cells of class switched memory B cells in the LN of pGal-Dsg3 treated mice as compared to saline, pGal-P1, or the mixture of pGal-P1 and pGal-Peptide pool treated groups as measured by flow cytometry. Notably there is no significant difference between pGal-Dsg3 and peptide 1 treated groups. No differences were found in the prevalence of ICOS+ Tfh cells, likely because we were not able to obtain the I-Ab tetramer using peptide 1 in time for the experiment endpoint and examine antigen specific T cell responses via flow cytometry. Taken together these results indicate that we induced disease in the pGal-Dsg3 and peptide 1 treated groups, but not in the saline treated group which is supposed to be the disease control.

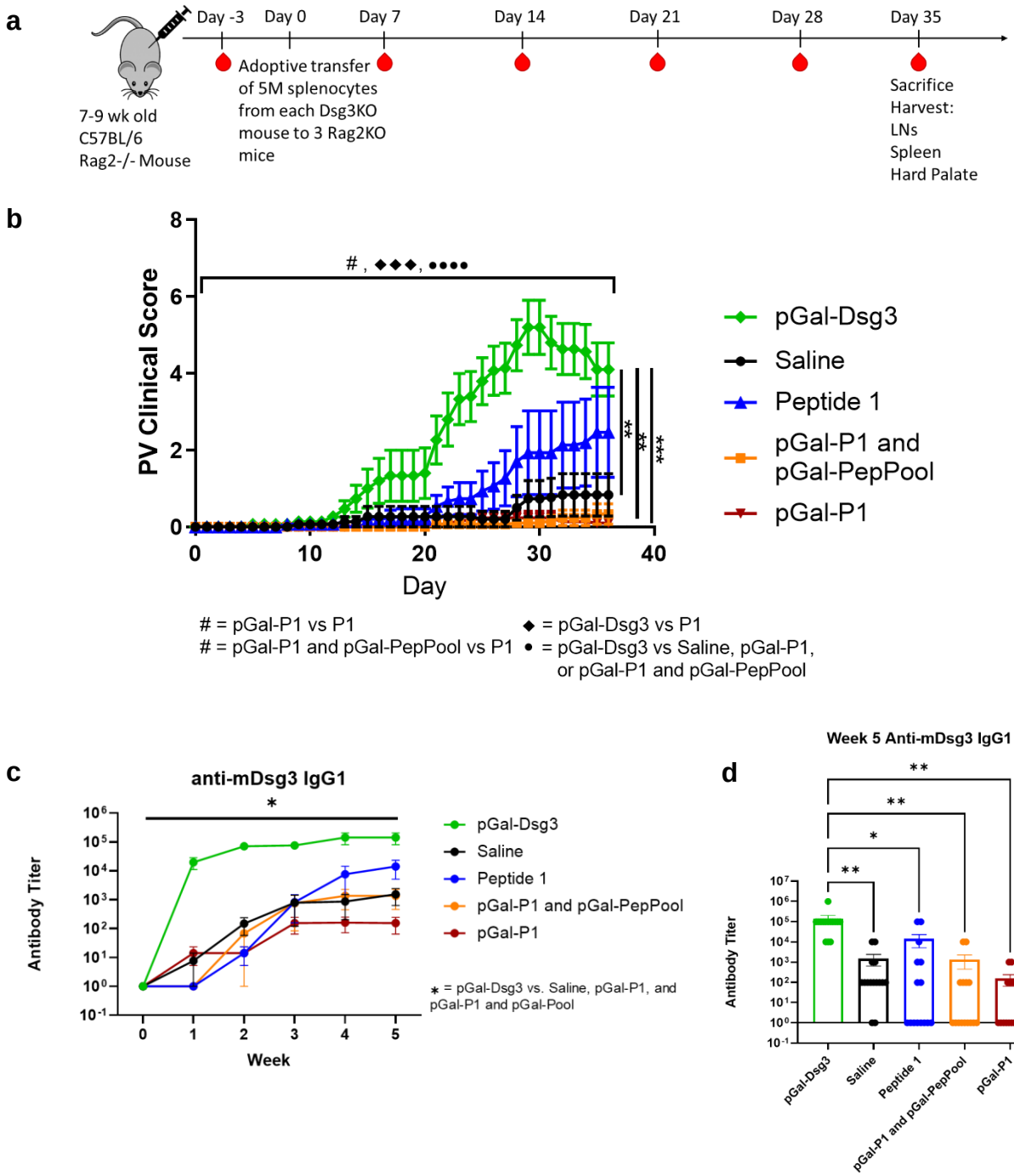


**Figure 2.11 | Adoptive transfer into Rag2$^{-/-}$ mice of Dsg3$^{-/-}$ splenocytes from mice prophylactically treated with pGal-antigen in pemphigus vulgaris peptide-immunized transfer model.** (A) Experimental design. (B) Disease progression as measured by clinical scoring of hair loss and lesions after adoptive transfer of Dsg3$^{-/-}$ mice splenocytes. (C) Antibody titer of anti-mDsg3 IgG1 in Rag2$^{-/-}$ mice. (D) Week 5 antibody titer of anti-mDsg3 IgG1 in Rag2$^{-/-}$ mice. Horizontal bars atop the graph indicate significant differences via AUC. All statistical comparisons were performed by one-way ANOVA using Tukey correction.

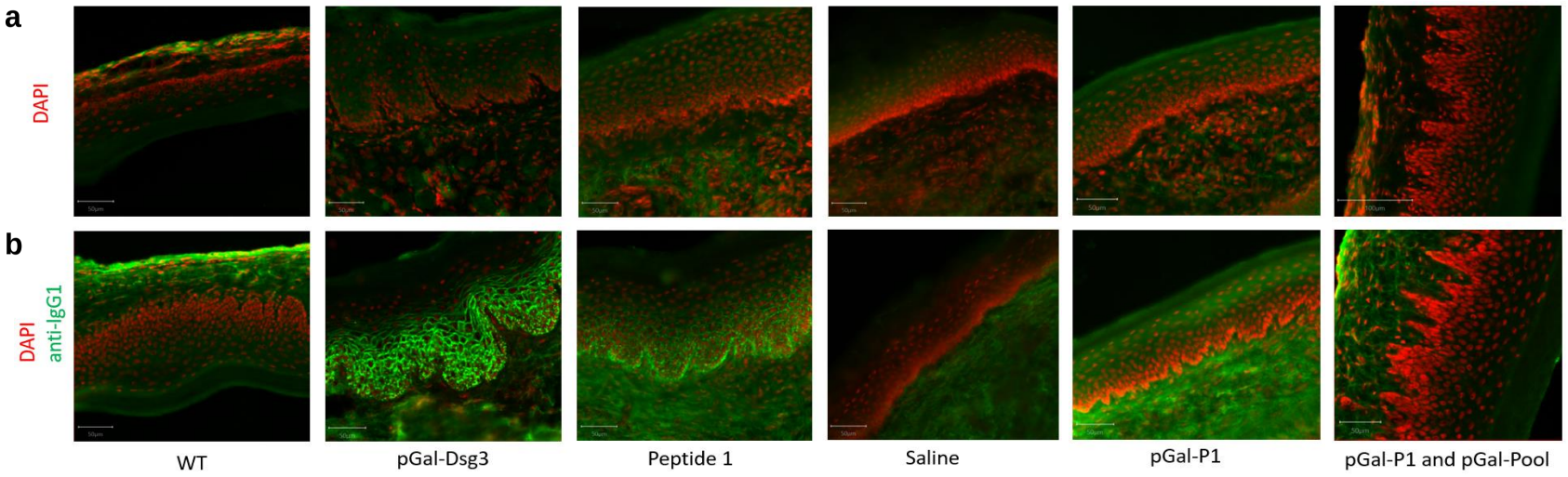


**Figure 2.12 | Detection of IgG antibodies in epidermal biopsies of areas with hair loss.**
(A) Nuclei were stained with 4'-6-diamidino-2-phenylindole, dihydrochloride ([DAPI], red). Green is autofluorescence. Bar = 50 μm.
(B) Representative images of direct immunofluorescent staining for the detection of IgG1 (green) deposition in the epidermis of the hard palate in each group. Characteristic weblike patterns seen in samples from pGal-Dsg3 and Peptide 1 treated mice reveal IgG1 deposition on keratinocyte cell surfaces. Wildtype, saline, pGal-P1, and the mixture of pGal-P1 and pGal-Pool do not exhibit the weblike staining pattern. Nuclei were stained with 4'-6-diamidino-2-phenylindole, dihydrochloride ([DAPI], red). Bar = 50 μm.

## 2.4 Discussion

There is a great unmet need for an antigen-specific immune therapy platform that is efficacious across a broad set of antigens. Our lab has dedicated enormous resources to the development of such platform therapies. pGal is one such antigen engineering approach for immunotherapy that has been demonstrated to successfully modulate T cell immunity in multiple animal models both prophylactically and therapeutically, as well as limit the development of anti-drug antibodies when given prophylactically. Here we have demonstrated how pGal performs in a B cell-mediated disease model. Furthermore, we have put the boundaries of the pGal platform to the test and revealed the importance of considering the properties of the antigen conjugated to pGal. In reaching these goals we have also developed new models of the B cell-mediated disease, pemphigus vulgaris.

When I set out to evaluate pGal in a B cell-mediated disease model, we first had to select which B cell-mediated disease model to use. Our criteria were a model with a known antigen and preferably a single antigen, clear and easy readouts, and an understood and relatively simple cause of disease. We had also considered a Parkinson's model, myasthenia gravis model, and autoimmune hepatitis (AIH). Pemphigus Vulgaris most clearly met the criteria of having known antigens and a single antigen mouse model, as well as no involvement of the complement cascade. Additionally, the readouts were clear with visible hair loss and lesions, and easily quantifiable with circulating antibodies.

We were able to recreate a reported naïve cell transfer model and confirmed autoantibody production as well as a dose dependence on the number of cells transferred. We struggled to see disease at the cellular level due to our technical limitations in measuring antigen-specific responses. We would later create Dsg3 tetramers to see antigen-specific B cells responses by flow

cytometry, but at this time we were limited in the amount of Dsg3 material we could acquire. We also did not have I-Ab tetramers as multiple potential mouse Dsg3 T cell epitopes have been reported, but extensive studies have not been done, unlike for human Dsg3. Despite these limitations, we were able to show a positive correlation between disease score and the percent of class switched B cells in $Rag2^{-/-}$ mice receiving $Dsg3^{-/-}$ splenocytes. We were interested in the naïve model as a low bar for tolerance induction, but we had concerns over the number of splenocytes needed and how that would require a large number of $Dsg3^{-/-}$ mice that must be bred as live mice are not available to order commercially. There was also a concern over the consistency of disease development as it had been previously reported that as low as 80% of mice developed disease.

For these reasons we also pursued establishing an immunized transfer model of pemphigus vulgaris. The currently reported models had the drawback of taking much longer than the naïve transfer model because of a lengthy immunization protocol involving five total immunizations. We hypothesized that the last two boosts were unnecessary and proceeded with a 3-dose immunization schedule. Another drawback of the immunized model regarding our goal of reducing disease score with pGal treatment was that suppressing an incredibly strong ongoing immune response would be a very high bar for efficacy. We decided to create an immunized model with B cell depletion to dampen the ongoing immune response. The rationale behind this design was two-fold. First, we have already shown that pGal is an effective therapy to suppress an ongoing T cell response. Second, B cell depletion is an approved therapy for PV in the clinic. We sought to mimic components of the clinical disease, namely having activated T cells present at the time of likely treatment and the possibility of also having a patient undergoing B cell depletion. A huge limitation here is that our model has no possibility of the return of naïve B cells, which does happen in the

clinic when the B cell depletion protocol is complete. We did a very small pilot of doing a secondary transfer of only naïve B cells into the Day 1 anti-CD20 treatment group, but we did not see return of disease (data not shown).

We tested three separate B cell depletion regimens. These were anti-CD20 given on day 1, anti-CD20 given on day 4 with bortezomib, and anti-CD20 given on day 4. Day 1 anti-CD20 effectively depleted B cells to a degree that resulted in no disease induction. Both day 4 anti-CD20 groups depleted B cells to a degree that delayed disease onset and decreased disease severity. However, the bortezomib treated group was largely toxic as demonstrated by a significant weight decrease immediately following treatment. There was also a decrease in the number of T cells in the lymph nodes which is particularly concerning in the $Rag2^{-/-}$ mice in which these T cells will not be replenished. Additionally, T cells are the cells in which pGal has had a demonstrated effect and so it is important that they are present at the time of treatment. High disease scores corresponded to high antibody titers. As we expected pGal-Dsg3 without B cell depletion was unable to suppress B cell responses. Due to a shortage in materials, we were unable to look for antigen specific T cell responses with a restimulation or antigen specific B cell responses with a Dsg3 tetramer and flow cytometry. We had planned to follow up with these readouts after identifying an effective pGal-Dsg3 dose. Unfortunately, we were surprised at the variability in disease induction and decided to focus on the naïve transfer model.

In our first naïve transfer pilot including pGal-Dsg3, we saw very intriguing results including a statistically significant difference in disease scores between saline and pGal treated mice. We also noted a pGal-Dsg3 treated mouse who developed a lesion which later resolved. These results were very encouraging despite seeing no differences in antibody abundance in multiple isotypes. At this time, we still did not have a way to effectively measure antigen-specific

B cell responses at the individual cell level. We attempted to see T cell responses to Dsg3 in a splenocyte restimulation but there was a technical challenge that as a group we've seen before, where certain proteins hinder the restimulation and at this time we did not have Dsg3 peptides to substitute.

In the naïve transfer model, we had similar misfortune in seeing a delayed and milder disease induction in our larger experiment. Disease induction was also highly variable. Every group had responders and non-responders. We confirmed disease seen by hair loss and lesions by examining skin samples and finding increased epidermal thickness and higher percentages of infiltrating CD3+ cells in diseased mice of all three groups. Unfortunately, even at this level there were no differences between the treatment groups. Here the evidence was clearer that there were pGal-Dsg3 mice with exacerbated disease as shown by two mice requiring euthanasia and significantly higher anti-Dsg3 IgG1 OD values. Kym had previously shown that administering another synthetically glycosylated antigen therapy, pGlu-antigen, mixed with unconjugated immunogenic antigen in a naïve environment did lead to higher antibody production than antigen alone, although it was not a statistically significant difference [72]. It appears that pGal-antigen in the presence of an immunogenic antigen may lead to increased immunogenicity.

To explicitly test the immunogenicity of pGal-Dsg3, we designed the prophylactic experiment to deliver pGal-Dsg3 in a completely naïve environment and without the presence of Dsg3 alone. We found that pGal-Dsg3 alone activated both B and T cells as evidenced by anti-Dsg3 IgG and IgG1 production, and IFNγ secreting T cells in response to Dsg3, peptide 1, and peptide pool. Our collaborators at Anokion found no difference between pGal-Dsg3 and Dsg3 in terms of anti-Dsg3 production. This is similar to what Kym saw in his pGal-Asparaginase (ASNase) experiment. However, the timing was off because the groups he was comparing were

pGal-ASNase tolerization followed by ASNase treatment and no tolerization followed by ASNase treatment [72]. Still he saw no difference between the groups and only a trend towards lower antibodies in the pGal-ASNase group. It has been shown that polyclonal antibodies to OVA had a 5-fold increase in affinity to OVA than to pGal-OVA, but it has not been shown if pGal-OVA itself is sufficient to produce anti-OVA antibodies. In fact, I would hypothesize that pGal-OVA would induce anti-OVA antibodies, given what has been demonstrated with pGal-Dsg3 and pGal-ASNase.

In this experiment I have also shown that pGal conjugated to a PV peptide or peptide pool did not induce antibodies to either Dsg3 or PV peptide 1. These pGal-peptide conjugations unfortunately did not completely prevent the induction of antibodies to Dsg3 or peptide 1 following peptide 1 immunizations. While the pGal-peptide conjugation treated groups did not have IFNγ secreting cell concentrations as high as the pGal-Dsg group, they also did not have significantly lower concentrations than the saline or peptide 1 groups. Without the saline and peptide 1 groups driving T cell and antibody responses to the extent of the pGal-Dsg3 group, it's impossible to say that the pGal-peptide conjugated groups could not have decreased responses in that context. In the second portion of the prophylactic experiment where splenocytes are transferred to $Rag2^{-/-}$ mice, it became even more clear that the most immunogenic treatments were pGal-Dsg3 and peptide 1. Unfortunately, because the saline treated group did not develop robust disease, we cannot conclude that either of the pGal-peptide conjugations induced tolerance. We can confidently conclude that the pGal-peptide conjugated groups were both less immunogenic than the peptide 1 treated group. Besides the evidence in clinical scores, there was also a significant difference in the anti-peptide 1 IgG1 titer on day 14 pre-transfer, as well as the differences seen in IgG1 deposition on the surface of keratinocytes in the hard palate. IgG1 deposition was only seen

in pGal-Dsg3 and peptide 1 treated mice.

This study provides insight into the use of pGal therapies in B cell-mediated disease, where the induction of autoantibodies is detrimental. We demonstrated that the ability of pGal to suppress or exacerbate the production of antibodies is antigen dependent. This highlights the importance of checking for the induction of antibodies with each new pGal construct, and perhaps altering conjugation ratios and checking for binding by antibodies to the antigen of interest before testing *in vivo*. We have also introduced multiple novel pemphigus vulgaris mouse models useful for interrogating potential therapeutics, although more work is required for their reliable use.

## 2.5 Materials and Methods

### 2.5.1 Mice

Mice were maintained in a specific pathogen-free facility at the University of Chicago. The experiments and procedures in this study were performed in accordance with the Institutional Animal Care and Use Committee. Dsg3$^{-/-}$ mice (stock no: 002911) and Rag2$^{-/-}$ mice (stock no: 008449) were purchased from The Jackson Laboratory.

### 2.5.2 Splenocyte adoptive transfer

Spleens were isolated from Dsg3$^{-/-}$ mice. Spleens were passed through a 70-micron filter and ACK lysed. Indicated numbers of splenocytes in IMDM were injected through the tail vein.

### 2.5.3 Subcutaneous immunization

All Dsg3 challenges consisted of 10 µg HEK cell produced Dsg3 emulsified with either CFA or IFA as specified, distributed evenly across each hock while mice were anesthetized with isofluorane. Peptide challenges were done similarly with 100 µg Dsg3$_{516\text{-}530}$. CFA/IFA (Sigma) emulsifications were prepared as a 1:1 mixture with antigen stock solutions in saline for a final antigen concentration of 0.125 mg/mL and 2.5 mg/mL, and 20 µL and 10 µL total injection volume per hock, for protein and peptide, respectively. Emulsions were vortexed immediately upon addition of adjuvant for 1 hour.

### 2.5.4 pGal antigen constructs

Dsg3$_{516\text{-}530}$ and Dsg3 (HEK produced) were conjugated to pGal using the same methods as previously described [36]. pGal-Dsg3 conjugation batches were purified by size-exclusion chromatography, and analyzed by SDS-polyacrylamide gel electrophoresis (Supplemental Figure 2.12).

### 2.5.5 Antibody titer ELISA

ELISA plates (Nunc Maxisorp, ThermoFisher) were coated overnight with 1 µg/mL Dsg3 or 20 µg/mL $Dsg3_{516-530}$. Mice were bled weekly, and blood was collected in a Microtainer™ capillary blood collector (BD) per IACUC protocol. Blood was spun down at 8000xg for 90 seconds and serum was collected. Sera was diluted in casein (Thermofisher) 1:100 for the first dilution with subsequent 10-fold dilutions. Plates coated with capture antigen were washed with 0.1% PBST, blocked with casein for 2 hours at room temperature, incubated with diluted sera for 2 hours at room temperature, and then washed again. Antibodies were detected using an HRP-conjugated anti-mouse IgG, IgG1, IgG2a, or IgG2b antibody (Abcam) for one hour at room temperature diluted in casein. After washing the plates again, TMB solution (Invitrogen) was added for 18 minutes at room temperature, and 10% sulfuric acid was added to stop the reaction. Titers were calculated by averaging 4 blank wells, adding 4 times the standard deviation of these wells. This value was then subtracted from the optical density (OD) 450-570 readings of the samples. The reciprocal of the last dilution with signal above a threshold of 0.02 is the titer plotted.

### 2.5.6 Pemphigus vulgaris model and scoring

Splenocytes were transferred from $Dsg3^{-/-}$ mice that were either immunized with Dsg3 protein or peptide as described above, or from naïve $Dsg3^{-/-}$ mice. The immunization and adoptive cell transfer schedules are as indicated in the figures. Mice were bled weekly and scored daily starting from the day of the adoptive cell transfer until the experimental endpoint. Scoring was done checking each of the following body areas: face/cheeks, top of head, back, underside, front right leg, front left leg, rear right leg, rear left leg, and tail. Scores were assigned as 1 point for hair loss, 2 points for mild erosive lesions up to 1.5 cm, 3 points for moderate erosive lesions 1.6 -2.5 cm, 1 point for the presence of elongated fore teeth (to then be trimmed), 0.5 point for 5-10% body

weight loss, 1 point for 10-15% body weight loss, and 1.5 points for 15-20% body weight loss. Immediate euthanasia was triggered by signs of the animal's overall health as measured by any single one of the following criteria: 1) severe hunched posture and ruffled, 2) increased respiration, 3) animal inactive but moves when stimulated, 4) deep lesions through the dermis, 5) a lesion exceeding 2.5 cm, 6) eye lid swelling with lid closure, or 7) 20% weight loss. Representative photos of $Rag2^{-/-}$ mice with hair loss and lesions are shown in Supplemental Figure 2.13.

### 2.5.7 B cell depletion

Rat anti-mouse CD20 (Clone SA271G2, Biolegend) 200 µg per injection was used for B cell depletion either one day or four days post adoptive transfer. Two doses of bortezomib 15 µg per injection and 36 hours apart were given as an alternative B cell depletion strategy starting six days post adoptive transfer. Rat IgG2b Isotype control antibody (Clone LTF-2, Bio X Cell) 200 µg per injection was used as an isotype control for the anti-mouse CD20 antibody. An equal volume of DMSO in saline as used in the bortezomib injections was administered in another group as a solvent control.

### 2.5.8 Tissue Processing

Draining lymph nodes of immunized mice (axillary, brachial, inguinal, and popliteal), lymph nodes draining from areas of lesions (axillary, brachial, inguinal, and iliac), spleens, or femurs were isolated from mice and kept on ice in DMEM until processing. Lymph nodes were digested at 37ºC for 40 min with 1 mg/mL collagenase IV (Worthington). Digested lymph nodes and spleens were processed into single-cell suspensions via passage through a sterile 70 µm screen. ACK lysis of red blood cells in splenocyte suspensions were done by resuspending in 3 mL ACK lysing buffer (Gibco), incubating for 5 min at room temperature, and then quenching with 30 mL 10% FBS in DMEM. Single cell suspensions were resuspended in 10% FBS and 1%

penicillin/streptomycin (pen/strep) in IMDM for counting with a fluorescent cell counter and subsequent use in restimulation experiments or direct staining for flow cytometry analysis.

### 2.5.9 Cytokine ELISA

3-day restimulation plates were removed from incubation and put on ice, followed by centrifugation at 2000g for 2 min. Supernatants were pipetted and stored at -20$^{o}$C until cytokine ELISAs were performed. Culture supernatants were measured using the LEGENDplex Mouse T Helper Cytokine Panel V3 kit (BioLegend, 741044), following the manufacturer's instructions.

### 2.5.10 Flow cytometry

For phenotypic analysis, 2 to 5 million cells were stained in PBS with 1:200 CD16/CD32 Fc Block (Biolegend) and 1:500 Live/Dead fixable dye (ThermoFisher) at 4$^{o}$C for 15 minutes. Cells were washed in 2% FBS in PBS. Cells were stained in 2% FBS in PBS with 1:200 surface antibodies at 4$^{o}$C for 20 minutes. Cells were washed in 2% FBS in PBS and fixed in 2% paraformaldehyde (PFA) in PBS. For intracellular staining, cells were fixed and permeabilized using Cytofix/Cytoperm (BD Biosciences) at 4$^{o}$C for 20 minutes and stained intracellularly in Perm Wash Buffer (Biolegend) with 1:200 antibodies at 4$^{o}$C for 30 minutes. For transcription factor stain, FoxP3 Transcription Factor Kit (eBioscience) was used per the manufacturer's protocol, and nuclear stains were applied for 1 hour at 4$^{o}$C.

### 2.5.11 *Ex vivo* restimulation

1 to 2 million cells from spleen or lymph node in single-cell suspensions were restimulated *in vitro* with the addition of 1 mg/mL Dsg3 as indicated on figures or peptide epitopes as described: 10 μg/mL $Dsg3_{516\text{-}530}$ (LDRGKYTGPYTVSLE), $Dsg3_{499\text{-}513}$ (KKDICTSSPSVTLSV) and $Dsg3_{503\text{-}5317}$ (CTSSPSVTLSVRTLD) also referred to as PVP1, PVP2, and PVP3, respectively (WatsonBio). Unstimulated (no peptide added) control wells were used to determine background

levels of non-specific activation.

### 2.5.12 Statistical Analysis

Statistically significant differences between experimental groups were determined using Prism software (v9, GraphPad). Unless otherwise specified in the figure legend, one-way ANOVA was performed with a Tukey's post-hoc test to correct for multiple comparisons. Comparisons were significant with p values < 0.05. Statistical significance is shown with stars as follows: *** means $p \leq 0.001$; ** means $p \leq 0.01$; * means $p \leq 0.05$, unless otherwise stated.

## 2.6 Appendix A: Supplementary Figures

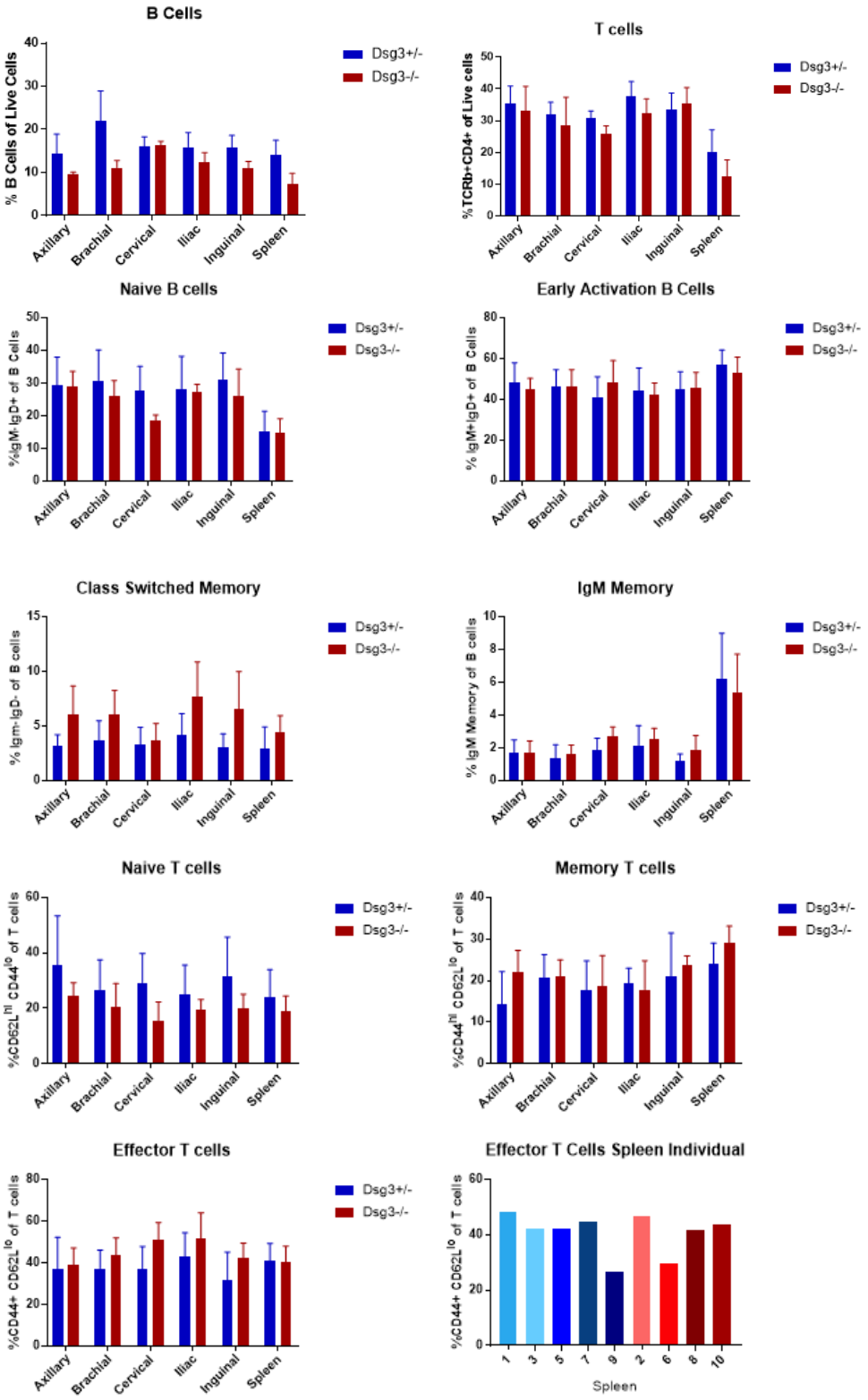


**Supplemental Figure 2.1 | Cell type distribution in Dsg3$^{+/-}$ and Dsg3$^{-/-}$ mice identified by flow cytometry.**

**Figure 2.1, continued.** Compared to Dsg3$^{+/-}$ mice, Dsg3$^{-/-}$ mice show greater amounts of class switched memory cells. Both mice groups have the highest percentage of IgM cells located in the spleen. All statistical comparisons were performed by one-way ANOVA using Tukey correction.

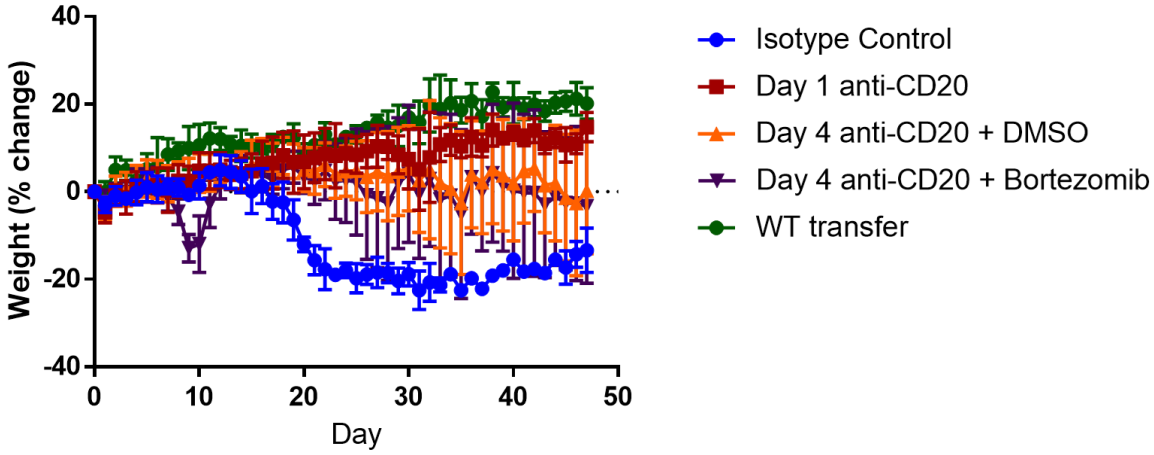


**Supplemental Figure 2.2 | Percent weight change in mice during treatment.** Weight change shown as a percent difference from the weight on Day 0. Compared to isotype control, weight loss was minimal for anti-CD20 treated mice. A dip in weight in the bortezomib treated group is seen immediately following bortezomib treatment days 8-11.

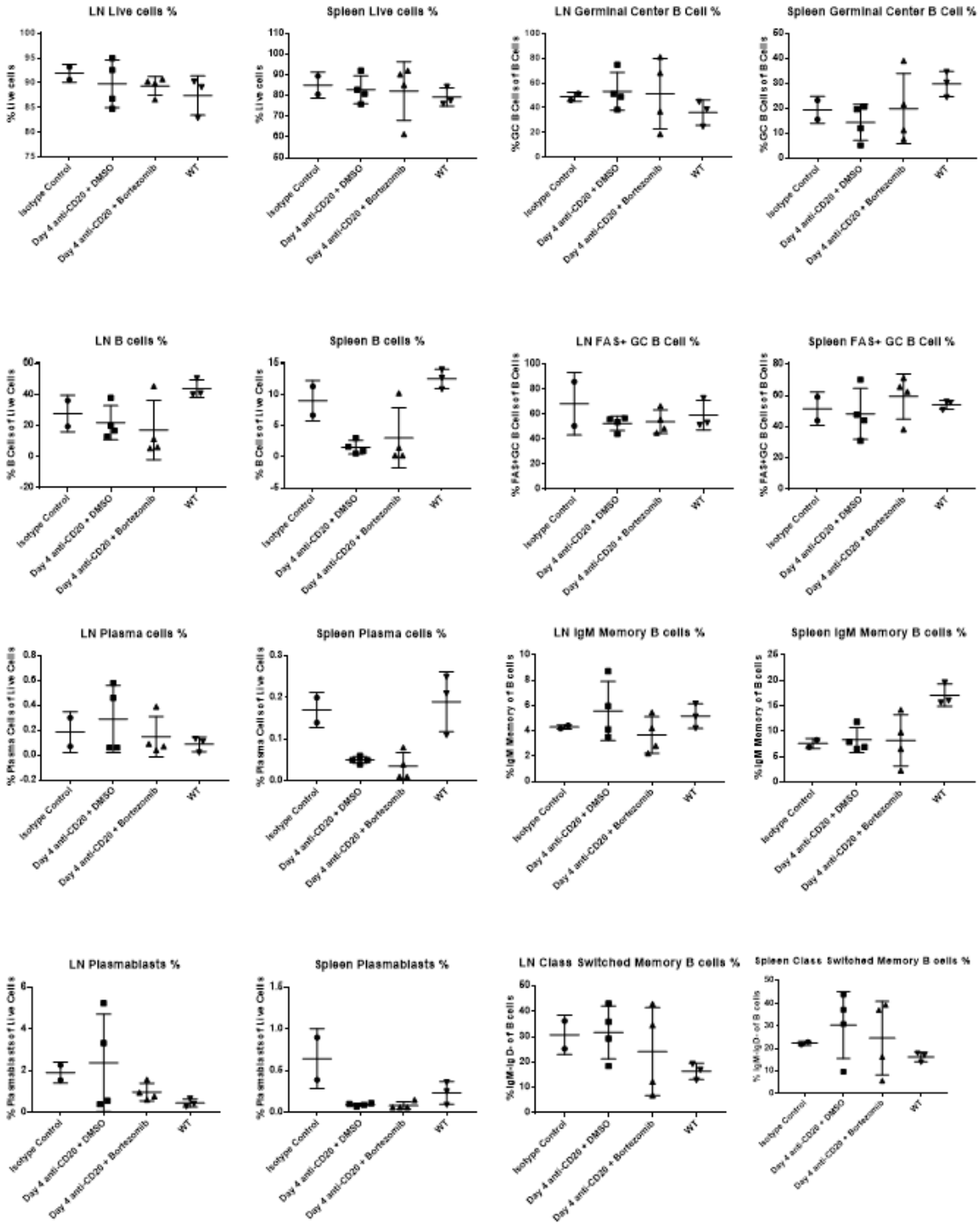


**Supplemental Figure 2.3 | Different cell types in lymph node and spleen captured by flow cytometry.** Spleen showing the most variation between wild type (WT) and anti-CD20 treated mice. All statistical comparisons were performed by one-way ANOVA using Tukey correction.

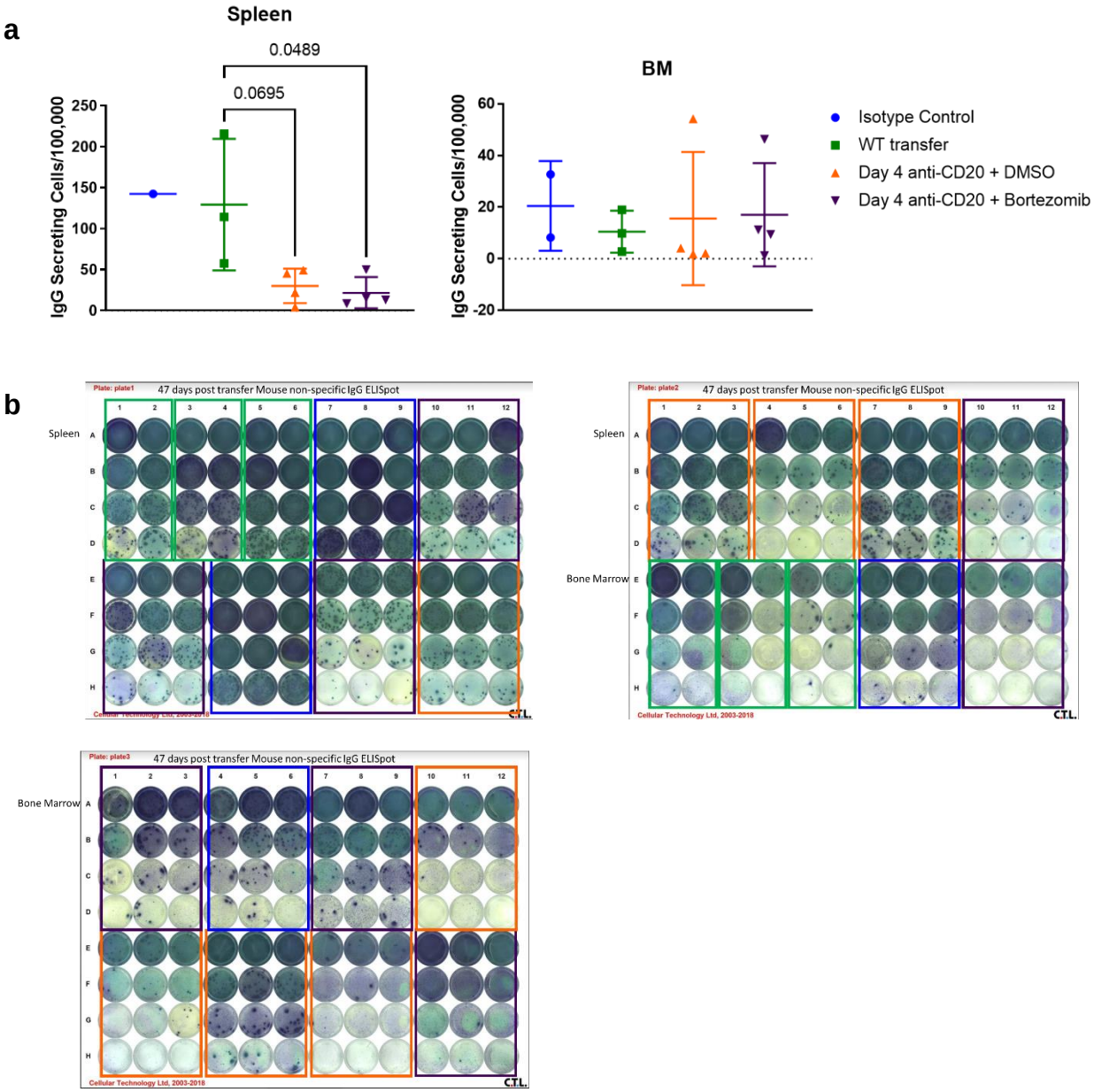


**Supplemental Figure 2.4 | ELISPOT analysis for non-specific IgG cells in spleen and bone marrow.** (A) Comparison of IgG secreting cells in spleen and bone marrow shows lower concentrations in spleens of mice treated with anti-CD20. (B) Spots indicative of non-specific IgG are shown in each well for each group of mice (color coded squares). All statistical comparisons were performed by one-way ANOVA using Tukey correction.

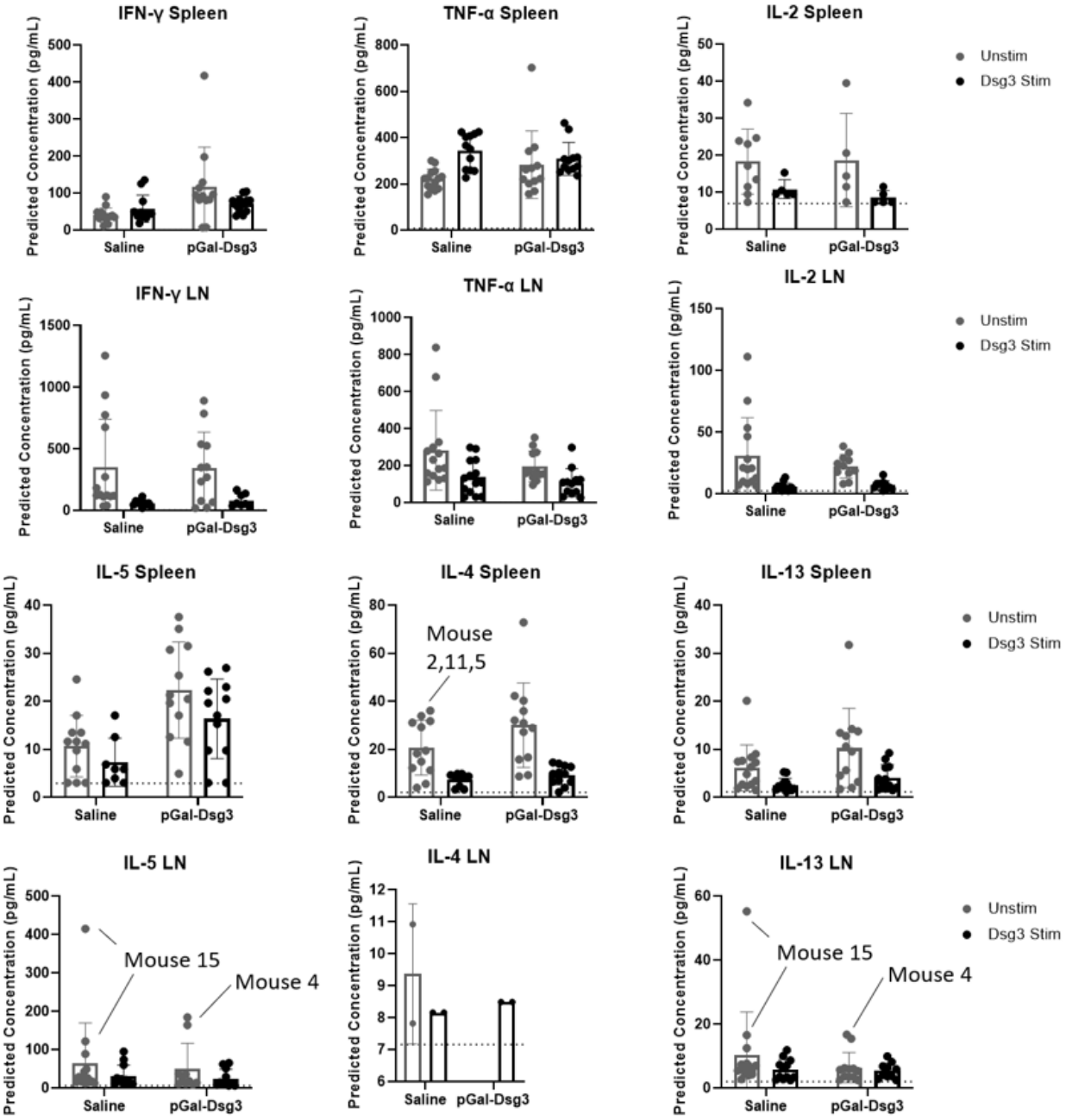


**Supplemental Figure 2.5 | Dsg3 failed to stimulate cytokine production *ex vivo*.**
**(continued on next page)**

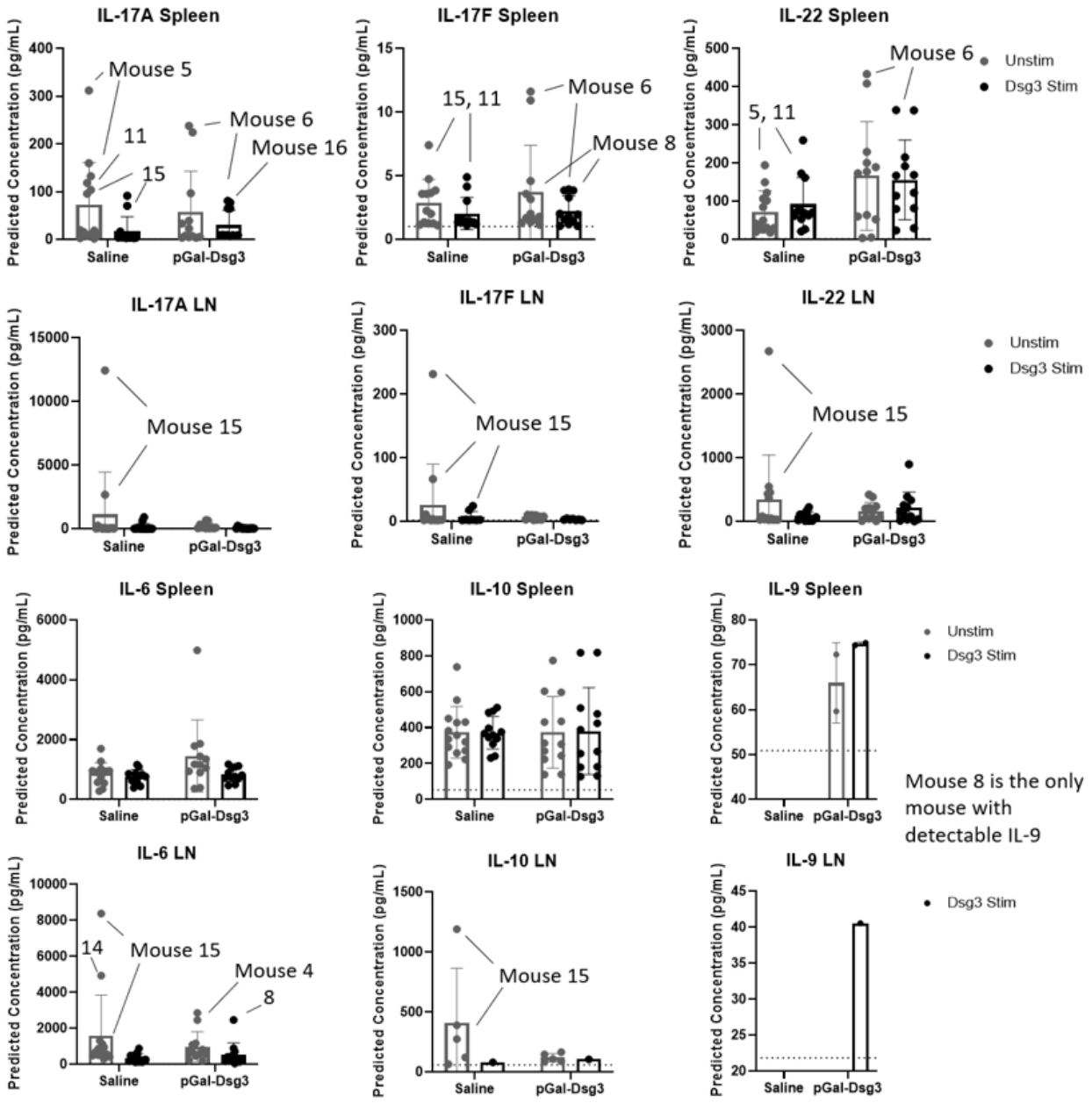


**Supplemental Figure 2.5 (continued from previous page)**

**Supplemental Figure 2.5 | Dsg3 failed to stimulate cytokine production *ex vivo*.** Three-day restimulations of splenocytes and lymphocytes were carried out for analysis of Th1, Th2, and Th17 associated cytokine production in culture supernatants. All statistical comparisons were performed by one-way ANOVA using Tukey correction unless otherwise indicated.

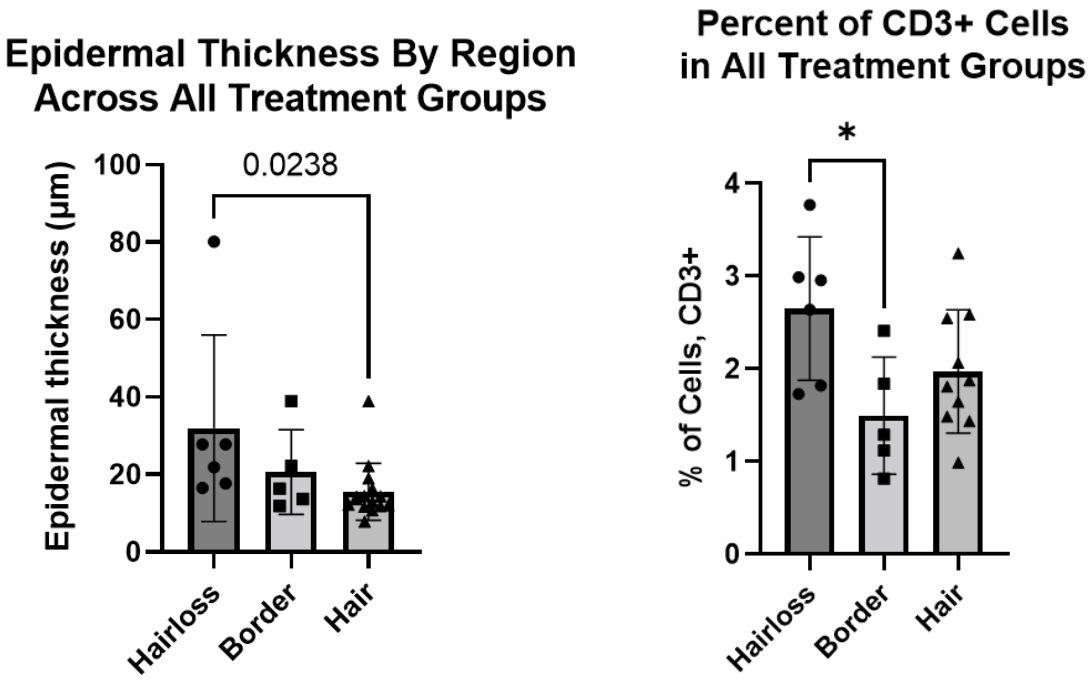


**Supplemental Figure 2.6 | Comparison of skin samples from areas of hair loss and areas with hair or the border between the two.** Areas of hair loss show an increase of CD3+ cells as well as an increase in epidermal thickness. All statistical comparisons were performed by one-way ANOVA using Tukey correction.

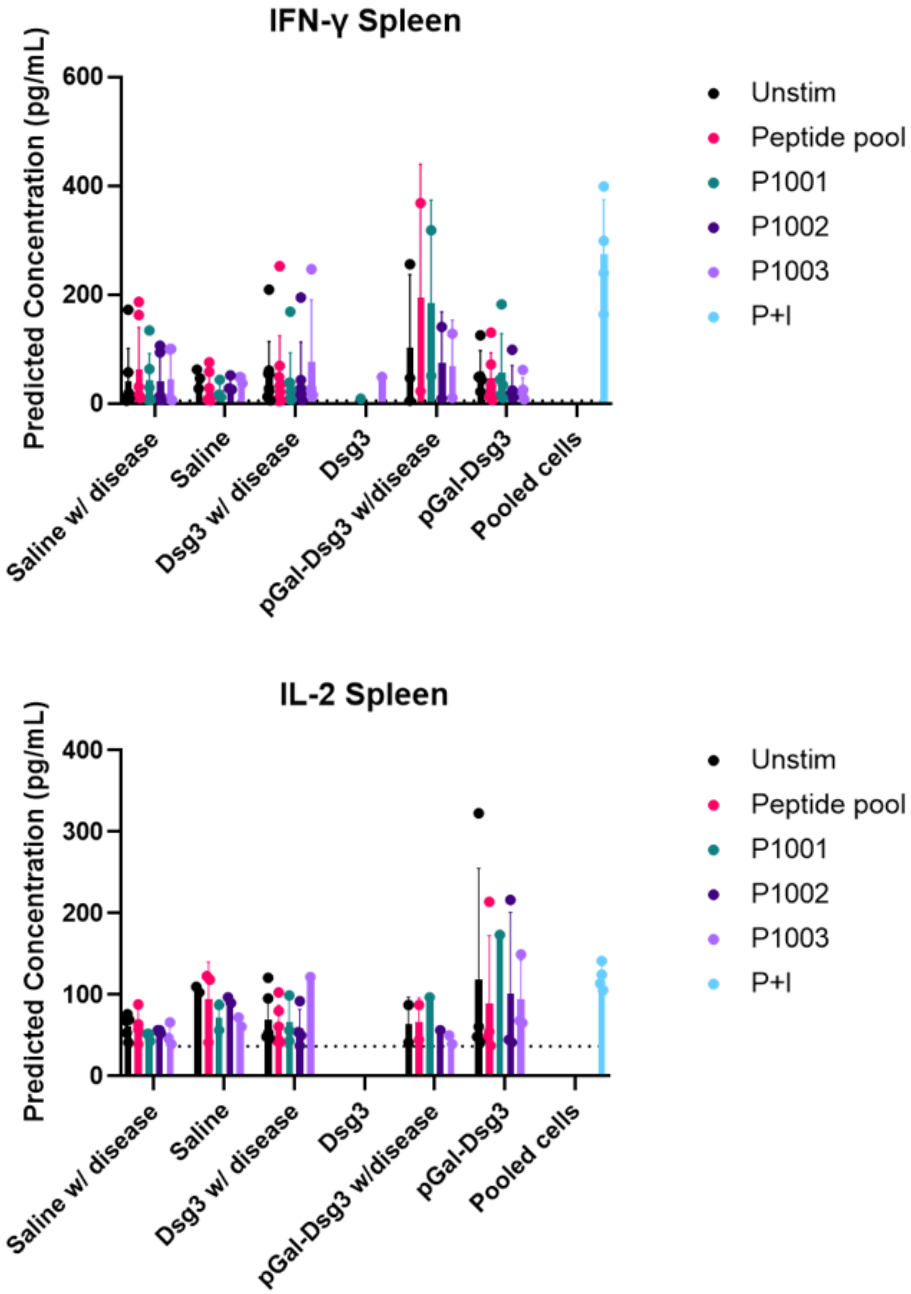


**Supplemental Figure 2.7 | Cytokine secretion by splenocytes after 3-day restimulation with Dsg3 peptides.** Three-day restimulations of splenocytes and lymphocytes were carried out for analysis of Th1, Th2, and Th17 associated cytokine production in culture supernatants. Cells were stimulated with Dsg3 peptide pool of 140 peptides, P1001 is PV peptide 1, P1002 is PVP2 and P1003 is PVP3. P+I is PMA and ionomycin as a positive T cell activation control. There were no significant differences between groups based on treatment and disease status. Select plots shown here. All statistical comparisons were performed by one-way ANOVA using Tukey correction.

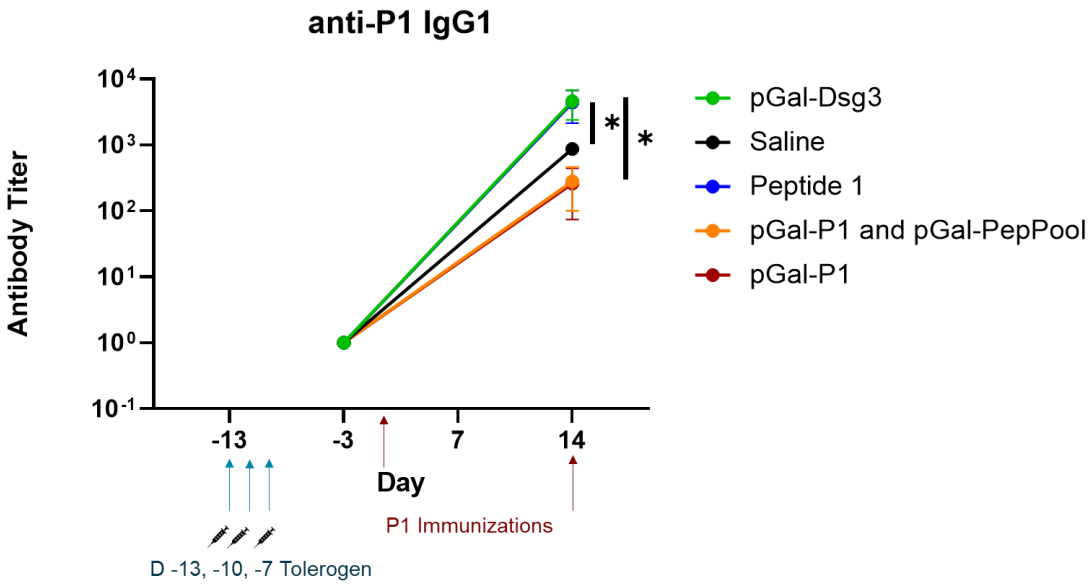


**Supplemental Figure 2.8 | No detectable anti-P1 antibodies before immunization.**
Antibody titer of anti-Peptide 1 IgG1 in Dsg3$^{-/-}$ mice. Blue arrows indicate tolerogen treatment. Red arrows indicate peptide 1 immunizations with CFA then IFA booster. No significant difference between pGal-Dsg3 and PV peptide 1, or the pGal-peptide conjugations, respectively. All statistical comparisons were performed by one-way ANOVA using Tukey correction.

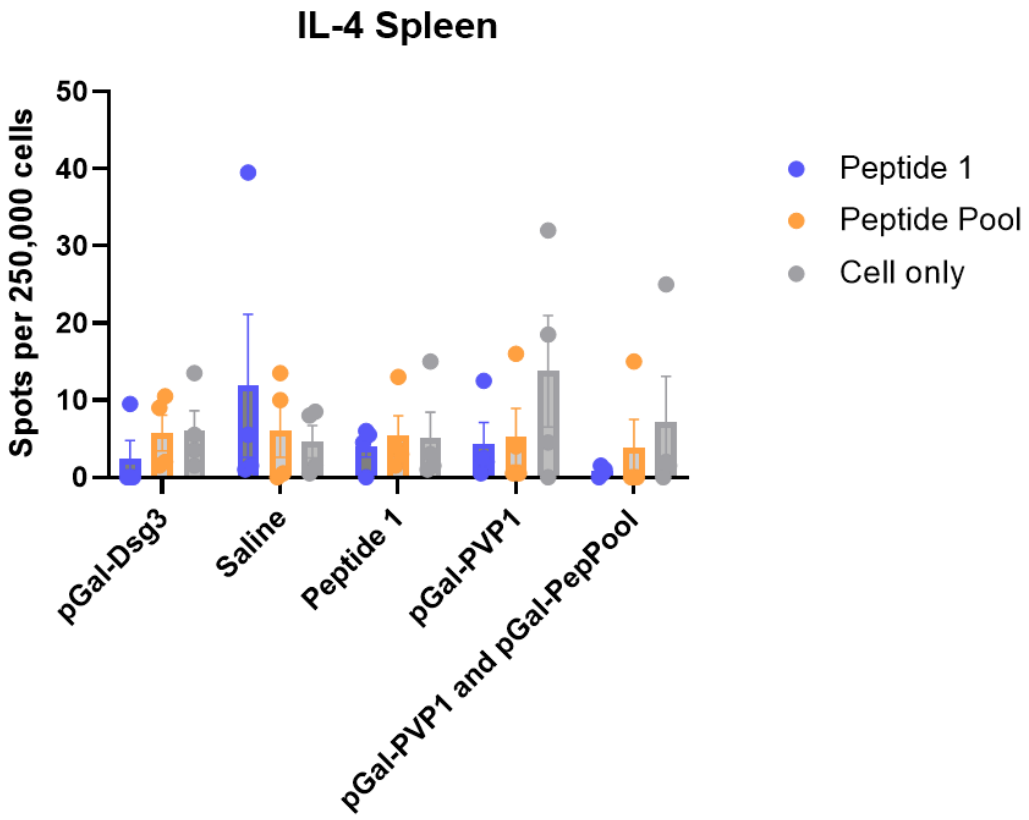


**Supplemental Figure 2.9 | IL-4 secreting splenocytes after restimulation with PVP1 or PV peptide pool.** IL-4 T cell ELISPOTs of spleens show no significant differences with only the saline group showing increased IL-4 secreting cells above the cells only condition. All statistical comparisons were performed by one-way ANOVA using Tukey correction.

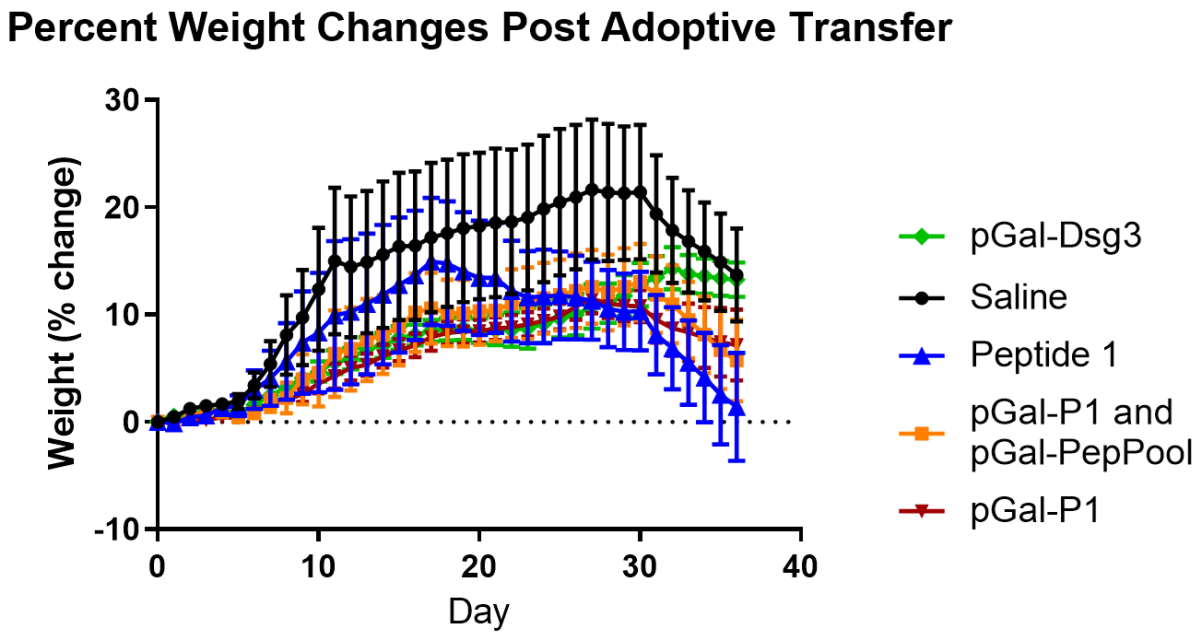


**Supplemental Figure 2.10 | Percent weight change in mice during treatment.** Weight change shown as a percent difference from the weight on Day 0. Interestingly, all groups except pGal-Dsg3 began losing weight at day 30.

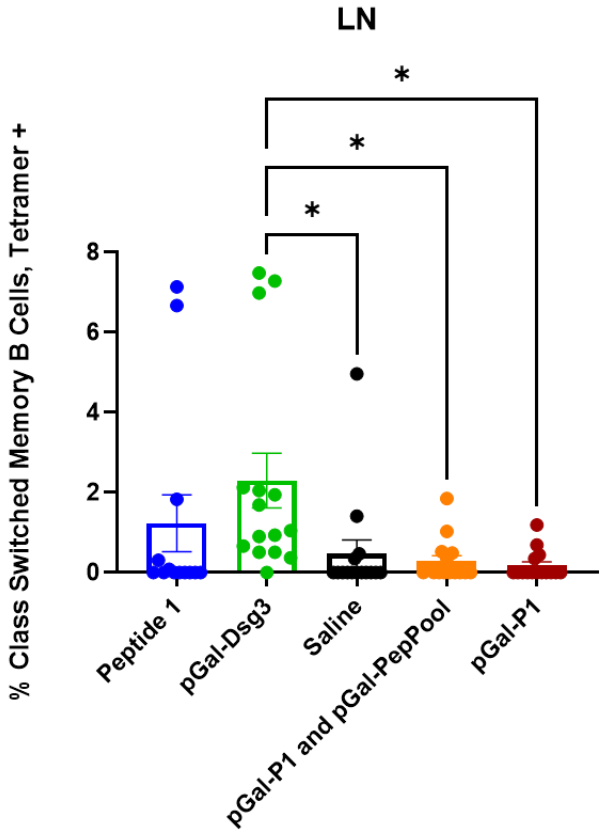


**Supplemental Figure 2.11 | Dsg3 tetramer+ cells of class switched memory B cells in the LN of pGal-Dsg3 treated mice.** The percent of class switched memory B cells that are positively stained for Dsg3 tetramer as measured by flow cytometry. All statistical comparisons were performed by one-way ANOVA using Tukey correction.

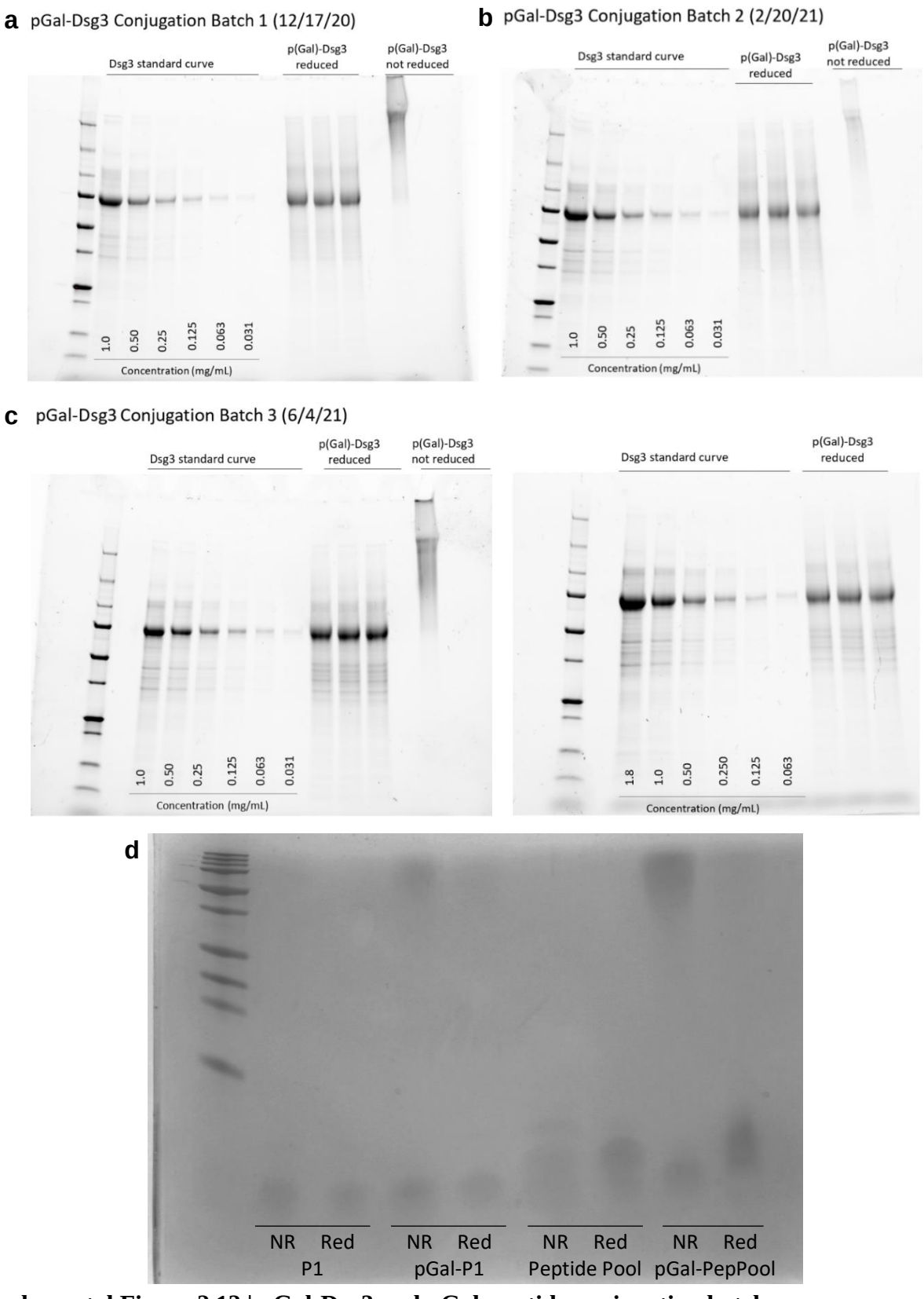


**Supplemental Figure 2.12 | pGal-Dsg3 and pGal-peptide conjugation batches.**

**Figure 2.12, continued.** All batches were purified by size-exclusion chromatography, and analyzed by SDS-polyacrylamide gel electrophoresis (SDS-PAGE). pGal-Dsg3 concentrations were calculated using a standard curve. A) SDS-PAGE of batch 1 with a conjugation Ratio of 1:30 and concentration of 573 µg/mL. 2 mg Dsg3 gave 618 µg pGal-Dsg3 (30.9% conjugation yield (Dsg3)). B) SDS-PAGE of batch 2 with a conjugation Ratio of 1:30 and concentration of 311.5 µg/mL. 1 mg Dsg3 gave 342 µg pGal-Dsg3 (34.2% conjugation yield (Dsg3)). C) SDS-PAGE of batch 3 with a conjugation Ratio of 1:30 and concentration of 801.4 µg/mL. 5 mg Dsg3 gave 2724 µg pGal-Dsg3 (54.5% conjugation yield (Dsg3)). (D) SDS-PAGE of P1, pGal-P1, peptide pool, pGal-peptide pool. NR = not reduced, Red = reduced.

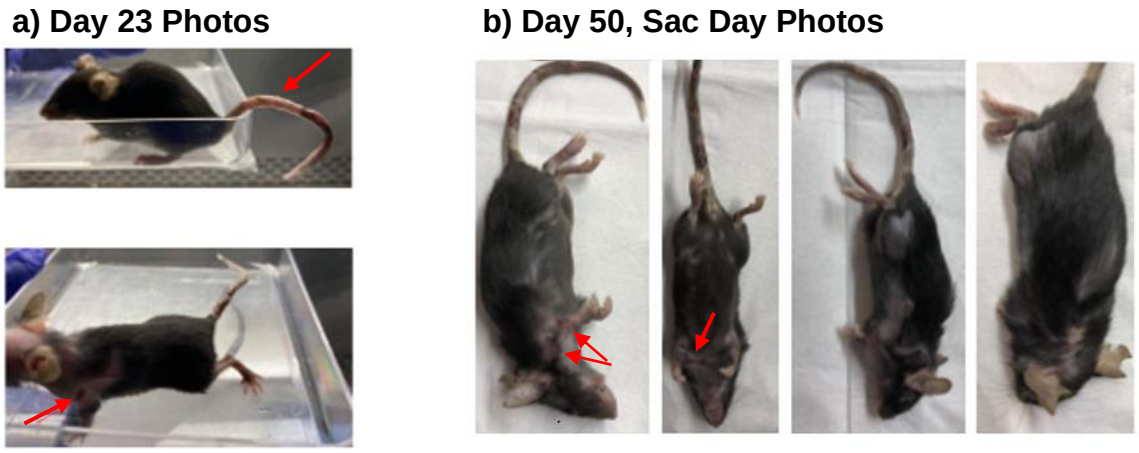


**Supplemental Figure 2.13 | Rag2$^{-/-}$ mice after adoptive transfer of Dsg3$^{-/-}$ splenocytes.** (A) Rag2$^{-/-}$ mice on day 23 showing lesions (red arrows) on tail (mouse #2) and on shoulder (mouse #4). (B) Rag2$^{-/-}$ mouse #8 on day 50. Erosive lesions (red arrows) are visible on left leg and shoulder, and on underside of neck. Patches of hair loss (whitish areas) appear on right side and back.

# CHAPTER 3

# LSECs AS KEY PLAYERS IN PROMOTING ANTIGEN-SPECIFIC TOLERANCE

## 3.1 Abstract

The liver is known as a tolerogenic organ, as evidenced by the spontaneous acceptance of liver transplants with low-dose immunosuppression, as well as less beneficial effects such as the persistence of chronic infectious liver diseases like hepatitis B or C, and malaria. This predisposition to induce immune tolerance is posited to be out of necessity due to the constant exposure to toxins and microbial byproducts from the portal vein and the need to avoid a constant and pathogenic state of inflammation. LSECs are especially exposed to these classically immune activating substances as they line the sinusoids of the liver. LSECs have been shown to induce T cell deletion and regulatory T cells. The aim of this study was to develop tools that could be used to understand the significance of the role LSECs play in the tolerogenic environment of the liver and to identify possible mechanisms of tolerance within the liver to enable the design of therapeutics for antigen-specific tolerance therapies. We developed an LSEC isolation protocol that achieves extremely high purity. A subset of LSECs that expressed MHC II was identified as part of our characterization efforts. An array of cell culture techniques failed to maintain LSECtin expression in primary LSECs *in vitro*. We reached an AAV transfer plasmid design that will be able to test LSEC-specific promoter candidates *in vivo*. In a proof of concept, transfected immortalized LSECs achieved similar antigen presentation as antigen-pulsed immortalized LSECs in a T cell coculture.

## 3.2 Introduction

### 3.2.1 Liver as a Tolerogenic Environment

Examples of the liver as a tolerogenic organ range from its success in long-term acceptance of liver allografts without immune suppression to the prevalence of chronic hepatic infections. Crispe et al. notes that long-term survival of human liver allografts has been shown to be successful without the use of immunosuppression. This implies that T cell mediated alloresponses do not play a major role in human liver transplants [73]. To understand why and how the liver operates as a tolerogenic organ, researchers have investigated the liver's vasculature and unique cell types. The liver receives 70-80% of blood from the portal vein, which provides constant exposure to gut-derived antigens [39]. Researchers hypothesize that this constant exposure to harmless antigens from food and commensal bacteria necessitates a tolerogenic environment to avoid unnecessary and chronic inflammation. However, the liver is also the target of viruses and parasites so the ability to switch to an activating/adaptive immune response is required to control infection. A network of liver-resident antigen presenting cells (APCs) carefully monitors antigens present in the liver and controls the switch from tolerance to activation. Out of these APCs, LSECs constitute the largest surface area of the liver sinusoids and therefore have the highest potential for frequent interactions with immune cells [74].

### 3.2.2 Role of LSECs in Clearance and in Regulation

LSECs occupy a strategic location in the liver sinusoid by forming the border between the bloodstream and the hepatocytes, and with the aid of hepatic stellate cells control the flow of blood reaching the hepatocytes as well as what particulates reach the hepatocytes [75, 76]. As the blood slowly flows through the sinusoids, LSECs remove pathogens, macromolecules, circulating antigens, and viruses [77]. In their role of clearance, LSECs employ receptors on their surface to

aid in the detection and endocytosis of various materials. The pattern recognition receptors (e.g., Toll-like receptors TLR2, TLR3, TLR4, TLR6/2, TLR8 and TLR9) [77, 78] expressed by LSECs bind distinct motifs evolutionarily conserved in pathogens. For example, LSECs release IL-6 when increased levels of lipopolysaccharides (LPS), a component of gram-negative bacteria, are detected [76, 79]. The LSEC-released IL-6 activates hepatocytes to initiate an innate immune response with the release of C-reactive protein and complement factors [76, 80]. With its strategic location and its ability to detect small amounts of LPS, LSECs serve in the crucial role of a sentinel raising the alarm of a potential microbial invader.

Other receptors on LSECs include endocytic receptors which are used for the clearance of various cellular and extracellular components. Examples of these receptors are stabilin-1, stabilin-2, scavenger receptors, mannose receptor, and FcγRIIb2. The FcγRIIb2 receptor is used to endocytose small IgG immune complexes. Because LSECs express an overwhelming proportion of RIIb in the body, researchers have suggested that exhausting LSECs' clearance capacity leads to the manifestation of immune complex disease [77]. Another type of LSEC receptor is C-type lectin receptors, such as L-SIGN and LSECtin. Expression of these receptors initiates the removal of a wide variety of molecules from the blood, primarily by the recognition of mannose residues. In this way, pathogens are cleared from the body [76].

The LSECtin receptor also serves in the regulation of T cells by silencing T cell activation. When LSECtin binds to CD44 on the surface of an activated T cell, the inhibition of T cell activation, proliferation, and effector function occurs [81]. LSECs can also prevent dendritic cells from activating CD8 T cells. LSECs accomplish this by first attaching to the T cell, then drawing the T cell LFA-1 receptors towards the LSEC. Facilitating binding to the dendritic cell, LFA-1 is critical for the immunological synapse between the T cell and the dendritic cell. By drawing LFA-

1 away from the immunological synapse, LSECs inhibit T cell activation [76]. These methods of LSEC regulation of T cells are especially effective because LSECs have an intercellular adhesion molecule (ICAM) receptor that allows lymphoid cells to adhere to their surface. This adherence increases the opportunity for LSECs to be in contact with T cells, and thus be able to regulate their activation.

### 3.2.3 Interaction between LSECs and CD8 T cells

LSECs have many shared attributes with antigen presenting cells (APCs), such as dendritic cells (DCs), only one of which is the ability to endocytose antigens. Similar to APCs, LSECs express major histocompatibility complex (MHC) I and MHC II, have costimulatory markers CD80 and CD86, can present antigen directly to T cells, and can cross-present antigen to CD8 T cells [76, 77, 78]. LSECs uptake antigen 10-50 times faster than DCs, however they do not retain the antigen as long as DCs. LSECs dynamically present antigen with the ability to quickly transport the endocytosed antigen transcytotically to hepatocytes [76].

Another difference between LSECs and DCs occurs when LSECs cross-present soluble antigen to CD8 T cells. Naïve CD8 T cells that interact with immature DCs, which have encountered antigen without the presence of danger signals, are clonally deleted or anergized. However, when naïve CD8 T cells encounter LSECs in conditions with no danger signals, tolerance results from programmed death-ligand 1 (PDL-1) signaling of the LSEC [39, 77, 82]. Grant et al. describes the interaction between LSECs and CD8 T cells [39]. A decrease in CD80 and CD86 expression occurs, and at the same time PDL-1 expression increases on the LSEC, and programmed death-1 (PD-1) expression increases on CD8 T cell. This results in co-inhibition, which occurs during a state of no infection and low antigen concentration. As a result, LSECs induce tolerance in CD8 T cells. LSEC antigen presentation increases linearly with increasing

antigen concentration, whereas PD-L1 expression reaches a ceiling. During an infection, the antigen concentration is high and CD8 T cells release IL-2 by autocrine signaling. Increasing TCR signaling overrides plateaued co-inhibition signals, and LSECs induce CD8 T cell activation [39]. Researchers have previously proposed that LSECs induce tolerance in the CD8 T cell compartment though clonal deletion and induction of anergy [83, 84]. Several studies have shown that LSEC cross-presentation of soluble antigen leads to anergy and deletion of naïve CD8 T cells [84, 85, 86, 87]. For example, one *in vivo* study demonstrated the ability of LSECs to cross-present soluble antigen and induce CD8 T cell tolerance. After 24h following treatment with OVA, LSECs from OVA treated C57BL/6 mice were adoptively transferred into untreated C57BL/6 mice. One week later the untreated C57BL/6 mice were challenged with a syngeneic tumor cell line transfected with ovalbumin (RMAova). Three of six mice that received LSECs from OVA-treated mice developed tumors, whereas all six control group mice rejected the tumor cells and did not develop tumors [84].

In addition to inducing tolerance, new evidence points to the induction of a memory-like T cell. One study shows that LSEC-primed CD8 T cells do not undergo clonal deletion, but travel to the lymphoid tissues after activation [88]. Unlike central memory CD8 T cells, LSEC-primed CD8 T cells have a more limited transcriptome profile, with transcription factors Eomes and Stat3 similarly to central memory T cells, and unique factors Zbtb32, E2F2.48 [76]. Knolle et al. proposes that LSEC-primed CD8 T cells serve an important role during the early stages of viral infections, when viral antigen concentrations are too low for DCs to become activated and initiate an immune response. The LSEC-primed CD8 T cell can travel to the lymph node where it can wait for re-activation when the infection or viral antigen concentration becomes high [76]. Further

studies are needed to reconcile these observations and form a cohesive model of LSEC and T cell interactions.

### 3.2.4 Interaction of LSECs and CD4 T cells

When LSECs interact with CD4 T cells, it can lead to the differentiation of naïve CD4 T cells into CD4+ Foxp3+ regulatory T cells (Tregs). LSECs can both produce and recruit TGF-β, which is essential to activate Tregs. When Tregs are activated by LSECs they induce tolerance. LSEC-induced Tregs have been shown to improve the condition of mice with autoimmune encephalomyelitis and autoimmune hepatitis [77, 82]. In another example, immune tolerance by LSEC generation of CD4+ Foxp3+ regulatory T cells (Tregs) was induced by using a nanoparticle-based autoantigen delivery system. The delivery system selectively delivered autoantigen peptides to LSECs. Carambia et al. prevented autoimmune encephalomyelitis (EAE) from developing in the mouse autoimmune disease model of EAE, and even reversed established EAE disease in mice [29]. This demonstrated Treg induction by LSECs for immune tolerance.

### 3.2.5 Why Study LSECs

We want to test the hypothesis that LSECs play a major role in peripheral tolerance. By expressing insulin in LSECs for presentation, we can recapitulate results from a study done by Akbarpour et al. that showed that insulin B chain 9–23 gene transfer to hepatocytes protected mice from type 1 diabetes by inducing Ag-specific FoxP3+ Tregs [18]. The rationale for this experiment is that LSECs have been shown to uptake antigen from hepatocytes for presentation on MHC II and cross-presentation on MHC I [76]. Directly expressing insulin in LSECs would show that LSECs are the antigen presenting cells mediating tolerance and not hepatocytes.

## 3.3 Results

### 3.3.1 LSEC Isolation and Characterization

Methods of LSEC isolation and characterization are diverse with no agreed-upon standard among the many researchers that work with them [77]. We have built upon existing isolation methods to create a reliable and rigorous isolation protocol. Murine livers are perfused and digested according to the specifications set out by Meyer et al. [89]. Briefly, we use a peristaltic pump to perfuse the liver with a catheter through the inferior vena cava and cut the portal vein. We perfuse with 25 mL Calcium-free Hank's Balanced Salt Solution containing penicillin, streptomycin, heparin, glucose, HEPES, and EGTA. We digest with 25mL Iscove's Modified Dulbecco's Medium (IMDM) containing Glutamax, collagenase type 4, and DNAse type 1. The liver is extracted and shredded in Dulbecco's Modified Eagle's medium (DMEM). The released cells are passed through a 70 μm filter and then centrifuged at 60 x g for 10 minutes to pellet hepatocytes. The supernatant is collected and the cells are pelleted at 680 x g for 10 minutes, then resuspended in 10mL DMEM. Following Smedsrød's protocol, the cells are laid on top of a density gradient of 50% cold Percoll in PBS and 25% cold Percoll in PBS [90]. With the centrifuge set for minimal acceleration and deceleration, the density gradient is spun at 1350 x g for 30 minutes. Cell separation is pictured in Figure 3.1a. The layer containing LSECs and lymphocytes is stained for CD45, CD31, Stabilin-2, and a live/dead stain. Cells are sorted using Fluorescence-activated cell sorting (FACS) and LSECs are selected as the population that is Stabilin-2 and CD31 positive. A representative plot is shown below in Figure 3.1b.

To verify that the isolated cells were indeed LSECs we used quantitative real-time PCR to validate expression of LSEC genes and the absence of genes not associated with LSECs. The results can be seen in Figure 3.2a where we can see expression of liver and lymph node sinusoidal

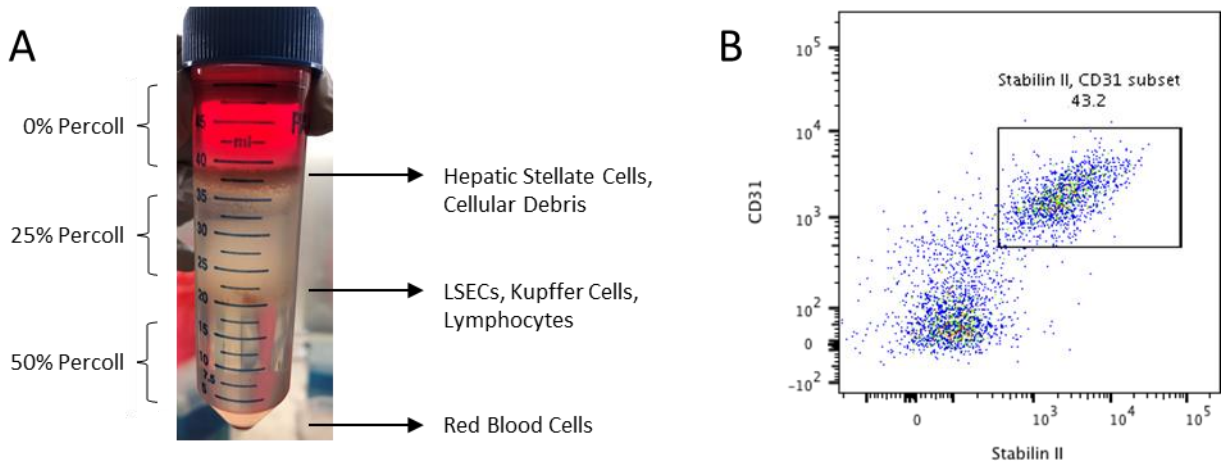


**Figure 3.1 | Density gradient and FACS steps in LSEC isolation technique.**
(A) Diagram of layers and cell separation in Percoll density gradient. The cell layer between 50% Percoll and 25% Percoll is collected for staining and sorting. (B) Representative plot of LSEC population P3 (CD31+ Stabilin-2+ CD45-) collected during FACS.

endothelial cell C-type lectin (LSECtin) with gene name Clec4g, Mannose Receptor C-Type 1 (Mrc1), and Von Willebrand factor (vWF). We also collected CD45+ cells and CD45+ CD19+ cells as controls that do not express LSECtin mRNA and do express CD45 and CD19 mRNA as expected.

A point of controversy between researchers that work with LSECs is how long LSECs can be cultured *in vitro* and retain their characteristics. Many studies focusing on the immunological role of LSECs do not publish data on cell identity and purity after the cells are cultured. As a preliminary experiment, we cultured LSECs on various coatings and in various media. In Figure 3.2b, our qPCR data taken at time of isolation (day 0), day 1, and day 3 show rapid loss of LSECtin, vWF, transforming growth factor beta (TGF- β), programmed death-ligand 1 (PD-L1), and Stabilin-2 expression. This presents a caveat when interpreting results from *in vitro* studies that meaningful LSEC changes are likely occurring during culture.

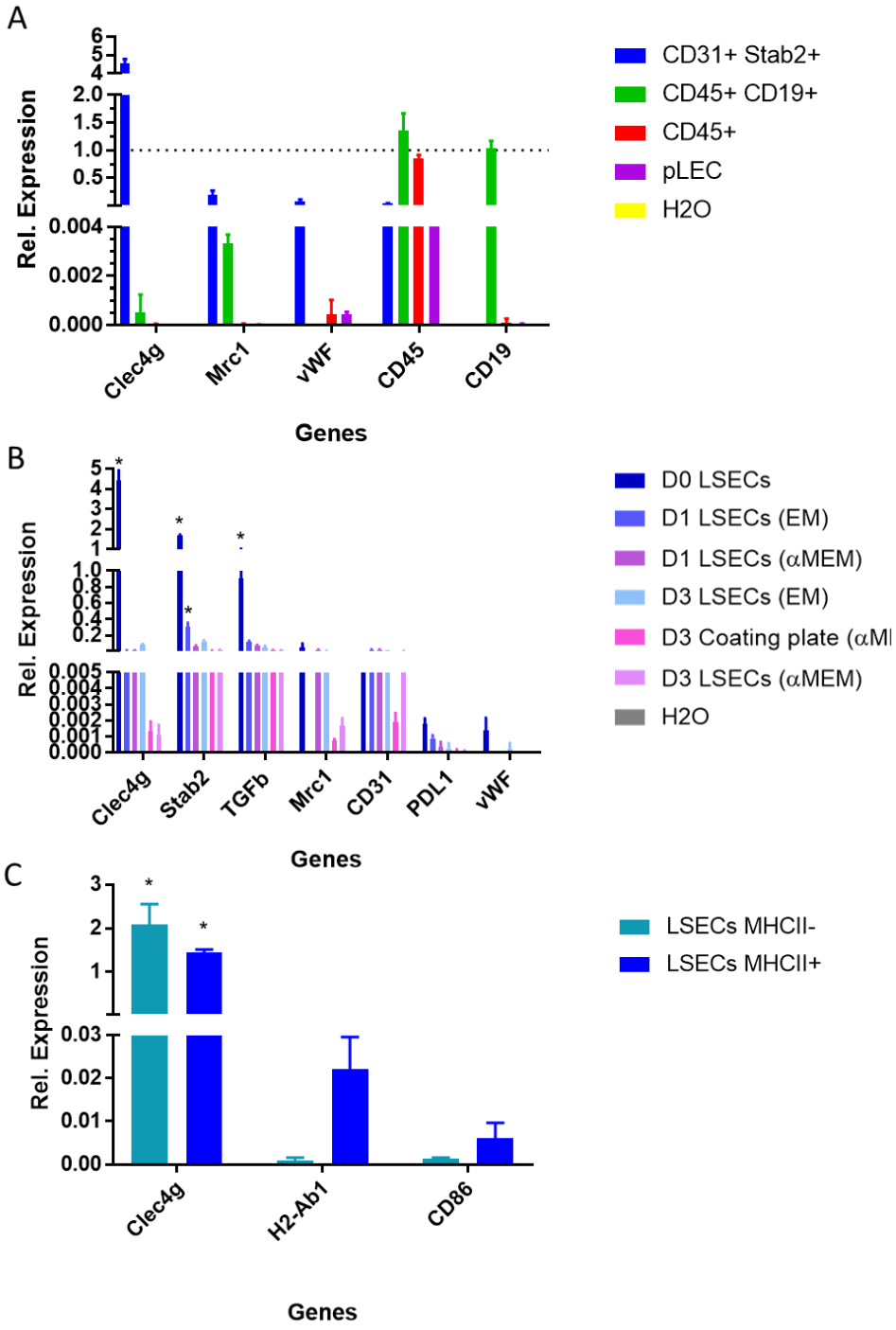


**Figure 3.2 | LSEC characterization through qPCR.** (A) Relative gene expression by LSECs, CD45+ cells, CD45+ CD19+ cells, and cultured primary lymphatic endothelial cells (pLECs) from C57BL/6J mice. (B) Relative gene expression by LSECS from Balb/c mice at time of isolation, day 1, and day 3 of culture in endothelial cell medium (EM) or modified Eagle's Minimum Essential Medium (αMEM) on collagen coated plates or plates coated with a coating solution of PureCol and human plasma fibronectin (Coating plate).

**Figure 3.2 continued.** (C) Relative gene expression of LSEC subsets from C57BL/6J mice. In all experiments gene expression is relative to housekeeping gene beta actin.

Abbreviations: C-Type Lectin Domain Family 4 Member G (Clec4g); Mannose Receptor C-Type 1 (Mrc1); Von Willebrand factor (vWF); cluster of differentiation 45 (CD45); cluster of differentiation 19 (CD19); Stabilin-2 (Stab2); Transforming growth factor beta (TGF-β); cluster of differentiation 31 (CD31); Programmed death-ligand 1 (PDL1);
histocompatibility 2, class II antigen A, beta 1 (H2-Ab1); cluster of differentiation 86 (CD86)

Another complicating factor in LSEC studies is the fact that at least two subpopulations of LSECs exist, and differing isolation techniques could be favoring different subpopulations. During our own characterization of LSECs we have isolated, we have seen two subpopulations using fluorescent staining and flow cytometry. One population was MHC II and CD80/86 high, and the other population was MHC II and CD80/86 low. Based on these results, we performed an isolation where we also stained for MHC II and during the FACS step we separated our two new LSEC subpopulations. Performing qPCR, we confirmed the difference in MHC II and CD 86 expression (Figure 3.2c). Single-cell RNA sequencing has shown clearly defined existing subpopulations and the extent of heterogeneity within LSECs [91, see 3.4 Discussion].

To further prove that our method of LSEC isolation was successful, we took scanning electron microscopy (SEM) of isolated cells to confirm the hallmark of LSECs, which is the fenestrations organized into sieve plates (Figure 3.3). With this proof, we were satisfied with our method of isolation.

Another way we characterized LSECs further was by fluorescently imaging liver sections. Figure 3.4 shows Stabilin-2 staining the sinusoids of the liver, showing that it is a potent surface marker of LSECs. We also observe nuclear staining of transcription factor prospero homeobox protein 1 (PROX1), which is a master control gene for lymphangiogenesis during early embryonic development, as well as punctate staining of gp38 which promotes DC migration. Both LSECs and LECs have minimal basement membranes and loosely organized cell junctions. Their

similarities have interesting implications for research in both cell types, including for the research covered in the next section, finding an LSEC-specific promoter.

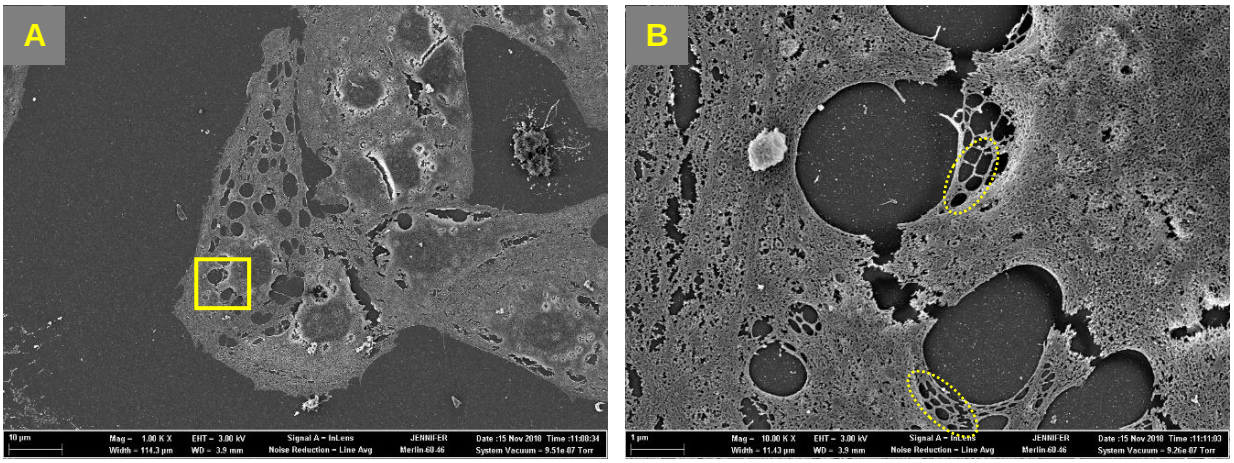


**Figure 3.3 | LSEC morphology confirmation by SEM.** Scanning electron microscopy (SEM) of isolated LSECs shows several sieve plates containing numerous fenestrations. (B) is 10x magnification of the region highlighted in (A) and shows multiple fenestrations arranged into sieve plates (yellow circles).

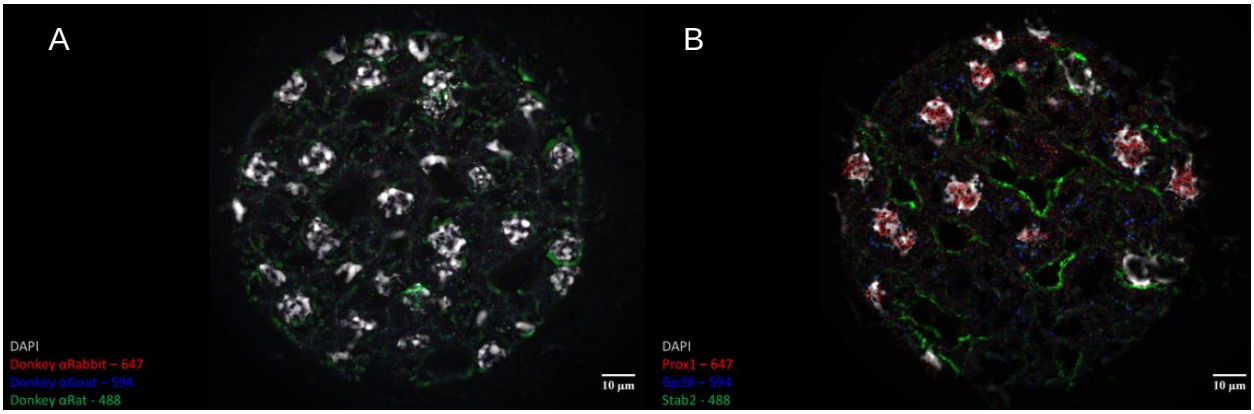


**Figure 3.4 | Shared LSEC and LEC markers on LSECs shown by immunofluorescent staining of liver sections.** (A) Background: Liver sections stained with Donkey αRabbit- 647, Donkey αGoat – 594, Donkey αRat – 488 secondaries only show no binding. (B) Liver sections stained with Stab2, a marker for LSECs, shows LSECs lining sinusoids of liver (green); transcription factor prospero homeobox protein 1 (PROX1) (red) and podoplanin (gp38) (blue), markers for lymphatic endothelial cells (LECs) shared by LSECs.

### 3.3.2 Generation of LSEC-Specific Promoter Candidates

The first step in identifying an LSEC-specific promoter is to find a protein that is expressed exclusively in LSECs. Possible candidates were identified by examining available liver transcriptomes and proteomes. These candidates were then screened using The Human Protein Atlas to check for expression in other tissues. LSECtin, gene name Clec4g, showed the most promise as expression is limited to the liver and lymph node. Because the vehicle and route of administration is a lentivirus delivered intravenously, the liver and spleen should be heavily infected compared to the lymph node [92]. Therefore, based on the anticipated distribution of lentivirus and the specificity of the Clec4g expression, the desired gene expression should be specific to LSECs in the liver. Although the LSEC-specific Clec4g promoter has not been used in published experiments and is not commercially available, gene databases such as Ensembl have predicted regions for the location of the promoter. Plasmids packaged into lentiviruses have a size limit of around 12 kilobases. This leaves around 1,000 base pairs for the promoter. The predicted promoter region of Clec4g is approximately 5,000 base pairs long. Therefore, a chromosome walking test is needed to identify a segment of the predicted region that properly initiates gene transcription. In a chromosome walking test, 1,000 base pair segments are used in plasmids as promoter candidates controlling the expression of a reporter, such as a fluorescent reporter. The plasmids are then transfected into LSECs and other cell types. Successful candidates induce expression of the reporter in the target cell type, LSECs, whereas other cell types will not express the reporter. A general promoter is used as a positive control that ensures the transfection was successful, and untransfected cells are used as a negative control that accounts for background fluorescence. Once a promoter is successful *in vitro*, it can be packaged in lentivirus and be delivered intravenously in mice for a biodistribution study.

Promoter candidates from predicted promoter regions identified by gene database Ensembl, company Genecopoeia, and a paper by Dominguez-Soto et al. (Figure 3.5) [93] were generated by using the chromosome walking test. These promoter candidates were cloned into a plasmid with a fluorescent reporter, green fluorescent protein (GFP). Plasmids were sent to the University of Chicago Comprehensive Cancer Center DNA Sequencing Facility for sequencing to


**Figure 3.5 | Promoter candidate location on mouse chromosome 8.**
Promoter candidates are shown as gray bars. LSECtin is encoded on the reverse strand, so transcription occurs in the anti-sense direction. Protein coding regions for LSECtin are shown by the blue and orange arrows. Promoter candidates cover the Ensembl predicted promoter region in 1,000 base pair segments. Additional promoter candidates focus on the predicted promoter regions reported by company Genecopoeia and promoter region predicted by Dominguez-Soto et al. Predicted promoter regions are shown in red relative to chromosome 8 position shown in turquoise. From Dominguez-Soto 2009 *Hepatology* [93].

verify their successful creation. Plasmids were then transfected into Human embryonic kidney cells 293T (HEK293T) cells, Chinese hamster ovary (CHO) cell line DG44, and primary lymphatic endothelial cells (pLECs) by first incubating the plasmids with the polycation polyethylenimine (PEI) to form positively charged complexes that bind to anionic cell surfaces. As expected, expression in HEK 293T cells and CHO-DG44 cells of GFP was lower for plasmids with the potential promoters than for plasmids with the constitutive cytomegalovirus (CMV) promoter (Figure 3.6). Primary LECs should express LSECtin, so we should see expression with the

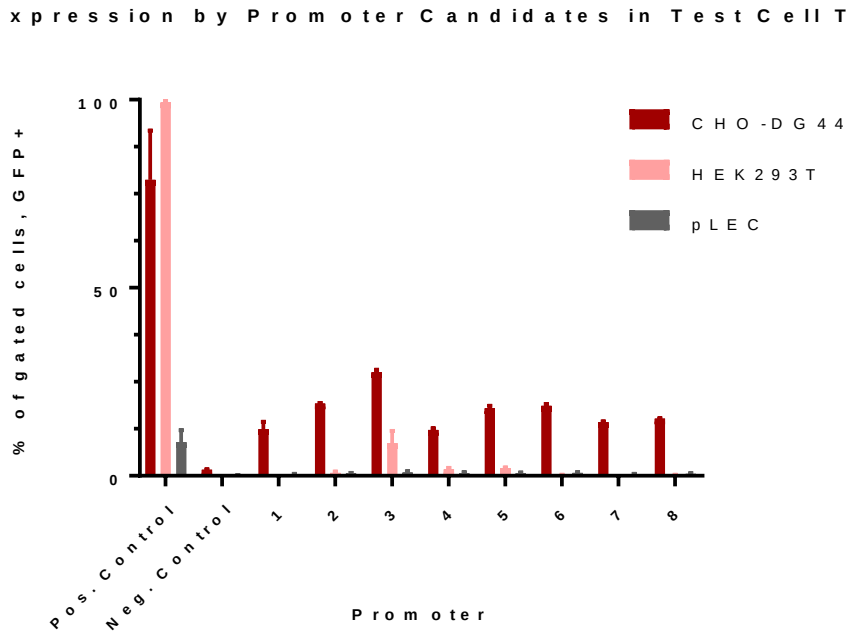


**Figure 3.6 | Green fluorescent protein expression in off-target cells and primary LECs.** Minimal GFP expression is seen in the transfection of pLECs due to loss of LSECtin expression and low transfection efficiency. CHO-DG44 and HEK293T cells show strong GFP expression with transfection with the positive control plasmid and minimal expression in the negative control plasmid. CHO-DG44 expression is less selective than HEK293T expression as seen by higher GFP expression levels by the percent of GFP+ cells across promoter candidates, and even in the negative control.

promoter candidates. However, since qPCR experiments showed no expression of LSECtin in the cultured pLECs, the lack of GFP expression in the transfection of pLECs is in agreement. Additionally, the results for pLECs were more difficult to interpret due to a low transfection efficiency of under 10% compared to efficiencies of 100% and 80% in HEK293T cells and CHO-DG44 cells, respectively. One complication in our current method of LSEC isolation is the use of an antibody that is fluorescent in the same channel as GFP. To address this issue, we cloned promoter candidates into a new plasmid with several advantages. The fluorescent reporter was mCherry, which has less background signal in cells. The plasmid was also compatible with lentiviral packaging. In the event of low transfection efficiencies using PEI or lipid-based

transfection agents with LSECs, we would be able to package the plasmids into lentivirus to maximize gene transfer.

In fact, we were met with three great challenges. The first, detailed in the next section is that LSECs proved difficult to transfect cells. The second is that as shown above, LSECs rapidly lose LSECtin expression *in vitro*. Despite many efforts to find culture conditions that kept LSECtin expression including various coatings and media, cocultures, and transwell plates, we could not find any conditions that kept LSECtin expression. The third challenge is that although we were able to transduce LSECs with lentivirus, our lentiviral production protocol did not produce titers high enough for *in vivo* delivery, which is necessary due to the loss of LSECtin expression *in vitro*. Therefore, we again went back to the drawing board and designed a new plasmid compatible with AAV packaging to be tested in future work.

### 3.3.3 LSECs as difficult to transfect cells

With our lentivirus transfer plasmid with mCherry reporter, we first tried multiple transfection methods using a positive control plasmid where the mCherry reporter expression was controlled by a constitutive CMV enhanced chicken beta actin promoter. As shown in Figure 3.7a, HEK cells were readily transfected with PEI yielding 80% mCherry+ cells. In contrast, LSECs did not reach over 1% of mCherry+ cells when transfected with PEI or Lipofectamine, and this was at similar levels as seen with the negative control. These results were also measured by the mean fluorescent intensity of mCherry+ cells (Figure 3.7b). After producing lentivirus and transducing LSECs, we saw a 2% increase in mCherry+ cells (Figure 3.7c). After calculating a functional titer, we realized that we could not achieve the volume of production needed for *in vivo* experiments, and began to clone AAV transfer plasmids.

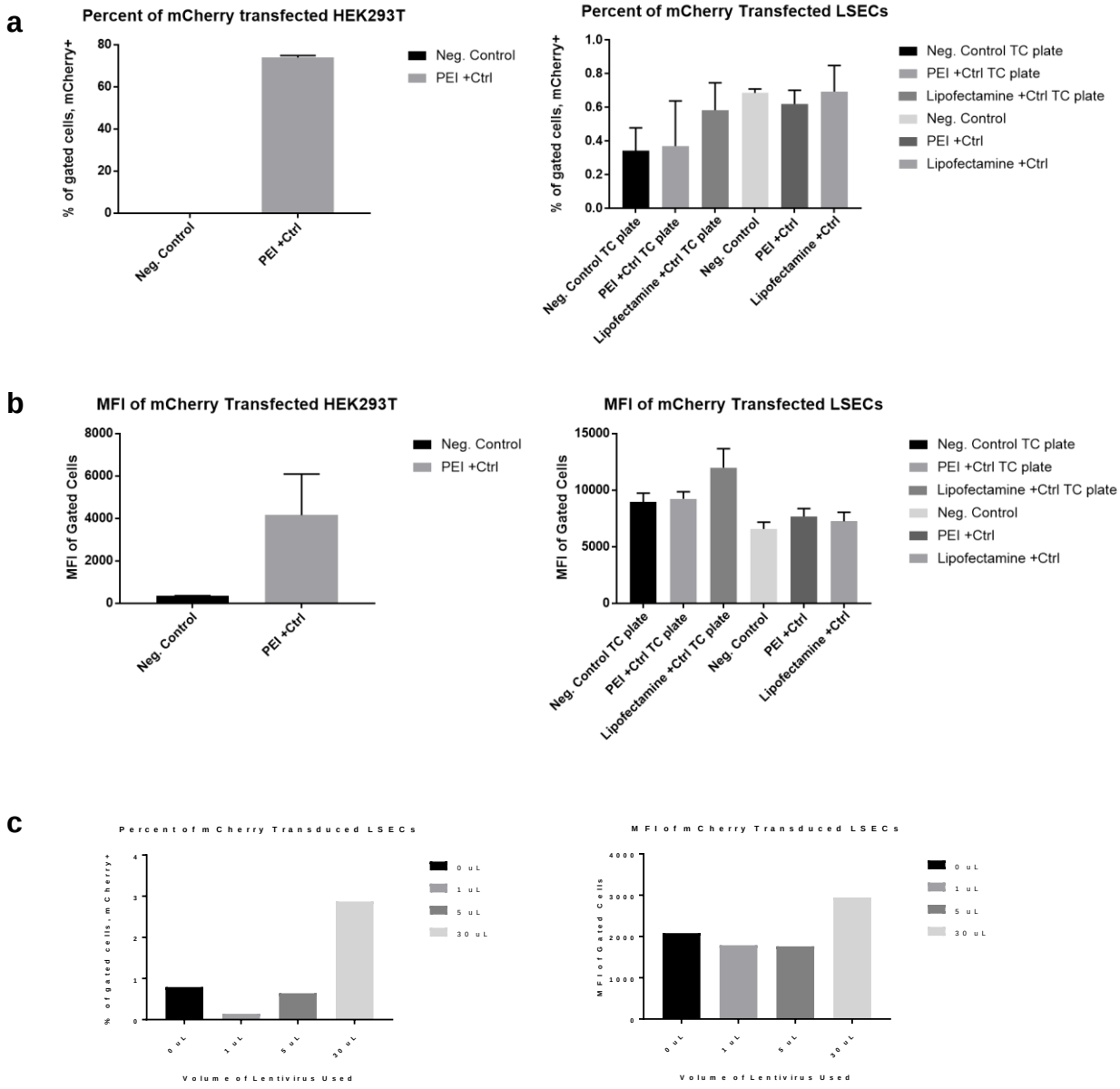


**Figure 3.7 | Fluorescent reporter mCherry.** (A) The efficiency of mCherry transfection into HEK293T and LSECs as shown by percent of mCherry+ cells. (B) The mean fluorescence intensity (MFI) of mCherry+ cells after transfection of HEK293T and LSECs. (C) Lentiviral transduction of mCherry into LSECs as shown by percent of mCherry+ cells and MFI of mCherry+ cells.

### 3.3.4 LSEC and T cell cocultures

In addition to the efforts to find an LSEC-specific promoter to enable *in vivo* studies of the role and potential use of LSECs in peripheral tolerance maintenance, we concurrently explored LSEC and T cell interactions via cocultures. LSEC isolations with the level of purity achieved by our technique do not yield large quantities, and this is especially true in B6 mice. Therefore, rather than performing cocultures with the standard OTI and OTII cells, we had to use DO11.10 cells, which are the equivalent of OTII cells but with a Balb/c mouse background. Figure 3.8a shows the proliferation of DO11.10 cells after a 3-day coculture with either Balb/c BMDCs or primary Balb/c LSECs and either no antigen, OVA, or MHC II peptide, ISQ stimulation. DO11.10 cells were CFSE labelled before culturing to track cellular divisions. BMDCs were chosen as a control because they are readily available and well-studied APCs with predictable activation in OVA pulsed T cell cocultures. Cocultures were done on collagen-coated or uncoated tissue culture plates. Polyinosinic:polycytidylic acid (Poly I:C) groups were included because Poly I:C is a synthetic analog of double-stranded RNA (dsRNA) and activates TLR3 signaling and cytoplasmic dsRNA sensors such as melanocyte differentiation-associated 5 (MDA5). LSECs express TLR3 and have been reported to respond to TLR3 agonists. We hypothesized that Poly I:C would activate LSECs, which in turn would activate T cells in coculture. This appears to have been the case in comparing the ISQ stimulated conditions on the uncoated plates. Coated plates without stimulation appear to have T cell division in both LSEC and BMDC cocultures, which is a surprising result. Poly I:C on the coated plate seems to have removed this effect in the BMDC coculture. Unfortunately, we did not have enough LSECs to include the Poly I:C and coated plate condition. Figure 3.8b shows IL-10 concentrations of BMDC and T cell cocultures in gray and LSEC cocultures in blue. IL-10 concentrations were highest in BMDC and T cell cocultures

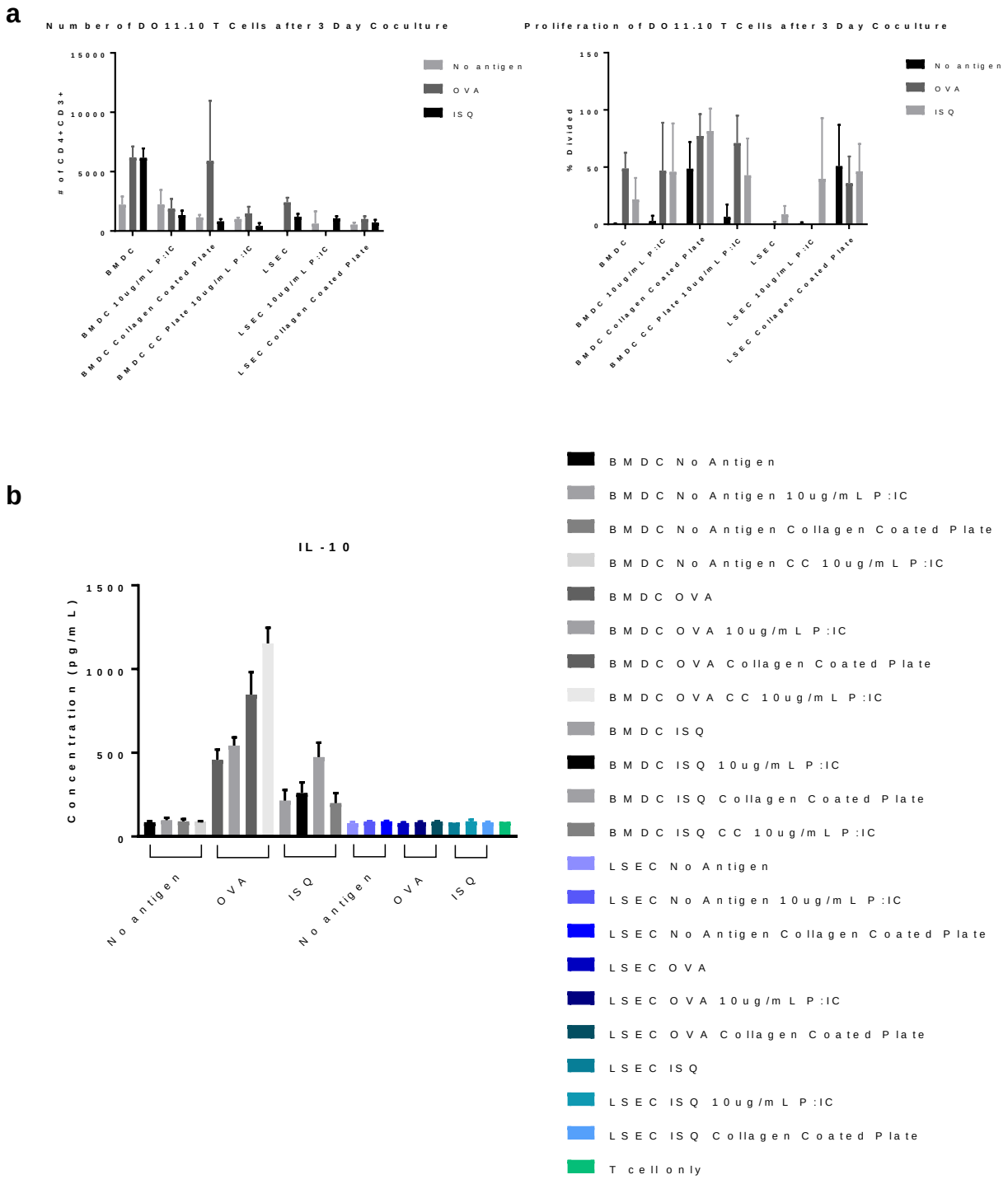


**Figure 3.8 | DO11.10 T cell cocultures with Balb/c LSECs or BMDCs.** (A) Number of CD4+CD3+ and % divided DO11.10 T cells after 3 days coculture with LSECs or BDMCs in coated or uncoated tissue culture plates and stimulation with OVA or ISQ. (B) IL-10 production by these same coculture groups as measured by cytokine ELISA.

stimulated with OVA. Stimulation with ISQ also led to IL-10 production. Interestingly we saw minimal IL-10 production in LSEC and T cell cocultures, matching that of T cell culture alone.

In order to further test why we did not see consistent activation using Poly I:C, we then tested a lower and a higher concentration of Poly I:C. Figure 3.9a shows the percent of divided T cells which were antigen experienced after coculture with Balb/c BMDCs or LSECs and stimulation with ISQ, OVA, or a Fab-OVA which targets LSECtin. The concentration of lack of Poly I:C had no effect on the percentage of divided cells that were antigen experienced. We also had the confusing result where T cells were CD44+ CD69+ despite having no antigen in the coculture. Figure 3.9b shows the percent of undivided T cells which were antigen experienced after coculture with Balb/c BMDCs or LSECs and stimulation with ISQ, OVA, or a Fab-OVA which targets LSECtin. We observed similar trends as for the divided cells but at a much lower percentage as we would expect because antigen experience drives division in activated T cells. We might have expected that LSECs not receiving Poly I:C signal would have a higher percentage of antigen experienced cells that were not dividing, and there does seem to be a trend that suggests that may be the case. In looking at CD25+ FoxP3+ divided T cells, we see an increase in the ISQ condition regardless of Poly I:C concentration (Figure 3.9c). However, we also see extremely high percentages of CD25+ FoxP3+ divided T cells in the BMDC cocultures with OVA or ISQ, which is not expected and suggests there was an issue with FoxP3 staining in those samples. Figure 3.9d shows similar trends in percentages of CD25+ FoxP3+ undivided T cells in the BMDC and LSEC cocultures, again at lower magnitudes. Overall, these results are not convincing that LSEC presentation with or without TLR3 signaling imparts a more tolerogenic phenotype on educated T cells.

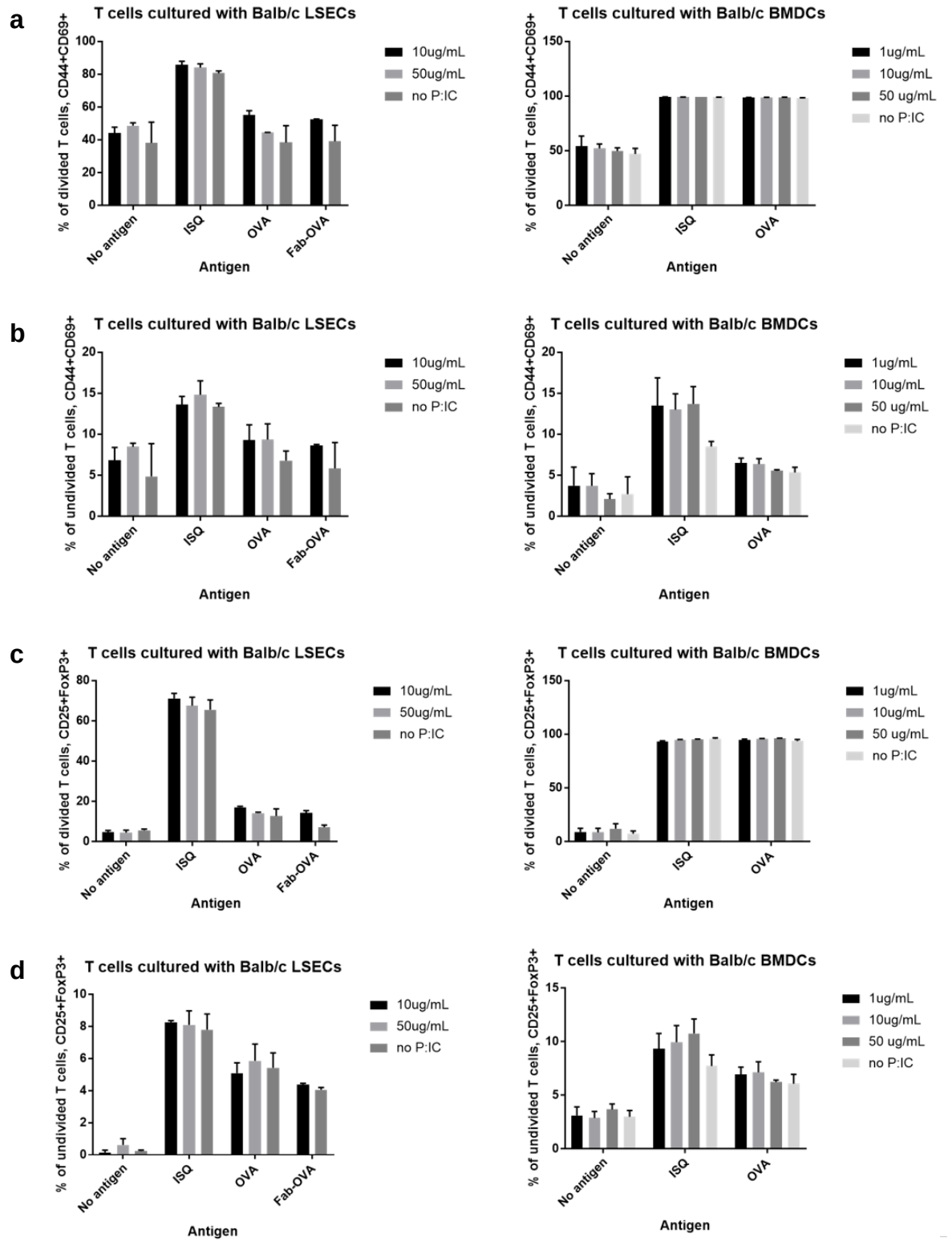


**Figure 3.9 | T cell phenotype of divided and undivided cells after coculture with Balb/c LSECs or Balb/c BMDCs.**

**Figure 3.9, continued.** (A) Percent of divided T cells that are CD44+CD69+ after 3 days coculture with LSECs or BDMCs and stimulation with OVA, LSECtin targeted OVA (Fab-OVA), or ISQ. (B) Percent of undivided T cells that are CD44+CD69+ after 3 days coculture with LSECs or BDMCs and stimulation with OVA, LSECtin targeted OVA (Fab-OVA), or ISQ. (C) Percent of divided T cells that are CD25+FoxP3+ after 3 days coculture with LSECs or BDMCs and stimulation with OVA, LSECtin targeted OVA (Fab-OVA), or ISQ. (D) Percent of undivided T cells that are CD25+FoxP3+ after 3 days coculture with LSECs or BDMCs and stimulation with OVA, LSECtin targeted OVA (Fab-OVA), or ISQ.

What is interesting is the difference we saw in the percent of T cells that divided after coculture with LSECs. In the no antigen and OVA stimulated conditions, we saw significantly less T cell division than in the ISQ stimulated group (Figure 3.10a). There is not a lack of MHC II as seen by the proliferation induced by the ISQ stimulated group. Therefore, the lack of proliferation in the OVA group is likely due to a lack of antigen processing. There was a trend towards increased proliferation with Poly I:C, but not in a dose dependent manner. Figure 3.10b shows numbers of CD25-FoxP3+ divided T cells were the largest in the groups cocultured with LSECs in presence of ISQ antigen. CD25-FoxP3+CD4+ T cells have controversial suppressive ability and may be a heterogeneous population including exhausted T cells and a reservoir for other types of CD4+ T cells. Additional studies would have to be done to directly assess the suppressive function of these T cells.

### 3.3.5 Antigen transfected immortalized LSEC and T cell cocultures

The wide range of reported *in vitro* antigen presentation by LSECs caused by varying degrees of purity and difficultly in preserving LSEC phenotype *in vitro* is highly motivating to develop tools to study LSEC antigen presentation *in vivo*. As an intermediate step, we wanted to see the effect of antigen presentation via transfection *in vitro*. As previously described, primary LSECs have extremely poor transfection efficiency. For this reason, we used an immortalized LSEC (iLSEC) line for T cell cocultures requiring transfection. Because the iLSEC line was

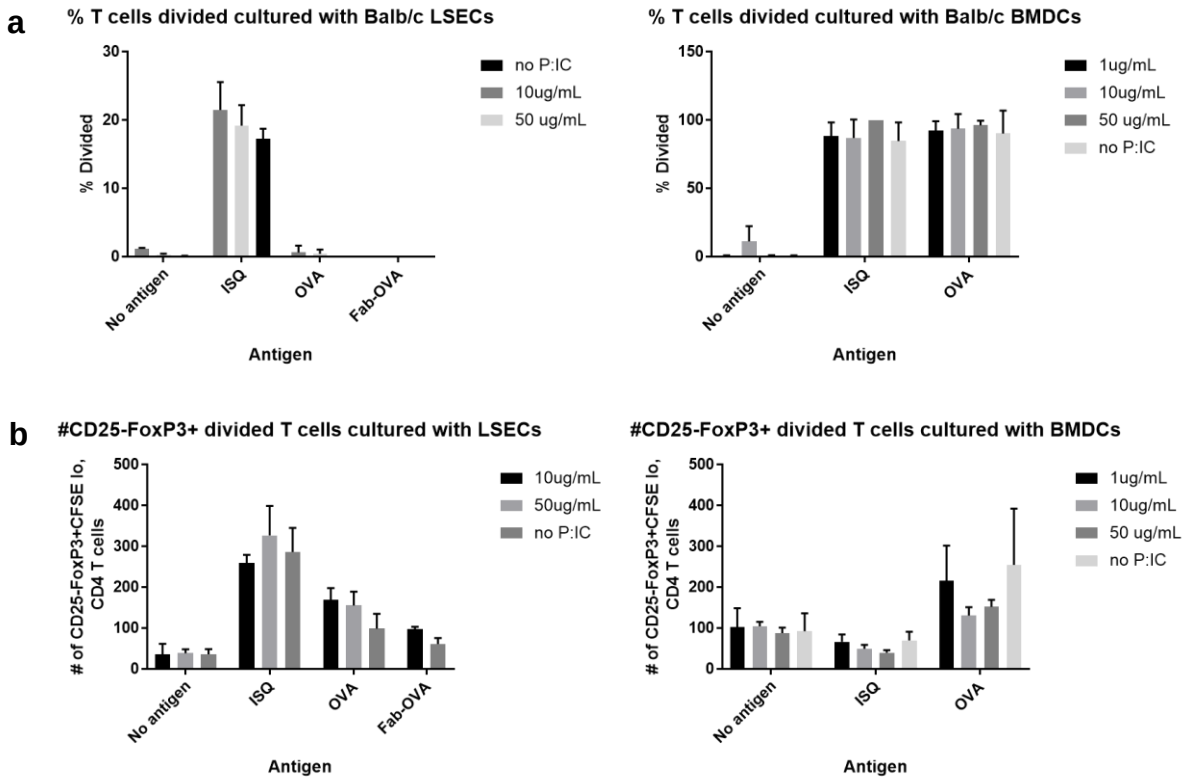


**Figure 3.10 | T cell proliferation and prevalence of CD25-FoxP3+ T cells following T cell coculture with Balb/c LSECs or Balb/c BMDCs in presence of antigen.** (A) Percent of T cells that have divided after 3 days coculture with LSECs or BDMCs and stimulation with OVA, LSECtin targeted OVA (Fab-OVA), or ISQ. (B) Numbers of CD25-FoxP3+ divided T cells were the largest in the groups cocultured with LSECs in presence of ISQ antigen.

created from cells with a B6 background, we were able to perform T cell cocultures using OVA antigens and OTI and OTII cells which also originate from mice with a B6 background. Figure 3.11a shows the division index of OTI cells after 3 days coculture with iLSECs or BDMCs and stimulation with OVA, SIINFEKL ($OVA_{257-264}$), or transfection with OVA plasmids using lipofectamine. OVA plasmids included pOVA cytosol, pOVA membrane, and pOVA secreted, which encode cytosolic, membrane bound, and secreted OVA, respectively. Division index is the average number of cells that a dividing cell became. Plasmids encoding mCherry were used as a transfection control that would not be expected to cause OTI proliferation. BMDCs required LPS to drive T cell proliferation in the secreted OVA and cytosolic OVA transfection conditions. There

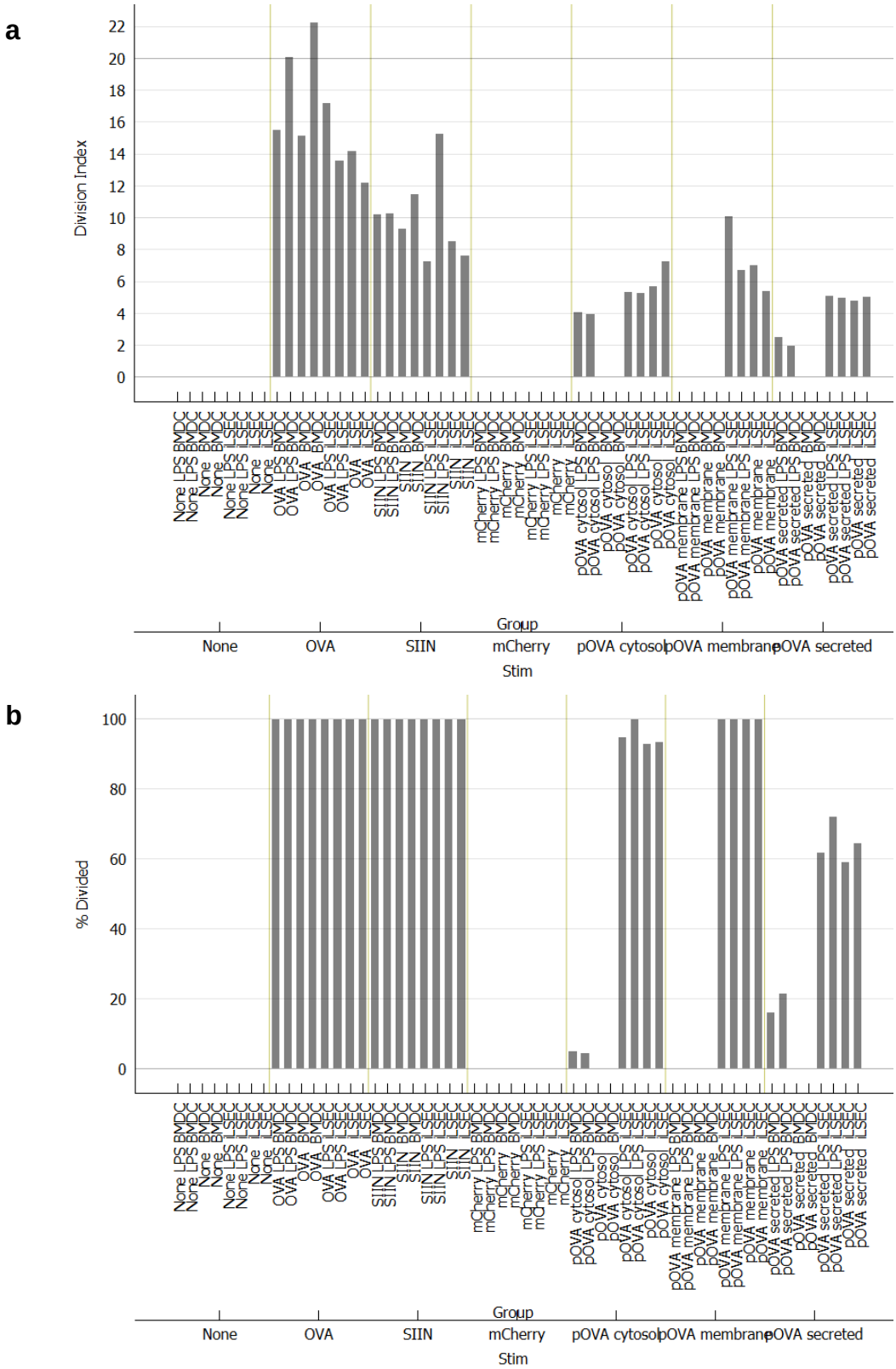


**Figure 3.11 | OTI cell proliferation after cocultures with antigen transfected or antigen pulsed immortalized LSECs or BMDCs.**

**Figure 3.11, continued.** (A) Division index of OTI cells after 3 days coculture with iLSECs or BDMCs and stimulation with OVA, SIINFEKL, or transfection with pOVA cytosol, pOVA membrane, or pOVA secreted. All conditions done with or without the addition of LPS. (B) Percent of OTI cells that have divided after 3 days coculture with iLSECs or BDMCs and stimulation with OVA, SIINFEKL, or transfection with pOVA cytosol, pOVA membrane, or pOVA secreted. All conditions done with or without the addition of LPS. OTI cell proliferation is highest for OVA and SIINFEKL stimulation of iLSECs and BMDCs with or without LPS, and iLSECs transfected with pOVA cytosol and pOVA membrane.

was no OTI proliferation with BMDCs in membrane bound OVA transfection condition. Figure 3.11b shows the percent of OTI cells that divided after 3 days coculture with iLSECs or BDMCs and stimulation with OVA, SIINFEKL, or transfection with OVA plasmids. iLSECs clearly have stronger antigen presentation after OVA plasmid transfections. Unfortunately, transfection efficiencies were not calculated using the mCherry transfected groups as planned. Therefore, we cannot determine if the difference between BMDC and iLSEC transfected groups is due to inefficient transfection of BMDCs or superior iLSEC antigen processing and presentation. We can however compare within a cell type. iLSECs transfected with pOVA cytosol or pOVA membrane drove a higher percentage of OTI division, which would be expected as those cellular locations would enable faster loading of MHC I as opposed to extracellular OVA from pOVA secreted that would require cross-presentation. However, OVA pulsing which is also extracellular had a high percentage of OTI division. It may be that the iLSEC produced OVA did not reach the concentrations of pulsed OVA, or perhaps the glycosylations are different.

Figure 3.12 shows the number of CTLA4+ OTI cells after 3 days coculture with iLSECs or BDMCs and stimulation with OVA, SIINFEKL, or transfection with OVA plasmids. Interestingly there were a large number of CTLA4+ OTI cells after coculture with OVA pulsed BMDCs, although this effect was partially lost with the addition of LPS. The number of CTLA4+ OTI cells is lower in iLSEC coculture groups, but it appears the induction is not LPS dependent.

Interestingly, there were not pronounced differences between transfected iLSEC groups and iLSECs pulsed with SIINFEKL, but there were dramatic decreases in OVA pulsed iLSECs, SIINFEKL pulsed BMDCs and transfected BMDCs compared to OVA pulsed BMDCs.

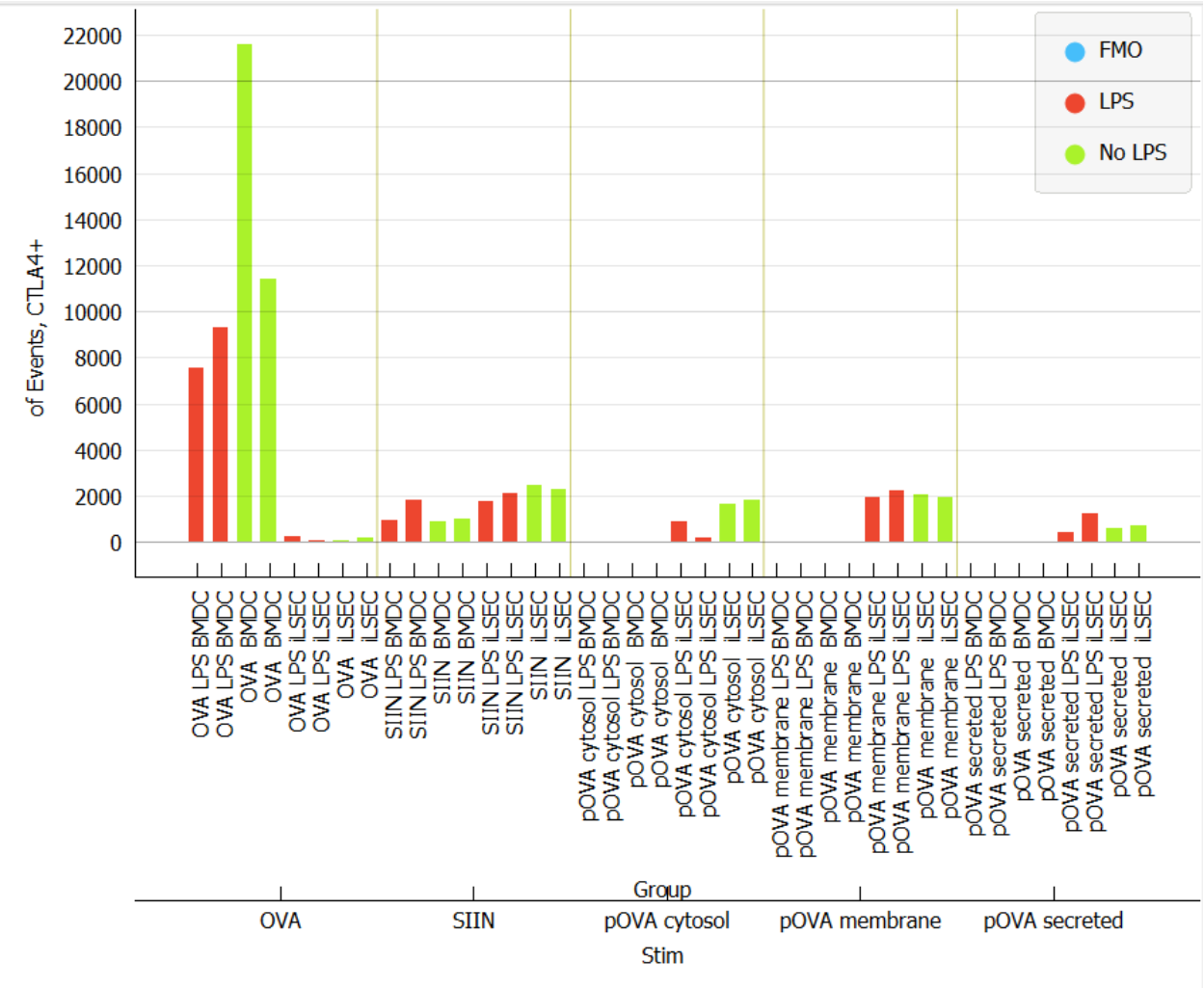


**Figure 3.12 | CTLA4+ OTI cells after cocultures with antigen transfected or antigen pulsed immortalized LSECs or BMDCs.** (A) Number of OTI cells that are CTLA4+ after 3 days coculture with iLSECs or BDMCs and stimulation with OVA, SIINFEKL, or transfection with pOVA cytosol, pOVA membrane, or pOVA secreted. All conditions done with or without the addition of LPS.

Figure 3.13a shows significant differences in the percent of OTI cells that became memory T cells after 3 days coculture with iLSECs or BDMCs and stimulation with OVA, SIINFEKL, or

transfection with OVA plasmids, done with or without LPS stimulation. iLSEC coculture groups show significantly lower percentages of memory T cells. Figure 3.13b specifically shows the marked decrease in the percentage of memory OTI cells after coculture with iLSECs as compared to BMDCs. This is particularly impressive given the greater proliferation seen in iLSEC coculture groups. Similar trends were seen in the percent of effector OTI cells (data not shown). It is possible that the proliferating cells in iLSEC pOVA transfected groups are exhausted as partially supported by CTLA4 expression, or anergic although further studies are needed to explore this possibility.

We performed 3-day cocultures of OTII cells with iLSECs or BDMCs and stimulation with OVA, class II peptide ISQAVHAAHAEINEAGR ($OVA_{323-339}$), or transfection with pOVA cytosol, pOVA membrane, or pOVA secreted. All conditions done with or without the addition of LPS. The percent of divided OTII cells was 5-10% for ISQ stimulated BMDCs and 10-25% for OVA stimulated BMDCs (data not shown). iLSECs cocultures did not have more than 5% of OTII cells divided. There were too few OTII cells to interpret phenotype.

Overall, these results support the further development of tools that enable gene delivery of antigens to LSECs *in vivo*. iLSECs are not clearly inducing tolerogenic fates *in vitro*, but there are no differences between antigen pulsed and antigen transfected iLSEC groups.

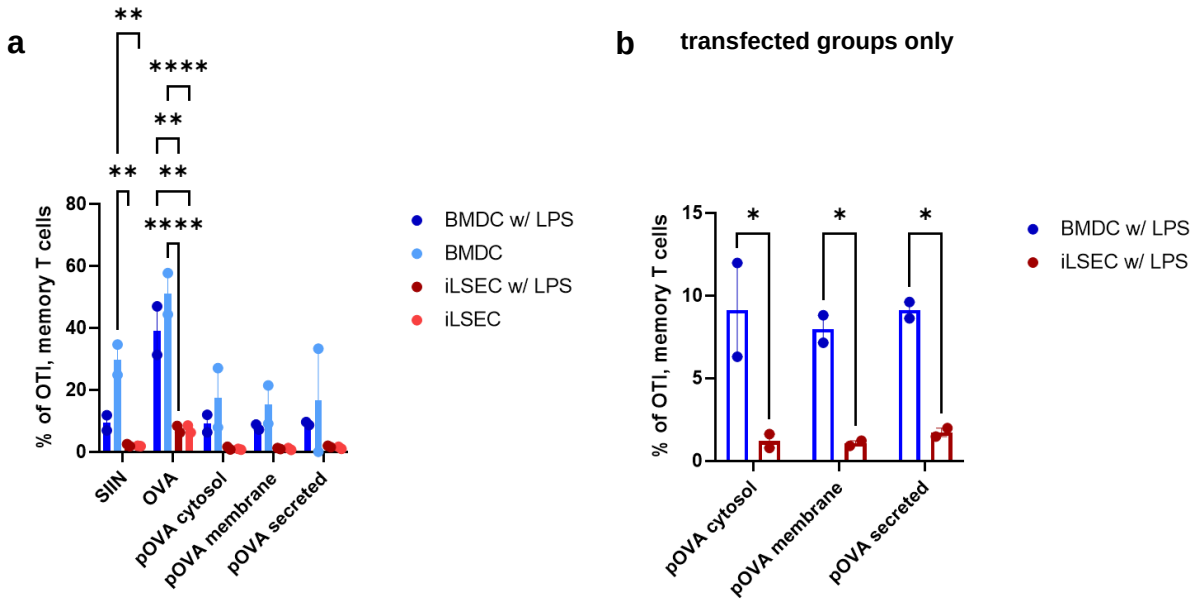


**Figure 3.13 | Percent of memory OTI cells after cocultures with antigen transfected or antigen pulsed immortalized LSECs or BMDCs.** (A) Percent of OTI cells that are memory T cells after 3 days coculture with iLSECs or BDMCs and stimulation with OVA, SIINFEKL, or transfection with pOVA cytosol, pOVA membrane, or pOVA secreted. All conditions done with or without the addition of LPS. All statistical comparisons were performed by one-way ANOVA using Tukey correction.

## 3.4 Discussion

LSECs are an important cell type in the liver that are understudied for their role as antigen presenting cells. The body of work that does exists has a large variety of isolation techniques, the most common of which being centrifuge gradients alone or selective attachment of Kupffer cells. These methods have been shown by our lab and others to have low purity. This adds a layer of complexity to interpreting conflicting reports of LSEC antigen presentation as contaminating macrophages would also be capable of antigen presentation.

In this work, I have described an isolation technique that includes sorting on CD31 and Stabilin-2 expression. Cells positive for CD31 and not Stabilin-2 were not taken as these were larger blood vessel endothelial cells. This isolation technique was shown to have even higher purity than CD146+ magnetic bead purification, which we found to have 5% contaminating cells [94]. Even though these cell marker dependent purification methods achieve high purity, the potential drawback is that we may be enriching for select LSEC subsets over others.

Here I have shown one such subset defined by MHC II expression, but there is also initial evidence in mice for many subsets with varying protein expression based on location within the liver microenvironment. In humans, single-cell RNA sequencing of liver cells has revealed two clusters of LSECs including an MHC II expressing subset (Figure 3.14 and Figure 3.15) [91].

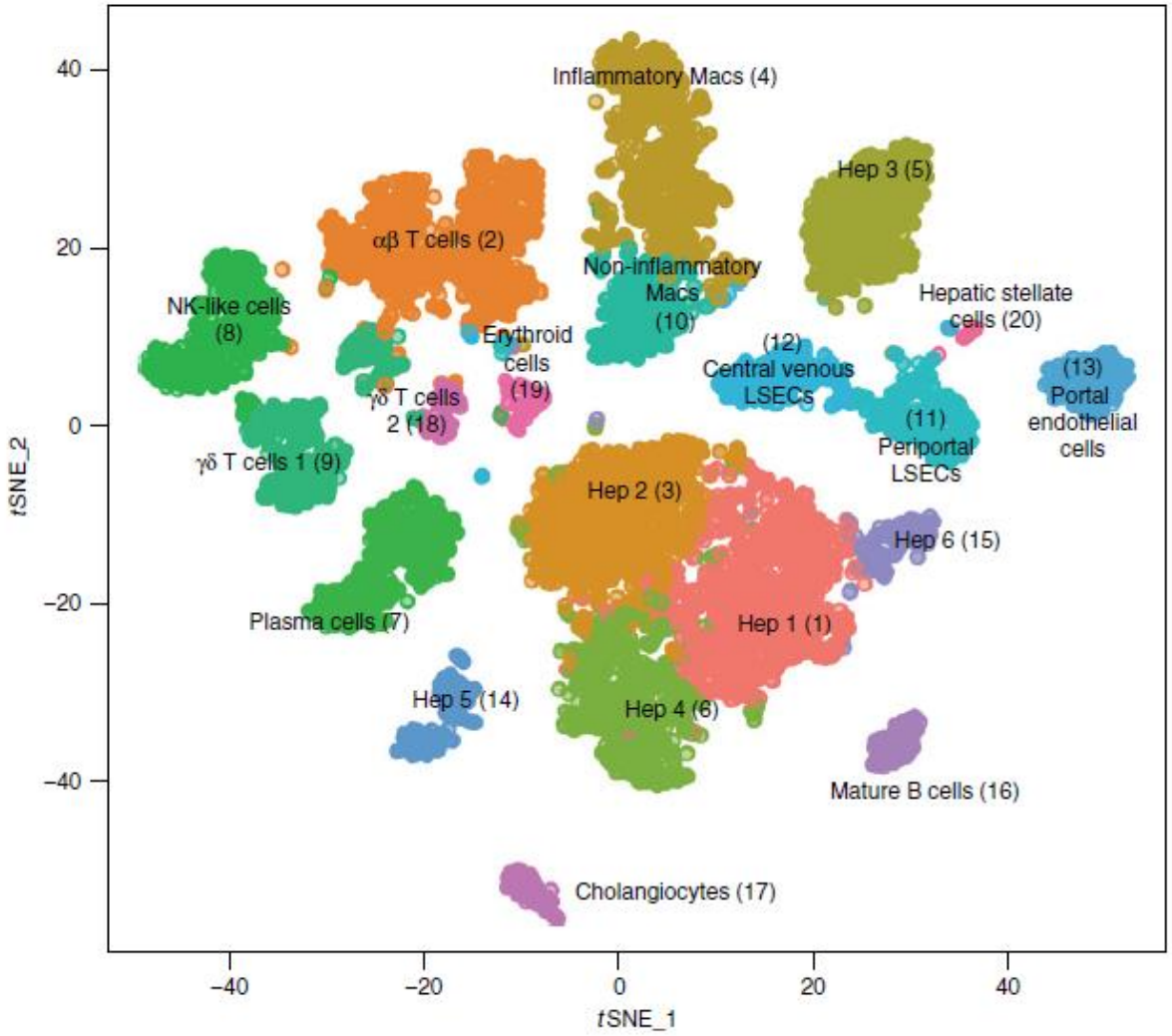


**Figure 3.14 | Excerpt from Fig. 2f, "20 distinct cell populations were revealed in healthy human livers".** t-SNE projection where cells that share similar transcriptome profiles are grouped by colors and assigned an identity for each cluster. 20 distinct cell populations from healthy human livers are shown. From MacParland 2018 *Nature Communications* [91].

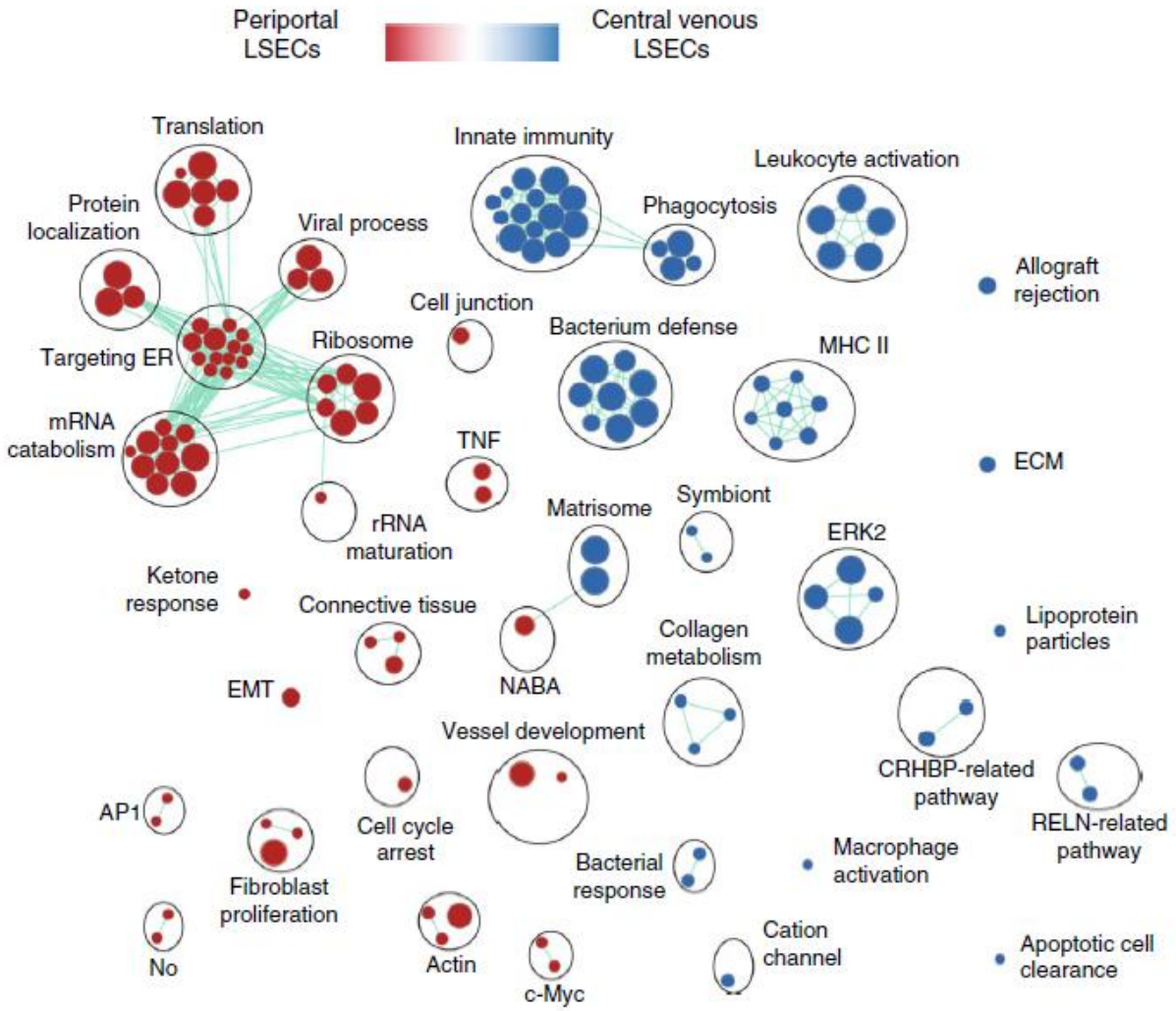


**Figure 3.15 | Excerpt from Fig. 5d, "ScRNA-seq analysis of LSEC populations".**
Pairwise pathway enrichment analysis of genes DE between clusters 11 and 12 defined in Fig 2f (see Figure 3.14 above). Pathways enriched in periportal LSECs (Cluster 11) are labeled in red and pathways enriched in central venous LSECs (Cluster 12) are indicated in blue. Colored circles (nodes) represent pathways, sized by number of genes they contain. Green lines depict intra- and inter-pathway relationships according to the number of genes shared between each pathway. Black circles group related pathways into themes that are labeled. From MacParland 2018 *Nature Communications* [91].

We have also shown that many LSEC culturing methods have failed to preserve LSECtin expression. While other *in vitro* studies have shown retention of other LSEC receptors and functions, it raises concerns that if the aim of a study is not extremely narrow, then it is impossible to know what pathways could be altered by *in vitro* cell culture. Because of these challenges in isolation and cell culture, there is a great need to develop tools that allow for the specific study of LSEC immune functions *in vivo*. In this thesis research, I have described the design of LSEC-specific gene promoter candidates based on the promoter region of LSECtin and required intravenous delivery to target LSECs over LECs and colonic macrophages, which also express LSECtin. Through the development and testing of these promoter constructs, I learned that LSECs and LECs are extremely difficult to transfect cells, and they both rapidly lose LSECtin expression *in vitro*. Further work is required for the successful identification of an LSEC-specific promoter.

In our own *in vitro* LSEC and T cell cocultures, we did not see IL-10 production as previously reported. We also saw better antigen presentation of ISQ than OVA by primary LSECs. It's possible that antigen processing capabilities were lost or weakened by *in vitro* culture. It's difficult to draw definitive conclusions from these *in vitro* experiments other than we were not surprised that we did not reproduce some aspects of published *in vitro* experiments due to our higher purity of LSECs. We do not claim that our results are more representative of how antigen presentation would happen *in vivo* however, because the increased purity is rendered useless by the likely loss of phenotype of cultured LSECs.

Immortalized LSECs retain LSEC features such as fenestrations, but lack LSECtin expression. It's unclear to what extent they can recapitulate *in vivo* LSEC antigen presentation, but we chose to use them because they were readily available and easily transfected. In OTI cocultures, we saw lower effector and memory T cell percentages in iLSEC coculture groups than in BMDC

coculture groups. We also saw relatively similar numbers of CTLA4+ OTI cells in OVA transfected iLSEC groups as in the SIINFEKL pulsed iLSEC group. Overall, there was no evidence that iLSECs presented antigen in a more activating manner when antigen was transfected as opposed to pulsed. This work supports the continued effort to develop tools for LSEC-specific antigen gene delivery to study LSEC antigen presentation *in vivo*.

## 3.5 Materials and Methods

### 3.5.1 Isolation of Murine LSECs

Mice were sacrificed and a catheter connected to a peristaltic pump was carefully inserted in the inferior vena cava. The liver was perfused at a rate of 5 mL/min with a wash buffer consisting of 12.5 mM EGTA, 125 units of heparin, 62.5 µL of 40% glucose, 625 µM HEPES, and 1% pen/strep in 25 mL of calcium-free Hank's Buffered Salt Solution (HBSS). The liver was then digested by perfusing with digestion buffer under a heat lamp. The digestion buffer was 25 µg Collagenase IV (Worthington) and 2 µg DNAse I (Sigma) in 25 mL of IMDM with GlutaMax. The liver was removed and gently torn open to release cells in a petri dish with IMDM with GlutaMax. The cell suspension was passed through a 70 µm filter and centrifuged at 68 x g to pellet hepatocytes. The supernatant was centrifuged at 600 x g and pelleted cells were resuspended in 10 mL DMEM to layer over a Percoll gradient. The Percoll gradient consists of a first layer of 20 mL of 50% Percoll in PBS and a second layer of 25% Percoll. The gradient was spun at 1350 x g with the lowest acceleration speed and no brake. The layer of cells between the two Percoll layers contains the LSECs to be purified by selective adherence, beads, or fluorescence-activated cell sorting (FACS).

### 3.5.2 Preparation of Liver Sections for Immunofluorescence Staining

Mice were perfused through the inferior vena cava with HBSS followed by zinc fixative to fix the liver. Livers were fixed overnight in zinc fixative, transferred to a 10% sucrose solution for 24 hours at 4$^{o}$C, and then to a 30% sucrose solution for 24 hours at 4$^{o}$C. Livers were flash frozen and cryosectioned in 8 mM slices. Sections were stained with 10 µg/mL A1A1 anti-LSECtin Fab [94] or irrelevant Fab control and rat anti-mouse Stabilin-2 (MBL International) at 4$^{o}$C in 0.5% casein in TBST. Sections were washed and stained with anti-human F(ab)2 Alexa Fluor 594

(Jackson Immunoresearch) and anti-rat Alexa Fluor 488 secondary antibodies for 1 hour at room temperature in 0.5% casein in TBST. Sections were mounted with ProLong Gold Antifade Mountant with DAPI (Life Technologies) and imaged on an Olympus confocal microscope.

### 3.5.3 Preparation of LSECs for SEM

Cells were incubated and allowed to adhere to a silicon wafer, and then fixed with 4% PFA in PBS. Cells were washed with PBS and underwent post-fixation with 1% osmium tetraoxide (Sigma-Aldrich) in PBS. Samples were then dehydrated in a graded ethanol series (50, 70, 95, 100%, 15 minutes each). Samples were dried in a Leica CPD3000 critical point dryer and then coated with a Pt/Pd sputter coater. Cells were imaged with a Carl Zeiss Merlin scanning electron microscope (Zeiss, Oberkochen, Germany).

### 3.5.4 RNA isolation

After FACS or cell culture, RNA was extracted following manufacturer's protocol with RNeasy kit (Qiagen) and RNA concentration was measured with the NanoDrop 2000.

### 3.5.5 qPCR

Equal quantities of RNA isolated from cell samples were converted to cDNA using The SuperScript™ III First-Strand Synthesis System (Thermofisher) following manufacturer's instructions. The qPCR reaction was set up with Taqman master mix and Taqman gene probes (Thermofisher) including a beta actin expression control, pipetting into a Lightcycler96 (Roche) compatible 96-well plate, and centrifuged for 1 minute at 2000 rpm. The samples were run in the Lightcycler96 with the following program: preincubation 1 cycle, 2 step amplification 50 cycles, and cooling 1 cycle.

### 3.5.6 LSEC Promoter Cloning

LSEC promoter g-blocks were ordered from IDT, PCR amplified, and cloned into the CMV promoter region of a GFP plasmid using restriction enzymes. Ligation reaction products were cloned into competent DH5alpha cells. Colonies were picked and sequenced. In-Fusion HD cloning kit (Takara Bio) was used for difficult to difficult to clone plasmids. Table 3.1 below shows promoter qualities such as length and the sites of the predicted promoter region to show overlap. Table 3.2 below shows the full sequences of the promoter candidates.

**Table 3.1 | LSEC promoter regions**

| Name | Length | Sites |
|---|---|---|
| Promoter 1 | 728 | 1-728 |
| Promoter 2 | 682 | 728-1409 |
| Promoter 3 | 1029 | 728-1756 |
| Promoter 4 | 347 | 1409-1755 |
| Promoter 5 | 956 | 1756-2711 |
| Promoter 6 | 956 | 2712-3667 |
| Promoter 7 | 956 | 3668-4623 |
| Promoter 8 | 577 | 4624-5200 |

**Table 3.2 | Full sequences of the promoter candidates.**

| Name | Sequence |
|---|---|
| Promoter 1 | CCCCACATTACCAGGCTCCTGGAACAAGGGATCTTATGGAAATGC<br>CAATGGGCTTGGAATACTCCCGTCCTGCCTGTGAAAAAACCTGGG<br>ACCCAAGACTGAGGAGGACTATCCAGAGGTGACTAAACTCCTCTT<br>AGAGGAGCTGAGAGGCTTAAGATACAGAGCCTCAGCCACGAAGG<br>CCCAAATCTGCCAGAGAAAAGTAAGTTATCTGGGCTACCTGCTGA<br>AGGACAGCGGGTTCTGCTCTCCAATGCTGGCTCATAGAGACCATC<br>CTGGACACGGACTTTGAGACCAGCCTATATTACTTAGCCTTTAAG<br>AGACCCTGTTTCCACATGAAACTCAAGAAGAAGAAAGACCAAAG<br>TGTGGATACTTTGTTCCTTCTTAGAATGGGGAACAAGATACCCAT<br>GGAAGGAATCACAGAGACAAAGTTCGGAGCTGAGATAGAAGGAA<br>GGACCATCCAGAGACTGCCCCACCCAGGGATCtATCCCATAAACA<br>ACCACCAAACCCAGACACTATTGCATATGCCAGCAAGATTTTGTT<br>GGCAGGACCCTGATATAGTTGTCTCTTGTGAGGCTATGCCAGTGT<br>CTGGCAAATTCAGAAGTGGATGCTCACAGTCATCTATTGGATGGA<br>ACGCAGGGCCCCCAATGAAGGAGCTAGAGAAAGTACCCAAGGGA<br>CTAAAGGGGTCTGCAACACTCTAGGAGGAACAACAATATGAATT<br>AACCAGTACCCCC |
| Promoter 2 | CAGAGCTCGTGTCCCTAGCTGCATATGTAGCAGAGGATGGCCTAG<br>TCGGCCATCATTGGGAGGACAGGCCCTTGGTCTTTCGAAAATTAT<br>ATGCCCCAGTACAGGGGAATGCCAGGGCCAGGAAGCAGGAGTGG<br>GTGGGTTGGAGAACAGGGCAGAGGGAGGGTATAGGGGACTTTTA<br>GAGAGGAAACTAGGAAAGGGGATAGCATTTGAAATGTAAATGAA<br>GAAAATATCCAATAAAAAATGTAACTTCAAATATATCACATTGCT<br>TTAGGTAGTAATTACATAATTTAACAAAGGGAACCTTACAATAAA<br>CTTTTAAAAGCTTTAAAAAAGAGAGAGAGACCCTGTTTCCAAAAA<br>AgAAAAAAGGTGGATGGGGGTCACCATGACAGCTCAATGAATAA<br>AGGAGCTTGCTGCCAAGTTTGGCAATTTGGCTTTGATCCCAGAAT<br>CCACATGGTGTAGAGAGAAAACCAATTCTCACACGTTGTCAGGTG<br>AATGTACATTAGAGGGATCTCTAATCCTATGCAAGAACCCAAAAC<br>ACACAATATAACTAAATAAATGCAATATTTAAAAGATAAATGGTG<br>CCTGGGTAACAACACTCCAATCTGTCCTCTGACCTCCACAATCAC<br>ACACATACATACATTTACACAGAGAGAGACAGAAGGTTGAGAAC<br>CACTGGTATAAA |

**Table 3.2, continued.**

| Name | Sequence |
|---|---|
| Promoter 3 | CAGAGCTCGTGTCCCTAGCTGCATATGTAGCAGAGGATGGCCTAG<br>TCGGCCATCATTGGGAGGACAGGCCCTTGGTCTTTCGAAAATTAT<br>ATGCCCCAGTACAGGGGAATGCCAGGGCCAGGAAGCAGGAGTGG<br>GTGGGTTGGAGAACAGGGCAGAGGGAGGGTATAGGGGACTTTTA<br>GAGAGGAAACTAGGAAAGGGGATAGCATTTGAAATGTAAATGAA<br>GAAAATATCCAATAAAAAATGTAACTTCAAATATATCACATTGCT<br>TTAGGTAGTAATTACATAATTTAACAAAGGGAACCTTACAATAAA<br>CTTTTAAAAGCTTTAAAAAAGAGAGAGAGACCCTGTTTCCAAAAA<br>AgAAAAAAGGTGGATGGGGGTCACCATGACAGCTCAATGAATAA<br>AGGAGCTTGCTGCCAAGTTTGGCAATTTGGCTTTGATCCCAGAAT<br>CCACATGGTGTAGAGAGAAAACCAATTCTCACACGTTGTCAGGTG<br>AATGTACATTAGAGGGATCTCTAATCCTATGCAAGAACCCAAAAC<br>ACACAATATAACTAAATAAATGCAATATTTAAAAGATAAATGGTG<br>CCTGGGTAACAACACTCCAATCTGTCCTCTGACCTCCACAATCAC<br>ACACATACATACATTTACACAGAGAGAGACAGAAGGTTGAGAAC<br>CACTGGTATAAACCAAACACATATCTTCTTGGCACTGTGTGTATA<br>CATTATGTATGTCTCCTATCTGTGCATGGGTGCTGTGTTCCTGGTC<br>TATGCCTCCATAGACACCAAAAGATGAGTCGTCACACCTTCTGTG<br>CAGGAAACACAGCTACAATGATCAAGCCACAGAGGTTTGATCTGC<br>CCCTCACAGTCCTAGCCTTGCCCAGCACTGCGACTGACCATTAGC<br>TGGCTTCCTACACAAAAGTATTGAGGCCACCGACATGGAAAGGA<br>AGGAAGGGAGGGAGGGAGGGAGATAGGATAGGGCTAGGGTGGA<br>GACTTAAATTTATATCTCTGTCCAGGGCTGGACGCCACCACCACC<br>A |
| Promoter 4 | ACCAAACACATATCTTCTTGGCACTGTGTGTATACATTATGTATGT<br>CTCCTATCTGTGCATGGGTGCTGTGTTCCTGGTCTATGCCTCCATA<br>GACACCAAAAGATGAGTCGTCACACCTTCTGTGCAGGAAACACA<br>GCTACAATGATCAAGCCACAGAGGTTTGATCTGCCCCTCACAGTC<br>CTAGCCTTGCCCAGCACTGCGACTGACCATTAGCTGGCTTCCTAC<br>ACAAAAGTATTGAGGCCACCGACATGGAAAGGAAGGAAGGGAGG<br>GAGGGAGGGAGATAGGATAGGGCTAGGGTGGAGACTTAAATTTA<br>TATCTCTGTCCAGGGCTGGACGCCACCACCACC |

**Table 3.2, continued.**

| Name | Sequence |
|---|---|
| Promoter 5 | ATGAACACTGGTGAATACAACAAGCTGGGCAGTGCAATTGAAGA<br>GGTCTCCAGAGGTAGGAGAAAGAGAATCACCCCATCGTCCTCCAT<br>GGGTTCTTCTGTTCTAATGTTTGCAGTTTGGGAGGGCTGGGGAGA<br>AGAAACGGCAAAACCATACAGGAGACACCACTGTATGGACAGAA<br>CTGTGGAATGGTGGTGCCCGCAGCACAGGCATGGGGACATCACAT<br>CCTGGAGTGAGGACTTCCCAGGGTCCTAAGGGCTGGGTCCTGGGT<br>CCTGGACTGAGAAACAGCATCACCCAAGTCTCCCCCAGAAAACCT<br>GTGTGGGGACAGGTATCACTCCAGCCACAGACACCTTGTTACATA<br>GATTCTGGTTACACTGGCATAAGAATTCTAAGACTGCTAAATATG<br>CAGCTGGAGCCATGGGTCCCTCCATGTGAACTCTTTGGTTGATGG<br>TTTAGTCCCTGGGAGCTCTGGAGGGTCTGGTTGGTTTATATTGTTG<br>TTCTTCCTATGGGGTTGCAAACCCCTTCAGCTCCTTCTTCAGTCCT<br>TCCTCTAACTCCTCCATCGGGATtCCCATGCTCAGTTCCGTGGTTG<br>GCTGCAAGCATCAGCCTCTGTATTTGTCAGGCTCTGGCAGAGCCT<br>CTCAGGAGACAGCTATTTCAAGCTCCTGTCAGCAAGCACTTCTTG<br>GCATCTGCAATAGTGTCTGGGTTTGGTGGCTGCATATGGTAGTCTC<br>TGGATGGCCTTTCTTTCAGTCTGTGTTCCACCTGTGAAGGCTCAGT<br>GCCCCAATGTAGGGGAAGTCTAGGGTGGTGAGGTGGGAGTGGGC<br>AGGTGGGTATGGGAGCACCCTCATAGAAGCAGTGGGGGGTGGAA<br>TGAGATGGGAGTTTGTGGAGGGAAACCCAGGAAGGGGGATAATA<br>TTTGAAATGTAAAAAAATAAAATAGCCAATTAAAGACTTTTTTAA<br>TTTTTAAAATT |

**Table 3.2, continued.**

| Name | Sequence |
|---|---|
| Promoter 6 | AAATTTAAAAAAATTCTAACTATGTTGTGTGGTGGTAGGAGGGTA<br>CTTAAGCTGTCTGTACCTCTGTCCTGGAGAGAGCCAGAATTTATCT<br>GTGTTCTACTAGGGCAATTGGGACGTTGGGAGTGCTACAAACAAA<br>GACTTTTCTTCCTGGTCTTGGCTCTGCTGGTGGCCACAGTTCTATG<br>GGCTCTCATTCTGAGCACCCTACTGTCCAGTGGTGAGTGATGTATT<br>TTCATGTGTACATGTCTGTGTCTGAGGGTATGCCGCGGGTGTACA<br>AGTGCCCACAGTGGGTAGATGGCATCAGATCCCCTACAGCTGGAG<br>TTGGAGACACTTGTGAGCCATTGCATGTGGGTGCGAGTGCTAAGA<br>ACCAAACTCAGGTTCTCTGGAACAGCATCTCTGAACCATCGCTCC<br>ACCGGAGTGATCCCTTTACAGGGACAAGTTATGCTGCCTGGCAGG<br>TAAGGCACAAACTTGCTTCCTATGCGGTGCACCACATGGGGTCCT<br>GGATAGCAATGAGTATAAACCATGGTTCCCATGGGTTTCACCAGG<br>TTTGCCTGAGACATCGGAAATCATATGGATTGTATGATATGATTTT<br>TATGTTATGAATGGAAATTCAAAACAGCAAAAAAATTAAAGTTAT<br>AAAGTAACAACGAAAATAATTTTATGGTTAGAGGTCACCACAACA<br>TAAACTATATTAAAGGGCCACCGCATTAGGAAGGTTGAGGACCAC<br>TGGTGCTTGGCACTGTATTATGCATTTTGTATGTCTCCTGTCCATA<br>CCCGGACATACCTGTGCCTCCGTGGATAACAACGTACGTGTCCTC<br>ACACACTCTGAGCAGGCGGAGGCTTCACAACTCATGCTTGCATCT<br>CTCTGCAGCCTCCAGCAAGCTCAGGGTGCTGCTCAGCCACCAGGA<br>CCTGCTGAGGACAAATGGTGCGTGAGGAGCTGCAGCGCAGGGCG<br>GCAGCGC |

**Table 3.2, continued.**

| Name | Sequence |
|---|---|
| Promoter 7 | ACCCTTGCGGTGGGAGGAGGAACTGCCAGGGAGGAGGACCTGGG<br>TAGTGAATAGCTGAGGCCGCTGCAATCGGGTTGACTGGTTTGTGT<br>GTGGTGGGTGGGGTCTTTCCAGCCTCAGAGCAGAAGATGACGTTG<br>AGTTCCCTGAAGGATGATATtGGAGCCTGCAGGAATTGCTGTAAG<br>AAAGAGGGGTTTGGTGAAAACTTGAAAGTTGAGGGGCTGGGAAA<br>TGGGGCAGGTGGTTTGGGAGAGGCAAGTGGGGGCAAGACTGGTT<br>TTTGCCCCATCCCCATATAGGCTCCGTGACAAAAGCGCAGTTGCA<br>AACCACACTGGCGGAGTTTAAGGACATACAAGCAAAGTTGATGG<br>AGCAGGAGAGCATCCTGAAAGAACTGCAAGAGCGTGGTGAGAGC<br>TGAACACAACCCCCTGGTCCCCGACCTTCATCCCTAATCATAGCC<br>ACACCGCTTCTTGGTAGTCCAGTCCTGGACCCTCAGGTCTCTGGTG<br>ACTGAACCCAGGACTTCGAATGCTAGGTAGGCTTTCCACACCTGA<br>GCCGTGCCCAGACCCTCAAAGCAGGATTCTAAGCAGGTGCTCTAC<br>CTTTGAGTCGCTCTCCCAGACCCTTGCTGGGGGATTCTAGGCAGG<br>TACTCTAATACCAACCTTATTACCAGCACTCATTTTATGTTTTGAG<br>ACAGGCTCCATTAAGTTACCAAGGATGGTCTTAAACTCTCTGTGT<br>AGTCCAAGTTAGCTTTGACCTTACAATCCTCCTCTACCTCAGCTTT<br>CTGGAGTAACTGAAACCGCCACGTTCAAATTGATGTTATTCTTGA<br>CCGTGACACCATGAACTGACCATGGATATATATTTTGACCTATAC<br>ATAAGTCCCGGTCTTAACCTCAACTATAAATGTCCACTCTTCTGAC<br>CTTGTAGTGACCCAGGACTTGGCTAAAGCAAGCAGAGACCGTGA<br>GAACATCCGCAGT |
| Promoter 8 | GAGCTGTTCCAGGCACTGGAAGCTGTCAAGCGCCAGAACAGTGA<br>GCCAGAGATAGGACGAGGGGTGGGGGAGGAATGGACCCAGCTGA<br>GGGTTTTCAGTGCTTCTCTTTCCACCAGACATTCCCTTGTTTCTCTG<br>GAACCCCACACCATCCGTCAAATTCCAATGGTCCCTTCCTATAAC<br>GGTCTATCTCTCTGACCCTCCCCACCCAACAGGCTCCTGTGAGCA<br>GTGCCCACCATCATGGCTACCCTTCCAAGGTTCCTGCTACTATTTC<br>TCTGAGACACAGGCCACATGGGATACAGCACAAAGCTACTGTGG<br>AGGCCAGGGTGCCCATCTGGTGATTGTCAGAGGCCTGAACGAGCA<br>GGTGCTCAGCTGGGACTTGGAAGAGGAGAAGCGGGGTTTGCCTG<br>AACTGGTGTGGCCCAGAACATTTGGCAGACTTGGCCAGCTGATGT<br>GTCTACCCACTCCTTCCAGGGCTTCCTGAGTCAGCACACACGTGG<br>CCGGGGCTATTGGTTGGGTCTGAGGGCAGTTCGCCACCTCAACAA<br>GATTCAAGGCTACCGGTGGGTAGATGGAGCCTCACTCA |

### 3.5.7 Lentivirus Production

Transfer plasmids contained a fluorescent mCherry reporter with expression controlled by a constitutive CMV enhanced chicken beta actin promoter. In a 15 cm dish, 10-10.5 million HEK 293T cells at not more than p15 were seeded 24 hours before transfection. 22.5 mL of complete IMDM was added 30 minutes to 2 hours before transfection. ENV (VSV-G), pMDL/RRE, REV, and the transfer plasmid were mixed with water/0.1x TE and $CaCl_2$ and then 2x HBS dropwise while mixing. The mixture was immediately added to the cells. The media of each transfected dish was changed 12-14 hours after transfection by adding 16.5 mL of complete IMDM. The supernatant was collected from each dish approximately 30-32 hours later and ultracentrifuged at 100000 x g for 2 hours at 4°C. The pellet was resuspended in PBS and frozen at least 10 min at –80°C before titration. Functional titers were calculated following Addgene's Fluorescence Titering Assay protocol.

### 3.5.8 AAV Production

AAVs were produced and titrated using AAVpro extraction solution (Takara, 6235), XFect Transfection Reagent (Takara, 631317), and AAVpro titration kit (Takara, 6233) all according to manufacturer's instructions. The control AAV had a constitutive CMV promoter initiating expression of a zsGreen fluorescent reporter.

### 3.5.9 ELISA

3-day restimulation plates were removed from incubation and put on ice, followed by centrifugation at 2000g for 2 min. Supernatants were pipetted and stored at -20$^{o}$C until cytokine ELISAs were performed. Culture supernatants were assessed for IL-10 using ELISA Ready-Set-Go Kit (eBioscience), following the manufacturer's instructions.

### 3.5.10 Flow Cytometry on LSECs

Cells were first stained with Live/Dead Viability Dye (Invitrogen) and 1:50 Fc block (BD). Cells were washed with 2% FBS in PBS. Cells were stained for CD31, Stabilin-2 and CD45 and with 5 µg/mL anti-LSECtin Fab for 30 minutes at 4$^{o}$C. Cells were washed in 2% FBS in PBS and stained with 1:400 dilution of anti-Fab for 15 minutes at 4$^{o}$C. Cells were washed and fixed in 2% paraformaldehyde for 15 minutes at 4$^{o}$C. Cells were washed and analyzed by flow cytometry.

### 3.5.11 HEK cells

The 293T cell line (ATCC # CRL-11268) was used to test the promiscuity of the LSEC promoter candidates because it is a highly transfectable derivative of human embryonic kidney 293 cells and it is an adherent cell type just like LSECs are an adherent cell type. HEK cells were cultured in complete DMEM containing 10% FBS and 1% pen/strep. Cells were split every 2-3 days at a 1:3 – 1:8 ratio.

### 3.5.12 CHO cells

CHO-DG44 cells were split to 1 million cells per mL one day prior to transfection. Cells were spun down at 300 x g for 5 minutes and resuspended in RPMI 1640 with 25 mM HEPES for a final concentration of 2 million cells per mL after adding PEI:DNA transfection mixture. After 5 hours shaking at 200rpm and 37$^{o}$C ProCHO5-CDM media (Lonza) was added to feed the cells.

### 3.5.13 BMDCs

Hematopoietic stem cells were obtained from mouse bone marrow and cultured in the presence of 200 U/mL GM-CSF, added at days 0, 3, and 6. BMDCs were ready to use at day 8. BMDCs were pulsed with 1 µg/mL OVA MHC class I peptide (SIINFEKL) or 2 µg/mL MHC class II peptide (ISQAVHAAHAEINEAGR) (Genscript) for 6 hours, washed, and CFSE-labeled OT-I or OT-II were added for 3 days.

### 3.5.14 T cells

Spleens were isolated from TCR transgenic mice and processed into an ACK lysed single cell suspension. OT-I and OT-II T cells were isolated from splenocytes with negative magnetic bead selection using a CD8 and CD4 negative selection kit (Stemcell), respectively. Cells were then CFSE labeled for coculture experiments.

### 3.5.15 Statistical Analysis

Statistically significant differences between experimental groups were determined using Prism software (v9, GraphPad). Unless otherwise specified in the figure legend, one-way ANOVA was performed with a Tukey's post-hoc test to correct for multiple comparisons. Comparisons were significant with p values $< 0.05$. Statistical significance is shown with stars as follows: *** means $p \leq 0.001$; ** means $p \leq 0.01$; * means $p \leq 0.05$, unless otherwise stated.

# CHAPTER 4

## CONCLUSIONS AND FUTURE DIRECTIONS

The aims of my thesis research shown above were to test the boundaries of the pGal tolerogen platform and improve our understanding of LSECs as a key APC in the liver. By suppressing activated autoreactive T cells with pGal in an antigen specific manner, we may be able to decrease the rate of relapse after B cell depletion therapies currently used in the clinic. By understanding LSEC subsets and identifying an LSEC specific promoter, we will be enabled to test the importance of LSECs in tolerance induction, which could then motivate the development of more targeted and hopefully more efficient and effective therapies.

One of the key findings of this work is that pGal-Dsg3 generated anti-Dsg3 titers to a much greater extent than pGal-ASNase. However, without the direct ASNase comparison starting dosing at the same time, we cannot say if this is due to the properties of the antigen alone. Regardless, for these cases where antibodies to the delivered antigen are unwanted, future work can be done to optimize the pGal-antigen conjugations. The ratio of pGal to linker (and subsequently antigen) can be increased to increase shielding of the antigen by the carbohydrate polymer. This phenomenon was shown previously by measuring the affinity for polyclonal anti-OVA IgG against plain OVA and pGal-OVA using surface plasmon resonance (SPR). It was shown that there was a five-fold decrease in affinity with pGal conjugation [95]. Importantly, serum IgG levels were measured only after OVA immunization and not following pGal-OVA treatment. Without knowing if pGal-OVA increased anti-OVA IgG, we do not know if a five-fold decrease in affinity was sufficient shielding to prevent off-target antigen uptake. More broadly, we also cannot be certain that increasing shielding will in fact prevent an increase in antibodies against the antigen delivered. Engineering how to prevent antibody production against pGal delivered antigen will be essential for

applications where antibodies are detrimental and protein antigen is necessary. This work suggests that pGal-peptide constructs may not induce antibody production against the delivered peptide.

In this work we were not able to demonstrate that pGal-Peptide 1 or a mixture of pGal-P1 and pGal-peptide pool were tolerogenic, but we also did not eliminate the possibility that they could be because the saline treated disease control did not develop disease. Future work should be done to test the potential of these pGal-peptide therapies for the treatment of pemphigus vulgaris. One option is to optimize the prophylactic model they were tested in. Potential ways to increase responses in the model include decreasing the time between initial immunization and boosting, adding a second IFA booster, transferring cells sooner after the last boost, or switching back to a Dsg3 protein immunization. Other opportunities include doing a mixed peptide and protein immunization to try to boost the response but still skew the responses towards one peptide for more robust readouts, or identifying more immunogenic peptides by epitope mapping in mice. Given the success in disease induction in the peptide 1 treated group, I hypothesize that one of the first strategies would be sufficient to successfully induce disease in the saline treated group and be able to see if there are differences in the pGal-peptide treated groups. Knowing that pGal-peptide therapies do not induce antibody production, it would also be possible to test these therapies in the B cell depletion pemphigus vulgaris model. However, this model is also not robust and would require optimization. One option would be to develop a screen by measuring antibody titers in the $Dsg3^{-/-}$ immunized mice before transfer and only transferring from high responders.

Extensive work was done to improve upon the purity achieved by current LSEC isolation methods. We developed a work flow that incorporates sorting on CD31 and Stabilin-2 expression. As more is learned about LSEC subsets in humans and in mice, this workflow could be adapted to sort specific subsets of LSECs for downstream uses such as qPCR profiling or restimulations for

cytokine analysis. Due to the challenges of preserving LSEC phenotype *in vitro*, downstream applications that do not require cell culture would be more reliable.

In the effort to design a system to test various LSEC-specific promoter candidates, the design went through multiple iterations to now where I have AAV transfer plasmid designs featuring a zsGreen reporter controlled by promoter candidates and mCherry constitutively expressed. This will allow an *in vivo* biodistribution study that shows which cells have been transduced and which transduced cells are transcribing zsGreen by recognizing the promoter candidates.

Not only would an LSEC-specific promoter unlock the ability to study the effects of targeted antigen presentation by LSECs in autoimmune disease models, but antigen presentation or other key pathways could be selectively turned off with the targeted delivery of silencing RNA. More broadly, LSECs are a cell type of interest in many fields of study involving the liver, including the study of cirrhosis and other liver diseases.

Despite concerns about how relevant *in vitro* experiments with iLSECs are to LSEC *in vivo* behavior, future studies should include further characterization and a search of markers of T cell anergy and exhaustion. These studies could support *in vivo* findings, and if iLSECs do recapitulate *in vivo* LSEC antigen presentation, then that would be extremely valuable to the field as they are readily available as compared to difficult and lengthy primary LSEC isolations.

In conclusion, this work seeks to further the field of antigen-specific tolerance. We have progressed from targeting tolerogenic organs and endogenous tolerogenic mechanisms in the body, to now studying specific cell types of interest within tolerogenic organs. The continued development of increasingly more efficient antigen-specific therapies will require a deep understanding of both key cell types contributing to peripheral tolerance and a deep understanding

of the limitations and corresponding design considerations of the current therapies in development in our lab and others. An immense amount of progress has been made in this field and is the foundation for further innovation that will improve the quality of life of millions of people affected by autoimmune diseases.

## REFERENCES


1. NIEHS Autoimmune Diseases fact sheet (2012, November). Autoimmune Diseases. Retrieved January 29, 2018 from https://www.niehs.nih.gov/health/materials/autoimmune_diseases_508.pdf

2. Lerner, A., Jeremias, P., Matthias,T. The World Incidence and Prevalence of Autoimmune Diseases is Increasing. *International Journal of Celiac Disease*, **3**, 151-155 (2015). doi: 10.12691/ijcd-3-4-8.

3. National Institute of Allergy and Infectious Diseases (2017, March 27). Food Allergy. Retrieved January 29, 2018 from https://www.niaid.nih.gov/diseases-conditions/food-allergy

4. Georgiev, V. S. (2009). National Institute of Allergy and Infectious Diseases, NIH Volume 2: Impact on Global Health. Chapter 1, Introduction. Humana Press: Springer.

5. Hayter, S. M., Cook, M. C. Updated assessment of the prevalence, spectrum and case definition of autoimmune disease. *Autoimmunity Reviews*, **11**, 754-765 (2012). https://doi.org/10.1016/j.autrev.2012.02.001

6. Weiner, H. L., Mackin, G. A., Matsui, M., Orav, E. J., Khoury, S. J., Dawson, D. M., et al. Double-blind pilot trial of oral Tolerization with myelin antigens in multiple sclerosis. *Science*, **259**, 1321-4 (1993).

7. Walczak, A., Siger, M., Ciach, A., Szczepanik, M., Selmaj, K. Transdermal application of myelin peptides in multiple sclerosis treatment. *JAMA Neurol*, **70**, 1105-9 (2013).

8. Streeter, H. B., Rigden, R., Martin, K. F., Scolding, N. J., Wraith, D. C. Preclinical development and first-in-human study of Atx-Ms-1467 for immunotherapy of MS. *Neurol Neuroimmunol Neuroinflamm*, **2**, e93 (2015).

9. McCarthy, D. P., Hunter, Z. N., Chackerian, B., Shea, L. D., Miller, S. D. Targeted immunomodulation using antigen-conjugated nanoparticles. *Wiley Interdiscip Rev Nanomed Nanobiotechnol*, **6**, 298-315 (2014).

10. Carambia, A., Freund, B., Schwinge, D., Bruns, O. T., Salmen, S. C., Ittrich, H., et al. Nanoparticle-based autoantigen delivery to Treg-inducing liver sinusoidal endothelial cells enables control of autoimmunity in mice. *J Hepatol*, **62**, 1349-56 (2015).

11. McCarthy, D. P., Yap, J.W.-T., Harp, C. T., et al. An antigen-encapsulating nanoparticle platform for TH1/17 immune tolerance therapy. *Nanomedicine: nanotechnology, biology, and medicine*, **13**, 191-200 (2017). doi:10.1016/j.nano.2016.09.007

12. Murphy, K. (2012). *Janeway's Immunobiology* (8th Edition). Garland Science.

13. Skapenko, A., Leipe, J., Lipsky, P.E. et al. The role of the T cell in autoimmune inflammation. *Arthritis Res Ther*, **7**, S4-S14 (2005). https://doi.org/10.1186/ar1703

14. Gottwick, C., Carambia, A., & Herkel, J. Harnessing the liver to induce antigen-specific immune tolerance. *Seminars in Immunopathology*, **44**, 475–484, (2022). https://doi.org/10.1007/s00281-022-00942-8

15. Bhandari, S., Larsen, A.K., McCourt, P., Smedsrød, B., Sørensen, K.K. The scavenger function of liver sinusoidal endothelial cells in health and disease. *Front. Physiol*., **12**, 757469. (2021). doi: 10.3389/fphys.2021.757469

16. Kim, M., Jeong, M., Hur, S., Cho, Y., Park, J., Jung, H., Seo, Y., Woo, H. A., Nam, K. T., Lee, K., Lee, H. Engineered ionizable lipid nanoparticles for targeted delivery of RNA therapeutics into different types of cells in the liver. *Science advances*, **7**, eabf4398, (2021). https://doi.org/10.1126/sciadv.abf4398

17. Keeler, G. D., Markusic, D. M., & Hoffman, B. E. Liver induced transgene tolerance with AAV vectors. *Cellular immunology*, **342**, 103728, (2019). https://doi.org/10.1016/j.cellimm.2017.12.002

18. Akbarpour, M., Goudy, K. S., Cantore, A., Russo, F., Sanvito, F., Naldini, L., Annoni, A., Roncarolo, M. G. Insulin B chain 9-23 gene transfer to hepatocytes protects from type 1 diabetes by inducing Ag-specific FoxP3+ Tregs. *Sci Transl Med*, **7**, 289ra81 (2015). doi: 10.1126/scitranslmed.aaa3032.

19. Keeler, G. D., Kumar, S., Palaschak, B., Silverberg, E. L., Markusic, D. M., Jones, N. T., & Hoffman, B. E. Gene Therapy-Induced Antigen-Specific Tregs Inhibit Neuro-inflammation and Reverse Disease in a Mouse Model of Multiple Sclerosis. *Molecular therapy: the journal of the American Society of Gene Therapy*, **26**, 173–183, (2018). https://doi.org/10.1016/j.ymthe.2017.09.001

20. Kontos, S., Grimm, A. J., & Hubbell, J. A. Engineering antigen-specific immunological tolerance. *Current opinion in immunology*, **35**, 80–88, (2015). https://doi.org/10.1016/j.coi.2015.05.005

21. Kontos, S., Kourtis, I. C., Dane, K. Y., & Hubbell, J. A. Engineering antigens for in situ erythrocyte binding induces T-cell deletion. *Proceedings of the National Academy of Sciences of the United States of America*, **110**, E60–E68, (2013). https://doi.org/10.1073/pnas.1216353110

22. Lutterotti, A., Ludersdorfer, T.H., Docampo, M.J., Hohmann, M., Sellés-Moreno, C., Hayward-Koennecke, H., et al. Establish Tolerance in MS with myelin-peptide coupled red blood cells – the Phase Ib ETIMS$^{red}$ trial. *Multiple Sclerosis Journal*, ECTRIMS 2019 – Late Breaking News Abstracts, **25**, 894 (2019). doi: 10.1177/1352458519869496

23. Cacicedo, M. L., Medina-Montano, C., Kaps, L., Kappel, C., Gehring, S., & Bros, M. Role of liver-mediated tolerance in nanoparticle-based tumor therapy. *Cells*, **9**, 1985, (2020). https://doi.org/10.3390/cells9091985

24. Casey, L. M., Hughes, K. R., Saunders, M. N., Miller, S. D., Pearson, R. M., & Shea, L. D. Mechanistic contributions of Kupffer cells and liver sinusoidal endothelial cells in nanoparticle-induced antigen-specific immune tolerance. *Biomaterials*, **283**, 121457, (2022). https://doi.org/10.1016/j.biomaterials.2022.121457

25. Freitag, T. L., Podojil, J. R., Pearson, R. M., Fokta, F. J., Sahl, C., Messing, M., Andersson, L. C., Leskinen, K., Saavalainen, P., Hoover, L. I., Huang, K., Phippard, D., Maleki, S., King, N., Shea, L. D., Miller, S. D., Meri, S. K., & Getts, D. R. Gliadin nanoparticles induce immune tolerance to gliadin in mouse models of celiac disease. *Gastroenterology*, **158**, 1667–1681.e12, (2020). https://doi.org/10.1053/j.gastro.2020.01.045

26. Prasad, S., Neef, T., Xu, D., Podojil, J. R., Getts, D. R., Shea, L. D., & Miller, S. D. Tolerogenic Ag-PLG nanoparticles induce Tregs to suppress activated diabetogenic CD4 and CD8 T cells. *Journal of autoimmunity*, **89**, 112–124, (2018). https://doi.org/10.1016/j.jaut.2017.12.010

27. *Topas Particle Conjugates*. (2022*).* Topas Therapeutics. Retrieved July 18, 2022 from https://topas-therapeutics.com/topas/rd/topas-particle-conjugates.html

28. Carambia, A., Gottwick, C., Schwinge, D., Stein, S., Digigow, R., Şeleci, M., Mungalpara, D., Heine, M., Schuran, F. A., Corban, C., Lohse, A. W., Schramm, C., Heeren, J., & Herkel, J. Nanoparticle-mediated targeting of autoantigen peptide to cross-presenting liver sinusoidal endothelial cells protects from CD8 T-cell-driven autoimmune cholangitis. *Immunology*, **162**, 452–463, (2021). https://doi.org/10.1111/imm.13298

29. Carambia, A., Freund, B., Schwinge, D., Bruns, O. T., Salmen, S. C., Ittrich, H., Reimer, R., Heine, M., Huber, S., Waurisch, C., Eychmüller, A., Wraith, D. C., Korn, T., Nielsen, P., Weller, H., Schramm, C., Lüth, S., Lohse, A. W., Heeren, J., & Herkel, J. Nanoparticle-based autoantigen delivery to Treg-inducing liver sinusoidal endothelial cells enables control of autoimmunity in mice. *Journal of Hepatology*, **62**, 1349–1356, (2015). https://doi.org/10.1016/j.jhep.2015.01.006

30. Liu, Q., Wang, X., Liu, X., Kumar, S., Gochman, G., Ji, Y., Liao, Y. P., Chang, C. H., Situ, W., Lu, J., Jiang, J., Mei, K. C., Meng, H., Xia, T., & Nel, A. E. Use of polymeric nanoparticle platform targeting the liver to induce Treg-mediated antigen-specific immune tolerance in a pulmonary allergen sensitization model. *ACS nano*, **13**, 4778–4794. (2019). https://doi.org/10.1021/acsnano.9b01444

31. *Our Pipeline and Programs*. (2022*).* Cour Pharmaceuticals. Retrieved July 12, 2022 from https://courpharma.com/pipeline/

32. *International Clinical Trials Registry Platform: Search Portal*. (2022, May 30). World Health Organization. Retrieved July 12, 2022 from

https://trialsearch.who.int/Trial2.aspx?TrialID=EUCTR2019-001727-12-DE

33. *Pipeline*. (2022*).* Topas Therapeutics. Retrieved July 18, 2022 from https://topas-therapeutics.com/topas/rd/pipeline.html

34. Debacker, A. J., Voutila, J., Catley, M., Blakey, D., & Habib, N. Delivery of oligonucleotides to the liver with GalNAc: From research to registered therapeutic drug. *Molecular Therapy*, **28**, 1759–1771, (2020). https://doi.org/10.1016/j.ymthe.2020.06.015

35. Cui, H., Zhu, X., Li, S., Wang, P., & Fang, J. Liver-targeted delivery of oligonucleotides with N-acetylgalactosamine conjugation. *ACS Omega*, **6**, 16259–16265, (2021). https://doi.org/10.1021/acsomega.1c01755

36. Wilson, D. S., Damo, M., Hirosue, S., Raczy, M. M., Brünggel, K., Diaceri, G., Quaglia-Thermes, X., & Hubbell, J. A. Synthetically glycosylated antigens induce antigen-specific tolerance and prevent the onset of diabetes. *Nature Biomedical Engineering*, **3**, 817–829, (2019). https://doi.org/10.1038/s41551-019-0424-1

37. Damo, M., Wilson, D. S., Watkins, E. A., & Hubbell, J. A. Soluble N-acetylgalactosamine-modified antigens enhance hepatocyte-dependent antigen cross-presentation and result in antigen-specific CD8+ T cell tolerance development. *Frontiers in immunology*, **12**, 555095, (2021). https://doi.org/10.3389/fimmu.2021.555095

38. *Pipeline: The potential to transform treatment*. (2022). Anokion. Retrieved July 21, 2022 from https://anokion.com/pipeline/

39. Grant, C. R., Liberal, R. Liver immunology: How to reconcile tolerance with autoimmunity. *Clinics and Research in Hepatology and Gastroenterology,* **41**, 6-16 (2017). http://dx.doi.org/10.1016/j.clinre.2016.06.003

40. Strauss, O., Phillips, A., Ruggiero, K., Bartlett, A., Dunbar, P. R. Immunofluorescence identifies distinct subsets of endothelial cells in the human liver. *Sci Rep,* **7**, 44356 (2017). doi: 10.1038/srep44356

41. Poisson, J., Lemoinne, S., Boulanger, C., Durand, F., Moreau, R., Valla, D., Rautou, P.-E. Liver sinusoidal endothelial cells: Physiology and role in liver diseases. *Journal of Hepatology,* **66**, 212–227 (2017). doi: 10.1016/j.jhep.2016.07.009.

42. Stubbington, M. J. T., Rozenblatt-Rosen, O., Regev, A., Teichmann, S. A. Single cell transcriptomics to explore the immune system in health and disease. *Science*, **358**, 58–63 (2017). doi: 10.1126/science.aan6828

43. Andrews S. FASTQC. A quality control tool for high throughput sequence data. Retrieved January 29, 2018 from http://www.bioinformatics.babraham.ac.uk/projects/fastqc/.

44. Conesa, A., Madrigal, P., Tarazona, S., Gomez-Cabrero, D., et al. A survey of best practices for RNA-seq data analysis. *Genome Biology*, **17**, 13 (2016). https://doi.org/10.1186/s13059-016-0881-8

45. Rosenblum, M. D., Gratz, I. K., Paw, J. S, Abbas, A. K. Treating Human Autoimmunity: Current Practice and Future Prospects. *Science translational medicine*, **4**, 125sr1 (2012). doi:10.1126/scitranslmed.3003504.

46. Horst, A. K., Neumann, K., Diehl, L., Tiegs, G. Modulation of liver tolerance by conventional and nonconventional antigen-presenting cells and regulatory immune cells. *Cellular & Molecular Immunology*, **13**, 277–292 (2016). doi:10.1038/cmi.2015.112

47. Krishna, M., Nadler, S. G. Immunogenicity to Biotherapeutics – The Role of Anti-drug Immune Complexes. *Front. Immunol.*, **7**, Article 21 (2016). doi: 10.3389/fimmu.2016.00021

48. Fogdell-Hahn, A. Antidrug Antibodies: B Cell Immunity Against Therapy. *Scand J Immunol*., **82**, 184–190 (2015). doi:10.1111/sji.12327

49. Van Brummelen, E. M. J., Ros, W., Wolbink, G., Beijnen, J. H., Schellens, J. H. M. Antidrug Antibody Formation in Oncology: Clinical Relevance and Challenges. *The Oncologist*, **21**, 1260-1268 (2016). doi:10.1634/theoncologist.2016-0061.

50. Egami, S., Yamagami, J., & Amagai, M. Autoimmune bullous skin diseases, pemphigus and pemphigoid. *J Allergy and Clinical Immunology*, **145**, 1031–1047, (2020). https://doi.org/10.1016/j.jaci.2020.02.013

51. Lim, Y. L., Bohelay, G., Hanakawa, S., Musette, P., & Janela, B. Autoimmune Pemphigus: Latest Advances and Emerging Therapies. *Frontiers in Molecular Biosciences*, **8**, 808536, (2022). https://doi.org/10.3389/fmolb.2021.808536

52. Ellebrecht, C. T., & Payne, A. S. Setting the target for pemphigus vulgaris therapy. *JCI Insight*, **2**, e92021, (2017). https://doi.org/10.1172/jci.insight.92021

53. Didona, D., Maglie, R., Eming, R., & Hertl, M. Pemphigus: current and future therapeutic strategies. *Frontiers in Immunology*, **10**, 1418, (2019). https://doi.org/10.3389/fimmu.2019.01418

54. *Pipeline DSG3-CAART*. (2022*).* Cabaletta Bio. Retrieved August 12, 2022 from https://www.cabalettabio.com/pipeline/dsg3-caart

55. Kasperkiewicz, M., Ellebrecht, C. T., Takahashi, H., Yamagami, J., Zillikens, D., Payne, A. S., & Amagai, M. Pemphigus. *Nature reviews. Disease primers*, **3**, 17026, (2017). https://doi.org/10.1038/nrdp.2017.26

56. Esensten, J. H., Muller, Y. D., Bluestone, J. A., & Tang, Q. Regulatory T-cell therapy for autoimmune and autoinflammatory diseases: The next frontier. *J Allergy Clin Immunol*, **142**, 1710–1718, (2018). https://doi.org/10.1016/j.jaci.2018.10.015

57. Liberal, R., Grant, C.R., Longhi, M.S., Mieli-Vergani, G. and Vergani, D. Regulatory T cells: Mechanisms of suppression and impairment in autoimmune liver disease. *IUBMB Life*, **67**, 88-97, (2015). https://doi.org/10.1002/iub.1349

58. Ujiie, H. Regulatory T cells in autoimmune skin diseases. *Experimental Dermatology*, **28**, 626-646 (2019). doi: 10.1111/exd.13535

59. Rocamora-Reverte, L., Melzer, F.L., Würzner, R., & Weinberger, B. The complex role of regulatory T cells in immunity and aging. *Frontiers in Immunology*, **11**, 616949, (2021). https://doi.org/10.3389/fimmu.2020.616949

60. Sugiyama, H., Matsue, H., Nagasaka, A., Nakamura, Y., Tsukamoto, K., Shibagaki, N., Kawamura, T., Kitamura, R., Ando, N., & Shimada, S. CD4+CD25$^{high}$ regulatory T cells are markedly decreased in blood of patients with pemphigus vulgaris. *Dermatology*, **214**, 210–220, (2007). https://doi.org/10.1159/000099585

61. Veldman, C., Höhne, A., Dieckmann, D., Schuler, G., & Hertl, M. Type I regulatory T cells specific for desmoglein 3 are more frequently detected in healthy individuals than in patients with pemphigus vulgaris. *Journal of immunology*, **172**, 6468–6475, (2004). https://doi.org/10.4049/jimmunol.172.10.6468

62. Kwon, E.J., Yamagami, J., Nishikawa, T., & Amagai, M. Anti-desmoglein IgG autoantibodies in patients with pemphigus in remission. *Journal of the European Academy of Dermatology and Venereology*, **22**, 1070–1075, (2008). https://doi.org/10.1111/j.1468-3083.2008.02715.x

63. Holstein, J., Solimani, F., Baum, C., Meier, K., Pollmann, R., Didona, D., Tekath, T., Dugas, M., Casadei, N., Hudemann, C., Polakova, A., Matthes, J., Schäfer, I., Yazdi, A. S., Eming, R., Hertl, M., Pfützner, W., Ghoreschi, K., & Möbs, C. Immunophenotyping in pemphigus reveals a $T_H17/T_{FH}17$ cell-dominated immune response promoting Desmoglein1/3-specific autoantibody production. *J Allergy Clin Immunol*, **147**, 2358–2369, (2021). https://doi.org/10.1016/j.jaci.2020.11.008

64. Bonasia, C.G., Abdulahad, W.H., Rutgers, A., Heeringa, P., & Bos, N.A. B Cell activation and escape of tolerance checkpoints: Recent insights from studying autoreactive B cells. *Cells*, **10**, 1190, (2021). https://doi.org/10.3390/cells10051190

65. *CAR T Cells: Engineering Patients' Immune Cells to Treat Their Cancers*. (2022*)*. NIH National Cancer Institute: About Cancer. Retrieved August 19, 2022 from https://www.cancer.gov/about-cancer/treatment/research/car-t-cells

66. Koch, P. J., Mahoney, M. G., Ishikawa, H., Pulkkinen, L., Uitto, J., Shultz, L., Murphy, G. F., Whitaker-Menezes, D., & Stanley, J. R. (1997). Targeted disruption of the pemphigus vulgaris

antigen (Desmoglein 3) gene in mice causes loss of keratinocyte cell adhesion with a phenotype similar to pemphigus vulgaris. *J Cell Biol*., **137**, 1091–1102. https://doi.org/10.1083/jcb.137.5.1091

67. Aoki-Ota, M., Tsunoda, K., Ota, T., Iwasaki, T., Koyasu, S., Amagai, M., & Nishikawa, T. A mouse model of pemphigus vulgaris by adoptive transfer of naïve splenocytes from Desmoglein 3 knockout mice. *Br J Dermatol*., **151**, 346–354, (2004). https://doi.org/10.1111/j.1365-2133.2004.06056.x

68. Amagai, M., Tsunoda, K., Suzuki, H., Nishifuji, K., Koyasu, S., & Nishikawa, T. Use of autoantigen-knockout mice in developing an active autoimmune disease model for pemphigus. *J Clin Invest*., **105**, 625–631, (2000). https://doi.org/10.1172/JCI8748

69. Holm, T. L., & Markholst, H. Confirmation of a disease model of pemphigus vulgaris: characterization and correlation between disease parameters in 90 mice. *Exp Dermatol*., **19**, e158–e165, (2010). https://doi.org/10.1111/j.1600-0625.2009.01033.x

70. Kim, A. R., Han, D., Choi, J. Y., Seok, J., Kim, S. E., Seo, S. H., Takahashi, H., Amagai, M., Park, S. H., Kim, S. C., Shin, E. C., & Kim, J. H. Targeting inducible costimulator expressed on CXCR5+PD-1+ TH cells suppresses the progression of pemphigus vulgaris. *J Allergy Clin Immunol*., **146**, 1070–1079.e8, (2020). https://doi.org/10.1016/j.jaci.2020.03.036

71. Hata, T., Nishimoto, S., Nagao, K., Takahashi, H., Yoshida, K., Ohyama, M., Yamada, T., Asano, K., & Amagai, M. Ectopic expression of epidermal antigens renders the lung a target organ in paraneoplastic pemphigus. *J Immunol*., **191**, 83–90, (2013). https://doi.org/10.4049/jimmunol.1203536

*72.* Brunggel, K.L. (2018). *Introducing tolerance to foreign and partly foreign proteins by erythrocyte binding and artificial glycosylations* (Thesis No. 8190) [Doctoral dissertation, École Polytechnique Fédérale de Lausanne]. EPFL Infoscience, EPFL scientific publications, doi: 10.5075/epfl-thesis-8190

73. Crispe, I. N., Giannandrea, M., Klein, I., John, B., Sampson, B. and Wuensch, S. Cellular and molecular mechanisms of liver tolerance. *Immunological Reviews*, **213**, 101–118 (2006). doi:10.1111/j.1600-065X.2006.00435.x

74. Knolle, P. A. Staying local – antigen presentation in the liver. *Current Opinion in Immunology*, **40**, 36-42 (2016). https://doi.org/10.1016/j.coi.2016.02.009

75. Bale, S. S., Golberg, I., Jindal, R., McCarty, W. J., Luitje, M., Hegde, M., Bhushan, A., Usta, O. B., Yarmush, M. L. Long-term coculture strategies for primary hepatocytes and liver sinusoidal endothelial cells. *Tissue Eng Part C Methods*, **21**, 413-22 (2015). doi: 10.1089/ten.tec.2014.0152

76. Knolle, P. A., Wohlleber, D. Immunological functions of liver sinusoidal endothelial cells. *Cellular & Molecular Immunology*, **13**, 347–353 (2016). doi:10.1038/cmi.2016.5

77. DeLeve, L. D., Maretti-Mira, A. C. Liver Sinusoidal Endothelial Cell: An Update. *Semin Liver Dis.*, **37**, 377-387 (2017). doi: 10.1055/s-0037-1617455.

78. Jenne, C. N., Kubes, P. Immune surveillance by the liver. *Nature Immunology*, **14**, 996-1006 (2013). doi:10.1038/ni.2691

79. Uhrig, A., Banafsche, R., Kremer, M., Hegenbarth, S., Hamann, A., Neurath, M., Gerken, G., Limmer, A., Knolle, P. A. Development and functional consequences of LPS tolerance in sinusoidal endothelial cells of the liver. *J Leukoc Biol*, **77**, 626-33 (2005). doi:10.1189/jlb.0604332

80. Zhou, Z., Xu, M.-J., Gao, B. Hepatocytes: a key cell type for innate immunity. *Cell Mol Immunol*, **13**, 301–315 (2016). doi: 10.1038/cmi.2015.97

81. Tang, L., Yang, J., Liu, W., Tang, X., Chen, J., Zhao, D., et al. Liver sinusoidal endothelial cell lectin, LSECtin, negatively regulates hepatic T-cell immune response. *Gastroenterology*, **137**, 1498-508.e1-5 (2009). doi: 10.1053/j.gastro.2009.07.051.

82. Doherty, D.G. Immunity, tolerance and autoimmunity in the liver: A comprehensive review. *Journal of Autoimmunity*, **66**, 60-75 (2016). https://doi.org/10.1016/j.jaut.2015.08.020.

83. Knolle, P. A., Limmer, A. Neighborhood politics: the immunoregulatory function of organ-resident liver endothelial cells. *Trends Immunol*, **22**, 432-7 (2001). doi: http://dx.doi.org/10.1016/S1471-4906(01)01957-3

84. Limmer, A., Ohl, J., Kurts, C., Ljunggren, H. G., Reiss, Y., Groettrup, M., Momburg, F., Arnold, B., Knolle, P. A. Efficient presentation of exogenous antigen by liver endothelial cells to CD8+ T cells results in antigen-specific T-cell tolerance. *Nature Medicine*, **6**, 1348-54 (2000). doi:10.1038/82161

85. Diehl, L., Schurich, A., Grochtmann, R., Hegenbarth, S., Chen, L., Knolle, P. A. Tolerogenic maturation of liver sinusoidal endothelial cells promotes b7-homolog 1-dependent CD8+ T cell tolerance. *Hepatology*, **47**, 296-305 (2008). doi: 10.1002/hep.21965

86. Schurich, A., Berg, M., Stabenow, D., Bottcher, J., Kern, M., Schild, H.-J., Kurts, C., Schuette, V., Burgdorf, S., Diehl, L., Limmer, A., Knolle, P. A. Dynamic regulation of CD8 T cell tolerance induction by liver sinusoidal endothelial cells. *The Journal of Immunology*, **184**, 4107–4114 (2010). doi: 10.4049/jimmunol.0902580

87. Hochst, B., Schildberg, F. A., Bottcher, J., Metzger, C., Huss, S., Knolle, P., Diehl, L., et al. Liver sinusoidal endothelial cells contribute to CD8 T cell tolerance toward circulating carcinoembryonic antigen in mice. *Hepatology*, **56**, 1924-1933 (2012). doi: 10.1002/hep.25844

88. Bottcher, J. P., Schanz, O., Wohlleber, D., Abdullah, A., Debey-Pascher, S., Hochst, B., Diehl, L., et al. Liver-primed, memory T cells generated under noninflammatory conditions provide anti-infectious immunity. *Cell Report*s, **3**, 779-795 (2013).

89. Meyer, J., Lacotte, S., Morel, P., Gonelle-Gispert, C., Bühler, L. An optimized method for mouse liver sinusoidal endothelial cell isolation. *Experimental Cell Research*, **349**, 291-301 (2016). https://doi.org/10.1016/j.yexcr.2016.10.024

90. Meyer, J., Gonelle-Gispert, C., Morel, P., Bühler, L. Methods for Isolation and Purification of Murine Liver Sinusoidal Endothelial Cells: A Systematic Review. *PLOS ONE*, **11**, e0151945 (2016). https://doi.org/10.1371/journal.pone.0151945

91. MacParland, S.A., Liu, J.C., Ma, X.Z., Innes, B.T., Bartczak, A.M., Gage, B.K., Manuel, J., Khuu, N., Echeverri, J., Linares, I., Gupta, R., Cheng, M. L., Liu, L.Y., Camat, D., Chung, S.W., Seliga, R.K., Shao, Z., Lee, E., Ogawa, S., Ogawa, M., … McGilvray, I.D. Single cell RNA sequencing of human liver reveals distinct intrahepatic macrophage populations. *Nature Communications*, ***9***, 4383, (2018). https://doi.org/10.1038/s41467-018-06318-7

92. Suwanmanee, T., Ferris, M. T., Hu, P., Gui, T., Montgomery, S. A., Pardo-Manuel de Villena, F., Kafri, T. Toward Personalized Gene Therapy: Characterizing the Host Genetic Control of Lentiviral-Vector-Mediated Hepatic Gene Delivery. *Molecular Therapy - Methods & Clinical Development*, **5**, 83-92, (2017). http://dx.doi.org/10.1016/j.omtm.2017.03.009.

93. Domínguez-Soto, Á., Aragoneses-Fenoll, L., Gómez-Aguado, F., Corcuera, M. T., Clária, J., García-Monzón, C., Bustos, M. and Corbí, A. L. The pathogen receptor liver and lymph node sinusoidal endotelial cell C-type lectin is expressed in human Kupffer cells and regulated by PU.1. *Hepatology*, **49**, 287–296 (2009). doi:10.1002/hep.22678

94. Watkins, E.A. (2021). *Antibody Targeting of Antigen to Endogenous Immune Surveillance Pathways for the Induction of Tolerance* (Record ID 2808) [Doctoral dissertation, University of Chicago]. Knowledge@UChicago, doi: 10.6082/uchicago.2808

*95.* Tremain, A. (2021). *Evaluation of Novel Engineered Strategies for Therapeutic Antigen Immunotherapy* (Record ID 3044) [Doctoral dissertation, University of Chicago]. Knowledge@UChicago, doi: 10.6082/uchicago.3044